di Bernardo, M., Budd, C., Champneys, A. R., Kowalczyk, P. S., Nordmark, A., Olivar, G., & Piiroinen, P. T. (2005). Bifurcations in nonsmooth dynamical systems.

Early version, also known as pre-print

University of Bristol - Explore Bristol Research
General rights

Bifurcations in Nonsmooth Dynamical Systems

M. di Bernardo[1,5], C. Budd[2], A.R. Champneys[1], P. Kowalczyk[1],
A.B. Nordmark[3], G. Olivar[4], P.T. Piiroinen[1,2,*]

[1] Department of Engineering Mathematics, University of Bristol, UK

[2] Department of Mathematical Sciences, University of Bath, UK

[3] Department of Mechanics, Royal Institute of Technology, Sweden

[4] Department of Applied Mathematics, Technical University of Cataloinia, Spain

[5] Department of Systems and Computer Science, University of Naples Federico II, Italy

[*] Corresponding author with email address **petri.piiroinen@bristol.ac.uk**

Abstract

A review is presented of the one-parameter, nonsmooth bifurcations
that occur in piecewise-smooth dynamical system. Motivated by ap-
plications, a pragmatic approach is taken to defining 'bifurcation' as
a nonsmooth transition with respect to a codimension-one discontinu-
ity boundary in phase space. Only local bifurcations are considered,
involving equilibria or a single point of boundary interaction along a
limit cycle. Three classes of system are considered; involving either
state jumps, jumps in the vector field, or in some derivative of the vec-
tor field. A rich array of dynamics are revealed, involving the sudden
creation or disappearance of attractors, jumps to chaos, bifurcation
diagrams with sharp corners, and cascades of period adding. For each
kind of bifurcation identified, where possible, a normal form is given,
together with a canonical example and an application. The goal is
always to explain dynamics that may be observed in simulations.

Key words: Nonsmooth dynamical systems, Bifurcations, Nonsmooth
transitions, equilibria, limit cycles

AMS Subject Classifications: 34A36, 34D08, 37D45, 37G15, 37G15,
37N05, 37N20

1   Introduction

Bifurcation analysis has shown considerable success in explaining, classi-
fying, and drawing analogies between the behaviour of dynamical systems
arising from a myriad of different application areas. A more or less complete
set of mathematical tools exist (e.g. [50, 1]), to describe bifurcations if the
system is sufficiently smooth. However many dynamical systems arising in
applications are nonsmooth; examples include the occurrence of impacting
motion in mechanical systems [7, 8], stick-slip motion in oscillators with
friction [69], switchings in electronic circuits [26, 4] and hybrid dynamics in
control systems [29, 79]. In all of these cases the assumptions behind most
of the results in bifurcation theory [50] for smooth systems are violated and
many new phenomena are observed.

Let us start with a motivating example. Figure 1 depics and experimen-
tal system where a free swinging pendulum is allowed to impact with a rigid
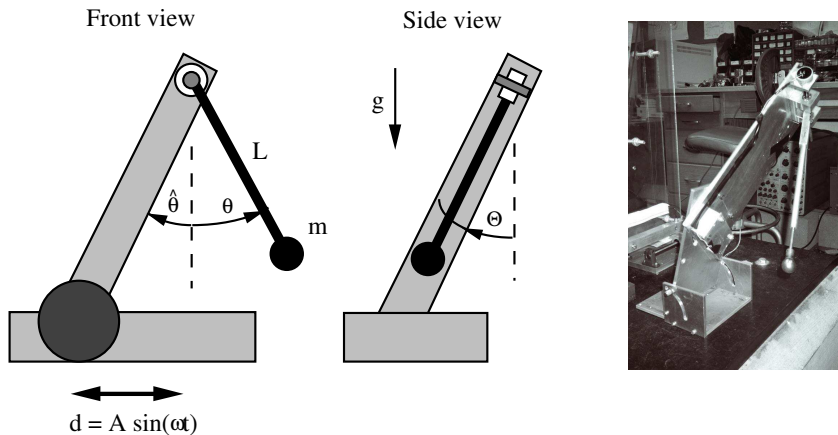stop (see [67] and Ex. 4.5 for more details). This is a cannonical example of

Figure 1: A schematic and a photo of the pendulum/impact barrier assem-
bly.

an impact oscillator, which have recieved a good deal of attention over the
last 30 years since the pioneering work by Peterka [66]. In this particular
study the table on which the pendulum rests is subjected to harmonic forc-
ing and the corresponding motion recorded under variation of the angular
position $\hat{\theta}$ of the stop. Furthermore, $d(t) = A\sin(\omega t)$ is the motion of the
support, L is the effective length of the pendulum arm, g is the gravity,

m is the mass, θ is the angle of the pendulum and Θ is the out of plane angle. Dissipation is included via a simple linear term $\kappa\dot{\theta}$ and a restitution at impact. Figure 2(a) shows the experimental results of the position of the pendulum at a fixed phase of the forcing, under gradual, quasi-static, variation of the dimensionless frequency η. Note several interesting features
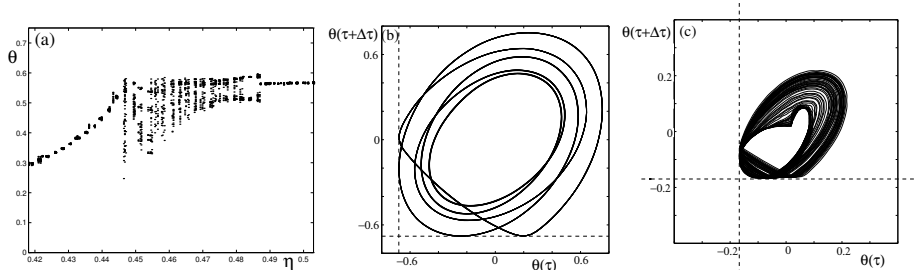

Figure 2: Experimental results for the impacting pendulum in Fig. 1, where (a) depicts a bifurcation diagram of θ, which is plotted once per forcing period, under frequency variation, (b) and (c) depicts delay plots of a period-five orbit and chaotic motion, respectively. The parameter values are (a) $\hat{\theta} = 40°$, (b) $\hat{\theta} = 10°$ and $\eta = 0.45$ and (c) $\hat{\theta} = 40°$ and $\eta = 0.35$.

of the dynamics. The most striking feature is the sudden transition around $\eta = 0.44$. This is where stable periodic motion is first observed to impact with the stop in a so-called *grazing bifurcation*. This creates a band of chaotic motion (Fig. 2(c)) where the amplitude range grows rapidly (seemingly discontinuously) with increasing η. The analysis in this review will seek to explain why we should expect to see such a transition, and other similar phenomena when a non-smooth event occurs such as a grazing of a periodic orbit. Moreover, further details of the dynamics can be explained using the theory we shall review such as the observed 'windows' (intervals of η-values) in which there is stable periodic motion embedded within the chaos (Fig. 2(b)). Here, there is a 'period-adding' sequence where the underlying multitple of the forcing period of the attracting limit cycle increases by one as η is reduced towards the grazing bifurcation value.

Finally, we remark that the dynamics created by such nonsmooth transitions can cause co-existence of different attractoes for the same parameter values, with highly complex basins of attraction. Figure 3 shows just such a case for a related impact oscillator, where again motion is depicted for a fixed value of the forcing phase. This picture shows the angle and and angular velocity of the pendulum at times $t = 2k\pi/\omega$, for $k = 1, 2, \ldots$ and where
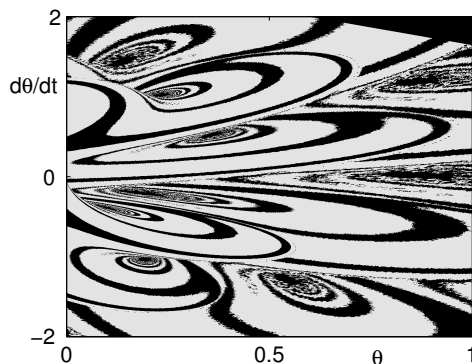
3

Figure 3: The domains of attraction of two stable periodic states (period-one and period-six) for a simple forced impact oscillator.

ω is the forcing frequency. The black regions correspond to initial conditions that are attracted to a stable period-one orbit and the grey regions to initial conditions attracted to a stable period-six orbit. See [56] for more details on domain of attraction calculations of impacting systems.

Returning to the general theme of this review, we note that in recent years there has been significant progress in identifying, classifying, unfolding and applying novel kinds of bifurcation that are unique to nonsmooth systems. Three problems emerge when trying to summarise this work and put it in context. What do we mean by a piecewise smooth system?, what do we mean by a bifurcation? and what do we mean by 'codimension' for a nonsmooth systems? Each of these questions alone warrant significant investigation in their own right. This review shall therefore take a pragmatic approach motivated by what is known to occur in applications. Lets take each of these questions in turn.

First, what do we mean by a *piecewise-smooth system*? There are several different formalisms for dealing with continuous-time nonsmooth systems. We mention that of hybrid systems, measure differential inclusions, complementarity problems, and set value ordinary differential equations, see e.g. [9, 43]. There is also a large literature for the dynamics of nonsmooth discrete-time maps – so-called border-collision bifurcations [32, 63, 5, 3]. Here we shall focus on the continuous-time case, although as we shall see, such nonsmooth mappings can arise as Poincaré maps when we study bifurcations of limit cycles. We will consider the simple paradigm of a piecewise smooth (PWS) system. That is, a set of ordinary differential equations in

4

$\mathbb{R}^n$, where the phase space is partitioned into finitely many open sets S_i in which the system is smooth[1]:

$$\dot{x} = f(x, \mu), \quad x \in \mathbb{R}^n, \quad \mu \in \mathbb{R}^p, \tag{1}$$

where

$$f(x, \mu) = F_i(x, \mu) \quad \forall x \in S_i \subset \mathbb{R}^n, \quad i = 1 \ldots, n,$$

and each function F_i is a smooth function of its argument. We shall also assume each boundary Σ_{ij} between regions S_i and S_j to be a smooth $(n-1)$–dimensional manifold, allthough we shall also be interested in corners termed by the intersections of two smooth Σ_{ij}. Broadly speaking, different classes of peicewise smooth systems can be classified according to what is allowed to happen when the flow intersects the boundary Σ_{ij}. Here we shall distinguish three classes of systems:

1. **Non-sliding PWS** The simplest assumption is that, the boundary Σ_{ij} is never simultaneously attracting (or repelling) from both sides under the dynamics, Hence all trajectories either cross Σ_{ij} transversally, or both vector fields are simultaneously tangent to it. See Fig. 4(a). Hence no *sliding* motion constrained to Σ_{ij} can take place. Such systems naturally arise as models of second-order bilinear oscillators (Example 2.1 below). This includes the case where the overall vector field f is continuous and has discontinuity across Σ in its first or higher derivative (PWS continuous). We also include in this class the the case where the vector field is discontinuous across Σ_{ij}, but the system dynamics means that the grazing sets of vector fields F_i and F_j coincide, so that no sliding can occur.

2. **Filippov PWS systems.** In this case, F is discontinuous across Σ and we allow the possibility that both flows in regions S_i and S_j have their components normal to Σ_{ij} of opposite sign. This implies the possible existence of sliding flow inside the discontinuity surface Σ_{ij} (along the bold portion of the boundary illustrated in Fig. 4(b). For many physical systems, this flow can be described by the Filippov convex method

$$F = \lambda F_i + (1 - \lambda) F_j, \quad 0 \leq \lambda = \frac{(H_{ij})_x F_j}{(H_{ij})_x (F_j - F_i)} \leq 1, \tag{2}$$

where H_{ij} is a function whose zero set is Σ_{ij} [34], see Chapter 4 below. Note that the flow corresponds with that in regions S_i and S_j when

---

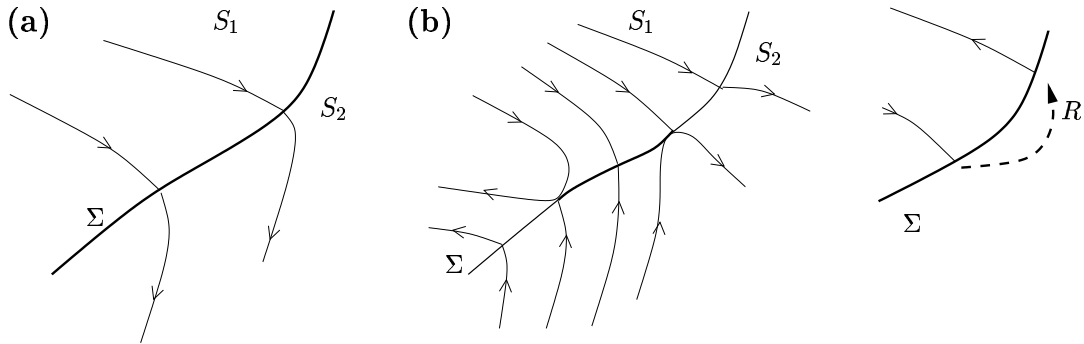[1]We take 'smooth' to mean C^r for r sufficiently large

Figure 4: Sketches of the phase space of the three classes of system under consideration; (a) non-sliding PWS, (b) Filippov and (c) impacting systems.

$\lambda = 0$ and $\lambda = 1$ respectively, see Figure 4(b). Such models arise, for example in models of dry friction oscillators and relay control systems (see example 3.1 below).

3. **Impacting systems.** Finally, we consider the case where Σ_{ij} is a hard boundary, and the region S_j is a forbidden region of phase space (Fig. 4(c)). On the boundary, the continuous dynamics is replaced by an instantaneous reset (or impact) map R.

$$x \to R(x), \quad x \in \Sigma_{ij}.$$

Depending on the properties allowed for the map R, many different dynamics may be seen. Much work in this area has been motivated by the case of mechanical systems where the phase space is composed of velocity and position variables and the the reset map acts to reverse the sign of a velocity variable at impact, see e.g. [66, 36], the introductory example presenmted above, and sec. 4 below. Hence we assume that the boundary Σ_{ij} is divided into regions Σ_i^- where it is attracting and Σ_i^+ where it is repelling. The reset is then assumed to to map $R : \Sigma_i^- \to \Sigma_i^+$. More complex situations can arise in three or more dimensions when motion under the dynamics can slide along the $(n-2)$-dimensional boundary between Σ_- and Σ_+. Motivated by mechanically impacting systems, we shall also restrict attention to the simplest forms of reset maps, avoiding the extra complexity that can arise in the case of impact with friction (e.g. [75]).

It is also possible to distinguish between the above three cases using

6

the concept of the *degree of discontinuity*. Using a concept widely used in control theory, this degree can be thought of as the relative degree between the state of the system $x(t)$ along a solution trajectory and a function which describes the jump that occurs across the boundary Σ_{ij}. Broadly speaking, for an impacting system we say the degree is zero since the jump is on the system state itself. By contrast, Filippov systems have degree one, since the jump is on the vector field which is the time derivative of the solution state. For PWS continuous systems, where the jump is on the kth-derivative of the vector field, then the degree is $k + 1$, since this is the number of times one has to differentiate the jump to obtain a discontinuity in the state. Note that there are other uses of relative degree in non-smooth mechanics, for example between the system state and the Lagrange multiplier (λ in (2) above) required to maintain a constraint (e.g. [43]). Of course, many systems may have the property that in different parts of their phase space or at different parameter values, they may exhibit different dynamics from the above list.

The second problem we face is to define what we mean by a *bifurcation*. There are in essence two approaches to defining bifurcation in smooth systems; analytical or topological. In the analytical approach, bifurcation is defined as the branching, folding or creation of additional paths of solutions of a certain class within a bifurcation diagram, e.g. [44, 13]. In the topological sense, a bifurcation is a parameter value within a class of systems at which the phase portrait is not structurally stable, e.g [42, 50]. A universal unfolding (or topological normal form) of the bifurcation includes a minimal number of terms and parameters to allow all possible structurally stable bifurcation diagrams to be seen at small values of the unfolding parameters. The number of parameters necessary defines the codimension of the bifurcation. For nonsmooth systems, these concepts are problematical. In the analytical approach, a small change in parameter can cause the instantaneous creation of a chaotic attractor together with infinitely many unstable periodic orbits (see e.g. [5]). For the topological approach, we need *a priori* to define a system topology. For example, does the topology allow a change in the number or relative position of the number of discontinuity boundaries Σ_{ij} as a parameter varies, or a change in the degree of discontinuity of the flow at those boundaries? For each class of nonsmooth system, there are likely to be several different possible notions of bifurcation.

Rather than deal with these technical issues, we again take a pragmatic approach. We are interested in describing situations that are unique to non-smooth systems; specifically, when the system dynamics does something degenerate with respect to a discontinuity boundary. For example, this might

involve an invariant set gaining a first contact with a certain Σ_{ij}, or the onset of sliding along the orbits of that invariant set. We shall refer to these events as *nonsmooth transitions* (NST) because, as we shall see, depending on the circumstances this may or may not lead to a bifurcation in either of the classical senses as a parameter is varied. NSTs were given the name C-bifurcations[2] in the Russian literature [33]. We shall concentrate on NSTs that involve the simplest kinds of invariant set only; equilibria or periodic orbits. In what follows, the term 'bifurcation' shall be used to mean such a nonsmooth transition. Of course, nonsmooth systems can also undergo regular bifurcatiopns too just like smooth systems, but the focus of this review is those bifurcations that are unique to nonsmooth systems. We should also contrast the C-bifurcations to so-called *border-collision bifurcations* [64, 3] which occur when fixed points of discrete-time maps cross a discontinuity. Here we shall be concerned exclusively with continuous-time systems.

For simplicity, we shall consider each NST in its simplest possible setting. So we will not allow systems which change their type between the three classes outlined above as parameters vary, and we shall assume that all discontinuity boundaries remain fixed. Also, we shall only deal with local bifurcations in the sense that the dynamics shall be governed by the point of interaction with the boundary and shall not involve possible heteroclinic connections to other invariant sets (but see [51] for a catalog of possible bifurcations, both local and global in two-dimensional Filippov systems with a single discontinuity boundary). A few remarks concerning bifurcations involving other invariant sets are given in Section 5.

This brings us to the issue of *codimension*. Broadly speaking we shall only treat codimension-one situations, that is NSTs that one should expect to see as a single parameter is varied. However, the classification by codimension relies heavily on what is assumed about the system topology. For example, in a system with four discontinuity boundaries that meet at a point, it may be possible for a bifurcation to occur upon varying one parameter whereby a periodic orbit passes through this point [53]. Hence we shall need to assume that the boundaries themselves are in general position. That is, any intersection between Σ_{ij} and Σ_{jk} occurs along a smooth $(n-2)$-dimensional manifold. For this reason, and since we only consider local neighbourhoods of the NST we shall only need consider cases where there are at most two discontinuity boundaries. The NSTs we consider shall then involve either an equilibrium approaching a single boundary Σ (or leav-

---

[2]The C stands for the Russian word for 'sewing', so that different trajectory segments are being sewn together at the bifurcation point.

ing the sliding region) or a periodic orbit either grazing with a boundary or approaching the intersection point between two boundaries Σ_1 and Σ_2. As we shall see, even considering this finite set of transitions leads to many possible dynamical consequences. Finally we should re-iterate that we are motivated by examples, and quite often the purely topological definition of codimension can then be unhelpful. For example in smooth dynamics, we know that conservative or symmetric systems can undergo bifurcations that would be of significantly higher co-dimension in the generic case. We already mentioned the case of degenerate piecewise discontinuous systems, where sliding is impossible. Also, motivated by examples with dry friction, there can be Filippov systems where there can exist non-isolated equilibria in the sliding region.

The next three sections of this review treat each of the three classes of system in turn, in each case dealing first with NSTs involving equilibria, then periodic orbits. In addition to reviewing the existing literature we include many new results, especially in Sections 2.1, 2.3, 3.1, and the whole of Section 4. For each NST we shall give a mathematical example, and where possible a *physical application*. We shall also give '*normal forms*' for the transition, where they are known to exist, and if not highlight a method for analysing what occurs. These normal forms shall, in the case of periodic orbit bifurcations typically take the form of maps. See Section 2.2 for a discussion on how to derive such maps using the *discontinuity mapping* idea. It might also be the case that the simple mathematical examples can serve as *canonical models* that contain all the essential features, that can occur in realistic applications. Where possible, we shall also indicate what is known about the dynamics of the unfolding of the transition, indicating which different sub-cases may occur. In some cases, where complete theory is available we give it with a motivation of the method rather than the complete proof. In other cases, complete results remain unknown and we merely sketch possible NST scenarios. We shall also introduce techniques of analysis and notation as we go along, thus later sections rely on concepts that are introduced in earlier one. In this way, we shall also highlight connections between the bifurcations that occur in the three different classes of systems. Finally, Section 5 indicates some of the many problems that are not treated by this review, including open questions and future directions for research.

2 Non-sliding Systems

This section describes the possible nonsmooth transitions of equilibria and periodic orbits of systems of relative degree one or two, i.e. piecewise smooth continuous and (degenerate) discontinuos vector fields with no sliding.

Example 2.1 (The bilinear oscillator, a motivating example)

Consider the bilinear oscillator defined by the equation (e.g. [71])

$$\ddot{X} + \zeta_i \dot{X} + k_i^2 X = \beta_i \cos(\omega t) + \Theta_i \tag{3}$$

where $i = 1$ if $X > 0$ and $i = 2$ if $X < 0$. This models a simple one-degree-of-freedom linear oscillator with sinusoidal forcing, where the value of the damping ζ, spring constant k, forcing amplitude β or offset Θ might change when the displacement X crosses a threshold value, which without loss of generality we take to be $X = 0$. We seek to understand the nature of the singularity in the flow map if a trajectory becomes tangent, i.e. *grazes*, with the threshold $X = 0$ at some time $t = t^*$. Now clearly for a grazing event we require $\dot{X}(t^*) = 0$ also.

First, to make the system autonomous, set time to be an extra state variable, via $x_3 := \omega(t - t^*)$, so that a grazing event happens automatically at the origin of the co-ordinate system

$$x := (x_1, x_2, x_3)^T = (X, \dot{X}, \omega(t - t^*))^T.$$

Then (3) becomes

$$\dot{x} = \begin{cases} A_1 x + B_1, & \text{if } H(x) = Cx > 0 \\ A_2 x + B_2, & \text{if } H(x) = Cx < 0 \end{cases} \tag{4}$$

where

$$A_1 = \begin{pmatrix} 0 & 1 & 0 \\ -k_1^2 & -\zeta_1 & 0 \\ 0 & 0 & 0 \end{pmatrix}, \quad B_1 = \begin{pmatrix} 0 \\ \beta_1 \cos(x_3 + \omega t^*) + \Theta_1 \\ \omega \end{pmatrix},$$

$$A_2 = \begin{pmatrix} 0 & 1 & 0 \\ -k_2^2 & -\zeta_2 & 0 \\ 0 & 0 & 0 \end{pmatrix}, \quad B_2 = \begin{pmatrix} 0 \\ \beta_2 \cos(x_3 + \omega t^*) + \Theta_2 \\ \omega \end{pmatrix},$$

$$C = \begin{pmatrix} 1 & 0 & 0 \end{pmatrix}. \tag{5}$$

In what follows, let

$$\hat{\beta}_i = \beta_i(\cos \omega t^*) + \Theta_i. \tag{6}$$

10

Consider first the case where $\hat{\beta}_1 \neq \hat{\beta}_2$. Then vector field itself is discontinuous at the grazing point since $F_i|_{x=0} = (0, \hat{\beta}_i, \omega)^T$. So, we have a jump in the value of the vector field anywhere along the set of potential grazing points. Moreover, at any point in the switching plane $\Sigma := \{x \in \mathbb{R}^3 : x_1 = 0\}$, the vector field undergoes a finite jump, since

$$F_i\big|_{x_1=0} = (x_2, \ \beta_i \cos\omega(c + x_3) + \Theta_i - \zeta_i x_2, \ \omega)^T. \tag{7}$$

This situation, where the degree of discontinuity of the vector field at all points of Σ is the same we refer to as representing *uniform discontinuity* of degree 1.

Definition 2.1 *A discontinuity boundary Σ is said to be* uniformly discontinuous *in some domain $\mathcal{D}$, if the degree of discontinuity of the vector field across Σ is the same throughout $\mathcal{D}$. Furthermore, we say that the discontinuity is* uniform with degree $m + 1$ *if the first $m - 1$ derivatives of $F_1 - F_2$, evaluated on Σ are zero.*

We note however from the form of F_1 and F_2 in (7) that Σ is never simultaneously attracting or repelling from both sides. This is because both vector fields graze along the same line $x_1 = x_2 = 0$. So there is no sliding possible in this example because in essence of second-order structure. (See condition (9) below).

Now suppose instead that $\Theta_1 = \Theta_2 := \Theta$ and $\beta_1 = \beta_2 := \beta$ so that at the grazing point the vector field is continuous. Then at the grazing point we have $\frac{\partial F_i}{\partial x}|_{x=0} = A_i$, $F_i|_{x=0} = (0, \ \beta, \ \omega)^T$ which if $\zeta_1 \neq \zeta_2$ or $k_1 \neq k_2$ implies that there is a jump in the first derivative of the vector field. Consider separately the cases where the damping coefficient ζ_i or the stiffness term k_i vary across the discontinuity boundary. If $\zeta_1 \neq \zeta_2$ but $k_1 = k_2$ then, at a general point in the switching plane Σ, we have (taking $t^* = 0$): $F_i|_{x_1=0} = (x_2, \ \beta_i \cos\omega x_3 + \Theta - \zeta_i x_2, \ \omega)^T$. Hence if $x_2 \neq 0$ we find that the vector field itself is discontinuous since $F_1 \neq F_2$. Only on the grazing line defined by $x_2 = 0$ is the lowest order discontinuity in the derivative of the vector field. This is an example of *non-uniform discontinuity*. As mentioned above, it is easy to see that there can be no sliding here though since both vector fields graze along the same line. In contrast if $k_1 \neq k_2$ but $\zeta_1 = \zeta_2 := \zeta$, then at a general point in Σ we have $F_i|_{x_1=0} = (x_2, \ \beta_i \cos\omega x_3 + \Theta - \zeta x_2, \ \omega)^T$, so that $F_1 = F_2$ and we have uniform discontinuity of degree 2.

In what follows, we shall be interested in two special forms of allowed jump across Σ. Uniform discontinuity of degree $m > 2$ is ensured by assuming

$$F_2(x) = F_1(x) + J(x)H(x)^{m-1} \tag{8}$$

11

where the boundary Σ is defined by the zero-set of the smooth function $H(x)$, and J, F_1 and F_2 are all sufficiently smooth in a neighbourhood of the grazing point $x = 0$. In the case of discontinuity of degree 1, that is where the vector fields are discontinuous across Σ, the generic situation is described by Filippov flows with sliding. However we saw that the special structure of the bilinear oscillator in the case of jumps in β_i or ζ_i caused discontinuity of degree 1 that did not lead to sliding. This special structure can be formalised by the assumption that

$$H_x(x)F_2(x) = N(x)H(x) + M(x)H_x(x)F_1(x), \qquad (9)$$

for functions N, M, F_1 and F_2 that are sufficiently smooth at the grazing point.

2.1 Nonsmooth Transitions of Equilibria

C-bifurcations or border-collisions, have been studied mostly with respect to fixed points of maps and limit cycles of continuous-time systems [28]. Comparitively less is known on the possible nonsmooth bifurcations of equilibria in piecewise smooth systems, that is [53] where equilibria of PWS flows can also interact with the switching manifolds as parameters are varied. In particular, we focus on nonsmooth continuous systems, i.e. systems with a degree of discontinuity equal to 2. We restrict our attention to a region of phase space, say $\mathcal{D}$, where the system under investigation can be described as follows in terms of a local set of coordinates. Namely, we have

$$\dot{x} = \begin{cases} F_1(x, \mu), & \text{if } H(x, \mu) > 0 \\ F_2(x, \mu), & \text{if } H(x, \mu) < 0 \end{cases}, \qquad (10)$$

where $x \in \mathbb{R}^n$, $F_1, F_2 : \mathbb{R}^{n+1} \mapsto \mathbb{R}^n$ are supposed to be sufficiently smooth, $H : \mathbb{R}^{n+1} \mapsto \mathbb{R}$ is a sufficiently smooth scalar function of the system states. Because of the continuity assumption we must have

$$F_2(x, \mu) = F_1(x, \mu) + G(x, \mu)H(x, \mu), \qquad (11)$$

so that when $H(x, \mu) = 0$ then $F_1 = F_2$ as required.

According to (10), H defines the switching manifold Σ as:

$$\Sigma := \{x \in \mathbb{R}^n : H(x) = 0\}$$

Locally, Σ divides $\mathcal{D}$ in the two regions S_1 and S_2 where the system is smooth and defined by the vector fields F_1 and F_2 respectively; namely:

$$S_1 = \{x \in \mathcal{D} : H(x, \mu) > 0\},$$
$$S_2 = \{x \in \mathcal{D} : H(x, \mu) < 0\}.$$

12

We assume that both the vector fields F_1 and F_2 are defined over the entire local region of phase space under consideration, i.e., on both sides of Σ.

We can identify different types of equilibria of system (10). Namely, it is possible to give the following definitions.

Definition 2.2 *We term a point $x \in \mathcal{D}$ as a* regular equilibrium *of (10) if x is such that either*

$$F_1(x, \mu) = 0 \ and \ H(x, \mu) > 0$$

or

$$F_2(x, \mu) = 0 \ and \ H(x, \mu) < 0.$$

Alternatively, we say that a point $y \in \mathcal{D}$ is a virtual equilibrium *of (10) if either*

$$F_1(y, \mu) = 0 \ but \ H(y, \mu) < 0$$

or

$$F_2(y, \mu) = 0 \ but \ H(y, \mu) > 0.$$

For some value of the system parameters, it is possible for an equilibrium to lie on the discontinuity boundary.

Definition 2.3 *We say that a point $z \in \mathcal{D}$ is a* boundary equilibrium *of (10) if*
$$F_1(z, \mu) = F_2(z, \mu) = 0 \ and \ H(z, \mu) = 0.$$

Note that under parameter variation the system might exhibit a boundary equilibrium for some value of its parameters μ. We shall seek to unfold the bifurcation scenarios that can occur when μ is perturbed away from the origin, i.e. the possible branches of solutions originating from a boundary equilibrium. Specifically we give the following definition.

Definition 2.4 *A regular equilibrium $x^* = x^*(\mu)$, which we assume depends smoothly on μ, is said to undergo a* boundary equilibrium transition *at $\mu = \mu^*$ if*

- $F_1(x^*, \mu^*) = 0$,

- $H(x^*, \mu^*) = 0$,

- $F_{1x}(x^*, \mu^*)$ *is invertible (or equivalently $det(F_{1x}) \neq 0$).*

While the first two conditions state that x^* is a boundary equilibrium when $\mu = \mu^*$, the third condition ensures that the branch of regular equilibria undergoing the bifurcation is isolated. Obviously, an equivalent definition can be given by considering flow F_2 rather than F_1.

Note that it is possible to interpret all of the scenarios described below, in terms of collisions of regular equilibria of the system with the discontinuity boundary. It is worth mentioning here that the definition given above is not equivalent to the one reported in [53]. There, bifurcations of equilibria are defined in terms of the eigenvalues of the system at the bifurcation point. Namely, the nonsmooth bifurcation of an equilibrium is defined as the point at which the eigenvalues of the system are set-valued and contain a value on the imaginary axis. Thus the definition given here is more general.

2.1.1 An overview of possible cases

The existence of different types of bifurcation scenarios following this type of nonsmooth transitions was discussed in [37], [53] and illustrated through some one and two-dimensional examples. It was shown, for example, that nonsmooth transitions of equilibria can be associated, in the simplest cases, to the *persistence* of the bifurcating equilibrium or its disappearance through a *saddle-node* like scenario. Namely, it was conjectured that a boundary equilibrium bifurcation can lead to the following simplest scenarios:

1. Persistence: at the bifurcation point, a regular equilibrium lying in region S_1 is turned into a regular equilibrium lying in region S_2 (or vice versa).

2. Nonsmooth Saddle-Node: at the bifurcation point, the collision of a stable and unstable equilibrium is observed on the boundary followed by their disappearance.

An extension of Feigin's classification strategy for border-collisions of fixed points of maps to the case of equilibria in flows was recently given in [27]. In the next section, we will present an alternative, more elegant derivation of conditions to classify between the two scenarios highlighted above, which will be further discussed in [57].

In addition to persistence and nonsmooth saddle-node scenarios, there might be other invariant sets involved in the bifurcation, for example, scenarios where one or more families of limit cycles are either created or destroyed at the nonsmooth bifurcation point. As shown later in Example 2.2, this

include the scenario where an equilibrium undergoes a boundary equilibrium transition, giving rise to a family of limit cycles. Such transition is the closest nonsmooth equivalent to a Hopf bifurcation for a smooth system.

More complex, non-generic scenarios are also possible in systems with symmetry, as for example the *multiple crossing transition* described in [54]. Note that all of these scenarios are due to the interaction between the bifurcating equilibrium and the discontinuity boundary in phase space. Thus, they are not necessarily associated to eigenvalues crossing the unit circle. We discuss now how some of them can be classified.

2.1.2 Persistence and Nonsmooth Saddle-Node

Despite their similarity to border-collisions, no general classification strategy has been proposed for nonsmooth bifurcations of equilibria in n-dimensional continuous-time systems. Our aim is to classify the simplest possible scenarios associated with a boundary equilibrium transition in n-dimensional nonsmooth continuous flows. We start by giving more precise definitions of the persistence and non-smooth saddle node scenarios introduced above. We assume that a boundary equilibrium bifurcation occurs at $x = 0$ when $\mu = 0$, i.e. $F_1(0,0) = F_2(0,0) = 0, H(0,0) = 0$.

Definition 2.5 *We say that (10) exhibits a* **border-crossing** *transition (persistence) for $\mu = 0$ (see Fig. 5(a)) if when μ is varied in a neighborhood of the origin, one branch of regular equilibria and a branch of virtual equilibria, cross at the boundary equilibrium point, $x = 0$ when $\mu = 0$, exchanging their properties. Namely, we assume there exist smooth branches $x^+(\mu)$ and $x^-(\mu)$ such that $x^+(0) = x^-(0)$ and w.l.o.g., (reversing the sign of μ if necessary)*

1. *$F_1(x^+, \mu) = 0, H(x^+, \mu) > 0$ and $F_2(x^-, \mu) = 0, H(x^-, \mu) > 0$ for $\mu < 0$,*

2. *$F_1(x^+, \mu) = 0, H(x^+, \mu) < 0$ and $F_2(x^-, \mu) = 0, H(x^-, \mu) < 0$ for $\mu > 0$.*

In terms of collision of equilibria with the boundary, this scenario describes how the only admissible equilibrium point x^+ for $\mu < 0$ hits the boundary when $\mu = 0$ and turns continuously into the admissible equilibrium x^- for $\mu > 0$.

Definition 2.6 *We say, instead, that the boundary equilibrium bifurcation is associated to a* **nonsmooth saddle-node** *for $\mu = 0$ (see Fig. 5(b)) if*

15

two branches of regular equilibria collide at the boundary equilibrium point, $x = 0$ when $\mu = 0$ and are both turned into two branches of virtual equilibria past the bifurcation point. Namely, there exist smooth branches $x^-(\mu)$ and $x^+(\mu)$ such that $x^-(0) = x^+(0)$ and

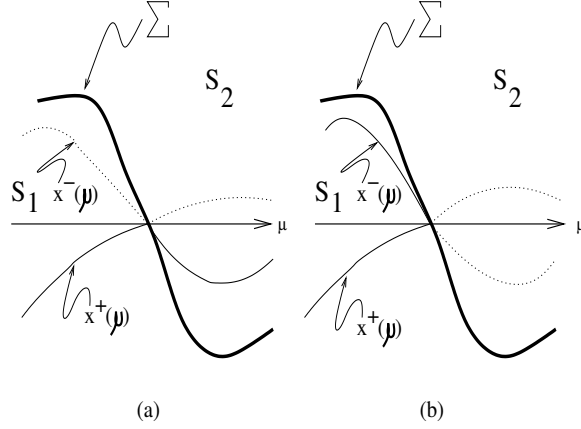1. *$F_1(x^+, \mu) = 0, H(x^+, \mu) > 0$ and $F_2(x^-, \mu) = 0, H(x^-, \mu) < 0$ for $\mu < 0$,*

2. *$F_1(x^+, \mu) = 0, H(x^+, \mu) < 0$ and $F_2(x^-, \mu) = 0, H(x^-, \mu) > 0$ for $\mu > 0$.*

Figure 5: Schematic bifurcation diagrams showing the two possible scenarios: (a) persistence; (b) saddle-node. Regular equilibria are represented by solid lines while virtual equilibria by dotted ones.

Here the two equilibria are both regular for $\mu < 0$ turning into two virtual equilibria past the border-collision point (leaving the system with no regular equilibrium either in region S_1 or region S_2). As will be shown later, one of the two equilibria has to be unstable.

We will now give conditions to distinguish between these two fundamental cases in the case of n-dimensional locally linearisable continuous nonsmooth flows. Namely, in order for x^+ and x^- to be two regular equilibria of the system, we must have

$$
\begin{aligned}
F_1(x^+, \mu) &= 0, \\
H(x^+, \mu) &:= \lambda^+ > 0
\end{aligned}
\tag{12}
$$

16

and, using (11),

$$
\begin{aligned}
F_2(x^-, \mu) &= F_1(x^-, \mu) + G(x^-, \mu)H(x^-, \mu), \\
H(x^+, \mu) &:= \lambda^- < 0
\end{aligned}
\tag{13}
$$

Now, linearizing about the the boundary equilibrium bifurcation point, $x = 0, \mu = 0$ we have:

$$
\begin{aligned}
Ax^+ + B\mu &= 0 \tag{14} \\
Cx^+ + D\mu &= \lambda^+ \tag{15}
\end{aligned}
$$

and

$$
\begin{aligned}
Ax^- + B\mu + E\lambda^- &= 0 \tag{16} \\
Cx^- + D\mu &= \lambda^- \tag{17}
\end{aligned}
$$

where $A = F_{1x}, B = F_{1\mu}, C = H_x, D = H_\mu$ and $E = G$ all evaluated at $x = 0, \mu = 0$.

Hence, from (14) we have

$$
x^+ = -A^{-1}B\mu
$$

and substituting into (15), we get

$$
\lambda^+ = (D - CA^{-1}B)\mu.
\tag{18}
$$

Similarly using (16) and (17), we have

$$
\lambda^- = \frac{(D - CA^{-1}B)\mu}{(1 + CA^{-1}E)} = \frac{\lambda^+}{(1 + CA^{-1}E)}.
\tag{19}
$$

Therefore we can state the following theorem.

Theorem 2.1 (Equilibrium points branching from a boundary equilibrium)
For the systems of interest, assuming the nondegeneracy conditions

$$
\begin{aligned}
det(A) &\neq 0 \tag{20} \\
D - CA^{-1}B &\neq 0 \tag{21} \\
1 + CA^{-1}E &\neq 0 \tag{22}
\end{aligned}
$$

- *a* persistence *scenario is observed at the boundary equilibrium bifurcation point if*

$$
1 + CA^{-1}E > 0;
\tag{23}
$$

17

- *a* nonsmooth saddle-node *is instead observed if*

$$1 + CA^{-1}E < 0; \tag{24}$$

This can be easily proved by considering that, from (18) and (19), λ^+ and λ^- have the same signs for the same value of μ (persistence) if condition (23) is satisfied, while they have opposite signs (nonsmooth saddle-node) if condition (24) is satisfied instead.

The strategy presented here is valid for n-dimensional systems. Much work is still needed to account for the other scenarios conjectured in [53]. A particularly interesting case is the case where a family of nonsmooth periodic oscillations is involved in the boundary equilibrium bifurcation scenario. Recently, some results have been presented in the literature to account for this type of transitions in planar nonsmooth dynamical systems.

It is worth mentioning here that, currently, there is no general result concerning the occurrence of such transitions in systems of dimension higher than two. After illustrating, a representative planar example, we shall seek to discuss the open problems and challenges lying ahead.

In what follows, we shall seek to illustrate a different scenario that might occur around a boundary equilibrium bifurcation point. Namely, we will discuss the case where a branch of limit cycles is generated or annihilated at the bifurcation point. We consider the case of planar nonsmooth continuous systems of the form (10).

Example 2.2 (A planar case)

Assume that $x^* = 0$ is a boundary equilibrium of (10) when $\mu = 0$. Linearising the system vector fields about the origin, we then get

$$\dot{x} = \begin{cases} A_1 x + B\mu, & \text{if} \quad Cx + D\mu < 0 \\ A_2 x + B\mu & \text{if} \quad Cx + D\mu > 0 \end{cases} \tag{25}$$

where $x^T = (x_1, x_2) \in \mathbb{R}^2$, $A_1 = F_{1x}, A_2 = F_{2x}, B = F_{1\mu} = F_{2\mu}$ and $C = H_x$, $D = H_\mu$. As discussed earlier, continuity of the vector field implies that $A_2 = A_1 + EC$ for some nonzero vector E of appropriate dimension. It is possible to show that under this assumption, a similarity transformation can be found that puts the system in a general canonical form, also termed observable canonical form in Control Theory [19] where the matrices A_1 and A_2 have all their last column equal to the vector $[0\ 1]^T$ and $C = [1\ 0]$.

As mentioned above, this class of planar dynamical system can exhibit numerous nonsmooth bifurcations. Obviously, there are many of the possible

18

scenarios involving the appearance (or disappearance) of one or more families of limit cycles. Rather than attempting a classification of all the possible ones, we focus on the one that is more reminiscent of the Hopf bifurcation in smooth system. Namely, we shall seek to find conditions for a family of stable limit cycles originating from a boundary equilibrium bifurcation.

In the case of planar nonsmooth continuous systems, we propose that such an event can be observed if

1. the boundary equilibrium bifurcation at $\mu = 0$ is associated to a persistence scenario with a regular stable focus becoming unstable as μ is varied in a neighborhood of the origin;

2. when $\mu = 0$ the origin is an asymptotically stable equilibrium of the linearised system of interest.

Note that, in this case, by using a continuity argument, it is easy to show that a stable attractor must exist in a neighborhood of the bifurcation point when the stable focus turns into an unstable one.

Now, condition 1 can be easily satisfied by using Theorem 2.1, i.e. assuming $(1 + CA^{-1}E) > 0$. Moreover, we require the eigenvalues of A_1 and A_2 to be complex with real parts characterised by opposite sign.

To fulfil condition 2 and hence ensure the existence of a limit cycle (the only other generically possible attractor locally for a planar system) for $\mu > 0$, we need to find conditions to ensure that the origin is asymptotically stable when $\mu = 0$. Since the system is in canonical form, we can assume $C = [1 \ 0]$, and the solutions for $\mu = 0$ are

$$\begin{cases} x_1(t) = e^{\alpha_i t}(x_{10}\cos(\omega_i t) + x_{20}\sin(\omega_i t)) \\ x_2(t) = e^{\alpha_i t}(x_{20}\cos(\omega_i t) - x_{10}\sin(\omega_i t)) \end{cases}$$

where $\alpha_i + j\omega_i, i = 1, 2$ are the eigenvalues of A_1 and A_2 respectively.

Now, without loss of generality, let x_{20} be positive and start from initial conditions on the x_2 axis given by $(x_{10} = x_1(0) = 0, x_{20} = x_2(0))$. Then, we have

$$\begin{cases} x_1(t) = e^{\alpha_1 t}x_{20}\sin(\omega_1 t) \\ x_2(t) = e^{\alpha_1 t}x_{20}\cos(\omega_1 t). \end{cases}$$

Then, the orbit will cross again the vertical axis at some time $t = t_1$ such that $x_1(t_1) = 0$, i.e.

$$e^{\alpha_1 t_1}x_{20}\sin(\omega_1 t_1) = 0.$$

19

Thus, we must have $\sin(\omega_1 t_1) = 0$ and therefore we find

$$t_1 = \frac{\pi}{\omega_1}.$$

Moreover, we have

$$x_2(t_1) = e^{\alpha_1 \frac{\pi}{\omega_1}} x_{20} \cos(\pi) = -x_{20} e^{\alpha_1 \frac{\pi}{\omega_1}} < 0.$$

Now, the vector field characterised by A_2 drives the system trajectory, and it can be shown similarly that the next time the orbit hits the vertical axis is $t_2 = \frac{\pi}{\omega_2}$, at which time

$$x_2(t_2) = x_{20} e^{\alpha_1 \frac{\pi}{\omega_1} + \alpha_2 \frac{\pi}{\omega_2}}.$$

Now, the origin will be stable as required if $x_2(t_2) < x_{20}$, thus we get the condition:

$$\frac{\alpha_1}{\omega_1} + \frac{\alpha_2}{\omega_2} < 0.$$

Hence, the origin is stable for $\mu = 0$ and for continuity for further variations of μ, past the bifurcation point an attractor must exist. As the system is planar and no other equilibria can exist, such an attractor must be a stable limit cycle.

Fig. 6 shows the bifurcation diagram of a planar system with

$$A_1 = \begin{pmatrix} -1 & 1 \\ -1 & 0 \end{pmatrix}, \quad A_2 = \begin{pmatrix} 2 & 1 \\ -5 & 0 \end{pmatrix}, \quad B = \begin{pmatrix} 0 \\ 1 \end{pmatrix}. \tag{26}$$

Here a stable focus hits the boundary and becomes unstable. We observe that, when this occurs, a limit cycle is indeed generated at the border collision point and that the amplitude of the limit cycle scales linearly with the parameter (rather than quadratically as in the classical Hopf bifurcation). A further analysis of this scenario can be found in [37].

2.1.3 Some non-generic phenomena

We close this section with a discussion of some other transitions recently studied in the literature which occur in non-generic piecewise smooth continuous systems of the form (10), such as systems, which are invariant under certain symmetries.

In this first case, we review an example from [54], where a branch of stable periodic orbits and an unstable focus existing for $\mu < 0$ collide on
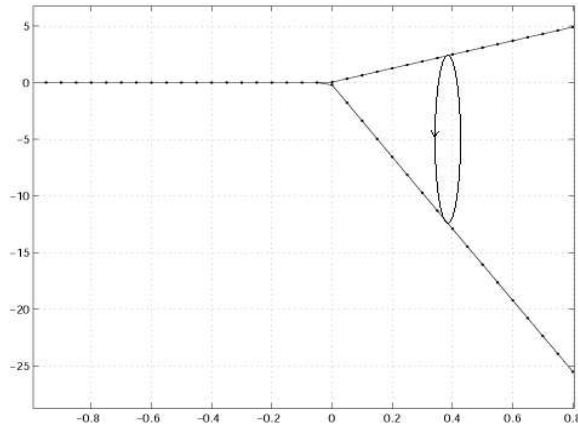
Figure 6: Bifurcation diagram for (25) and (26) showing the occurrence of an Hopf like transition at $\mu = 0$.

the boundary Σ at the bifurcation point. For $\mu > 0$, the unstable focus becomes a saddle, the periodic orbit disappears and two further stable equilibria appear (see Fig. 7). Phase portraits corresponding to representative parameter values ($\mu = -1, 0, 1$) have also been computed and are depicted in Fig. 8. This transition, named *multiple crossing bifurcation* in [53] has no counterpart in smooth systems.

As a second case, we refer again to Example 2.2, the system (25). Depending on the value of the parameters, regular equilibria can collide with Σ giving rise to one of the local transitions discussed above. In addition to this, for some degenerate cases, nonsmooth *global* bifurcations are also possible involving interactions of stable and unstable manifolds with Σ. Indeed, it has been shown that global phenomena like single or double saddle connections (homoclinic or heteroclinic loops) can occur when parameters of the system are varied. To illustrate the occurrence of such global nonsmooth phenomena, we briefly outline below some results presented in [37].

It can be proved for planar systems that the so-called Lum-Chua's conjecture is true; namely, that a continuous piecewise linear vector field with one discontinuity surface Σ has at most one limit cycle. Moreover, it it exists, the limit cycle is either attracting or repelling. Also, under some additional conditions, existence of homoclinic loops can be proved. For example, Fig. 9 shows a bifurcation diagram with bifurcation parameter μ_1, where a continuum of homoclinic loops (shaded region) is born at the bifurcation value. At this point, the global attractor at the origin changes its
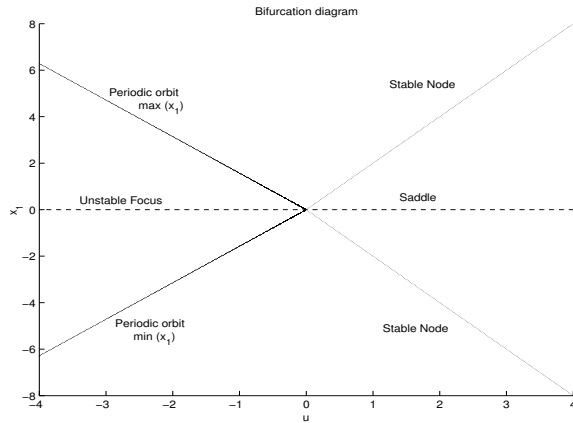
21

Figure 7: Bifurcation diagram for the example in [54] (eqs. (25) and (26)) showing the disappearing of a branch of limit cycles and an unstable focus and the appearing of two branches of stable nodes and a saddle at $\mu = 0$.

stability character. A phase portrait corresponding to $\mu = 1.75$ is shown in Fig. 10, where the homoclinic loops are clearly seen (see [37]).

2.2 Nonsmooth Transitions of Limit Cycles 1; Grazing

We consider two possible NSTs for periodic orbits. Here, the case of grazing with an isolated discontinuity boundary, and in Section 2.3, the case where a periodic orbit passes through a point where two boundaries cross. In the case of grazing, we shall start with some preliminary discussion which introduces the main technique of analysis that we shall use when dealing with bifurcations of limit cycles.

2.2.1 Discontinuity mappings

Suppose that the PWS system (1)

$$\dot{x} = f(x, \mu), \qquad x \in \mathbb{R}^n, \quad \mu \in \mathbb{R}$$

depends smoothly on a parameter μ, and that at $\mu = 0$ there is a T-periodic orbit $x(t) = p(t)$ that grazes with a discontinuity set Σ. That is, there is a point of tangency between the orbit p at Σ, which without loss of generality (with a translation of phase space and time if necessary), we assume to occur at the point $x = 0 = p(0)$. More precisely, the tangent vector to the flow is
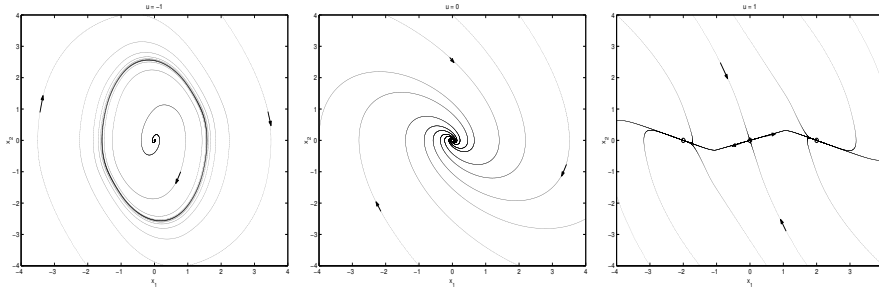
22

Figure 8: Phase portraits for Fig. 7 corresponding to $\mu = -1$, $\mu = 0$, and $\mu = 1$.
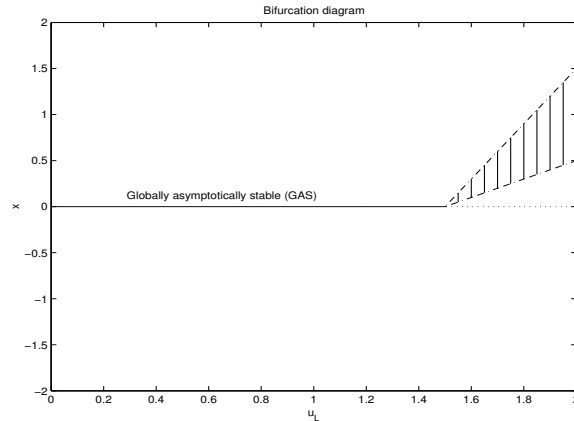

Figure 9: Bifurcation diagram showing the occurrence of a continuum of homoclinic orbits.

assumed to be in the tangent space to Σ at $x = 0$

$$f(0,0) \in T|_{x=0}\Sigma.$$

Moreover we suppose that $p(t)$ is hyperbolic and hence isolated (we shall not consider the Hamiltonian case here) and for simplicity that Σ is the unique discontinuity boundary of the system (see Fig. 11(a)).

As with smooth bifurcations, we also need a non-degeneracy hypothesis, that the paremater μ really does unfold the bifurcation. This can be stated in terms of the periodic orbit of the system obtained by removing the boundary Σ being such that it really does penetrate as μ is varied. This is effectively a nondegeneracy condition with respect to μ of the smooth global Poincaré map around $p(t)$. Figure 11 illustrates one possible fate of such a bifurcation,
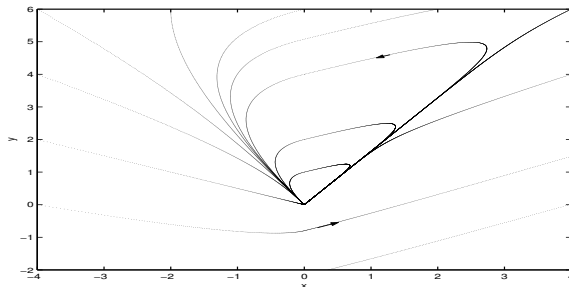
23

Figure 10: Phase portrait for corresponding to a parameter value with a continuum of homoclinic orbits.
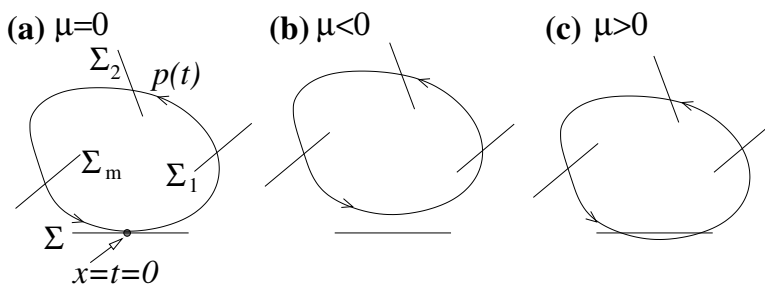

Figure 11: A possible fate of a hyperbolic periodic orbit undergoing a grazing bifurcation with boundary Σ at $\mu = 0$.

that a periodic orbit is generated on the far side of the bifurcation which penetrates Σ, but as we shall see this is only one possibility.

Let us now introduce the key concept of the (local) *discontinuity mapping* (DM) introduced by Nordmark [58, 59, 16]. This map near a grazing point is the correction that must be applied to a trajectory to take account of the passage through region S_2 on the far side of the discontinuity set Σ, when solving trajectories as if the boundary Σ were not there.

This DM is defined for all trajectories in a neighbourhood of the grazing one, and has no reference to grazing trajectories being part of a periodic orbit. Also, assuming some non-degeneracy conditions, it may be assumed that the entire phase portrait in the neighbourhood of the grazing point is qualitatively unchanged under small parameter variation (the grazing bifurcation occurs because of the fate of a certain distinguished trajectory, namely a periodic orbit). Hence we shall drop explicit parameter dependence when presenting the local discontinuity mappings. Notice that, by definition, the discontinuity map will be the identity for non-Σ-crossing trajectories.
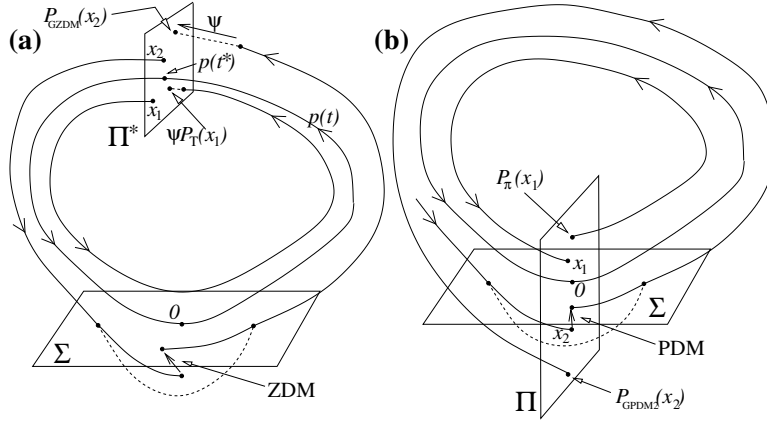
24

Figure 12: Comparison between the construction of global Poincaré maps GPDM and GZDM. For the GZDM (a), the local correction is composed with the non-crossing time-T map P_T, to give a new time-T map that must be composed with a smooth projection ψ in order to obtain the complete Poincaré map at some remote Poincaré section Π^*. For the GPDM (b), the local correction is computed with respect to a Poincaré section Π that contains the grazing point, so that the full Poincaré map may be obtained by composition of this local correction with the non-crossing Poincaré map P_Π.

Two forms of discontinuity map can be distinguished: The *zero-time discontinuity mapping (ZDM)* is defined in a full neighbourhood of the grazing point, and maps trajectories onto ones which have the same value of t. That is, the total time spent by following trajectories which define the ZDM is zero. The *Poincaré-section discontinuity mapping (PDM)* is defined on a suitably chosen Poincaré section Π that is transverse to the flow and contains the grazing point $x = 0$. That is, the PDM takes initial conditions on Π back to themselves. In fact the PDM is just a smooth projection of the ZDM (see, for example, [22]) so that the two maps will be topologically equivalent.

The difference in concept between the ZDM and the PDM comes about when one considers how to embed them into a more global picture containing the dynamics around the periodic orbit, see Fig. 12.

2.2.2 The local geometry near the grazing point

Consider an n-dimensional piecewise-smooth autonomous ODE system (1) that for small x can be written in the form

$$
\dot{x} = \begin{cases} F_1(x), & \text{if } H(x) > 0 \\ F_2(x), & \text{if } H(x) < 0 \end{cases}. \tag{27}
$$

Here $x \in \mathcal{D} \subset \mathbb{R}^n$ and $F_1, F_2 : \mathcal{D} \to \mathbb{R}^n$ and $H : \mathcal{D} \to \mathbb{R}$ are assumed to be smooth. The discontinuity set $\Sigma := \{H = 0\}$ defines a smooth boundary in phase space which for simplicity can be assumed to be linear (see [22] for co-ordinate transformations to which allow one to rectify a nonlinear smooth boundary into a linear one). The boundary Σ separates regions S^+ and S^- in which smooth dynamics governed by F_1 and F_2 apply:

$$
S^+ = \{x \in \mathcal{D} : H(x)) > 0\} \quad S^- = \{x \in \mathcal{D} : H(x)) < 0\}.
$$

We assume that both the vector fields F_1 and F_2 are defined over the entire local region of phase space $\mathcal{D}$ under consideration, i.e., on both sides of Σ.

We say that a *grazing* occurs at $x = 0$, $t = 0$ if the following conditions are satisfied for $i = 1, 2$:

$$
\left. \frac{d[H(x(t))]}{dt} \right|_{t=0} = H^0{}_x F_i^0 = 0, \qquad \left. \frac{d^2[H(x(t))]}{dt^2} \right|_{t=0} = (H^0{}_x F_i^0)_x F_i^0 > 0, \tag{28}
$$

where a superscript '0' denotes quantities evaluated at $x = 0$ (which superscript is dropped in what follows). The first condition states that the vector

field there is tangent to Σ. The second condition ensures that the curvature of the trajectories in the direction normal to Σ is of the same sign in S^+ and S^-. Without loss of generality we assume this sign to be positive so that grazing occurs from the side S^+

We are now in a position to state normal form results for grazing bifurcations, by constructing discontinuity maps within these local co-ordinates.

2.2.3 Normal forms for grazing bifurcations

We do not give the details here of the construction of discontinuity mappings, merely the results, the interest reader is referred to [16, 22, 61] for the details. The key idea is to use Taylor series expansion and the implicit function theorem to construct expressions for the local DMs purely in terms of quantities evaluated at the grazing point itself.

Theorem 2.2 (The ZDM normal form for uniform discontinuity [61])
Given the above assumptions and the assumed form of discontinuity (8) for $m \geq 2$, let $y(x) = H_{\min}(x)$ be the minimum value of $H(x)$ attained along a trajectory of flow ϕ_1, then the ZDM is given by

$$x \mapsto \begin{cases} x & if \quad y \geq 0 \\ x + e(x, \sqrt{-y})(-y)^{m-\frac{1}{2}} & if \quad y \leq 0 \end{cases} \tag{29}$$

where e is a sufficiently smooth function of its arguments within $\mathcal{D}$ whose lowest order term is given by

$$e(0,0) = 2(-1)^{m+1} I(m) J(0) \sqrt{\frac{2}{(H_x F_1)_x F_1(0)}}$$

with

$$I(m) = \int_0^1 (1 - \xi^2)^{m-1} d\xi; \qquad I(2) = \frac{2}{3}, \quad I(3) = \frac{8}{15}, \quad I(4) = \frac{16}{35}, \dots.$$

If we do not assume uniform discontinuity then we have the much more cumbersome expressions given by the following result, which include the case of degree of discontinuity 1, provide we include a condition that avoids sliding taking place.

Theorem 2.3 (The ZDM normal form at a general grazing bifurcation [22])
Given the above assumptions but not (8), the local zero-time discontinuity

27

mapping ZDM describing trajectories in a neighbourhood of the grazing trajectory generically has: (i) a square-root singularity at the grazing point if $F_1^0 \neq F_2^0$, and a non-sliding condition such as (9) holds; (ii) a 3/2-type singularity at the grazing point in the case where $F_1^0 = F_2^0$ while $\frac{\partial F_1^0}{\partial x} \neq \frac{\partial F_2^0}{\partial x}$ or $\frac{\partial^2 F_1^0}{\partial x^2} \neq \frac{\partial^2 F_2^0}{\partial x^2}$.

Specific formulae for these maps are given in the two cases as follows, where a subscript x denotes partial differentiation, and all quantities are evaluated at $x = 0$ (the superscript 0 being omitted).

(i) *If the vector field is discontinuous at grazing we have:*

$$x \mapsto \begin{cases} x & \text{if } H_{\min}(x) > 0 \\ 2\sqrt{\dfrac{-2H_{\min}(x)}{(H_x F_1)_x F_1}}\, v + O(x) & \text{if } H_{\min}(x) < 0, \end{cases} \tag{30}$$

where

$$v = \frac{(H_x F_2)_x F_1}{(H_x F_2)_x F_2}(F_2 - F_1) \tag{31}$$

$$H_{\min}(x) = H_x x + O(x^2). \tag{32}$$

(ii) *If the vector field is continuous, i.e. $F_1 = F_2 := F$, but has discontinuous first or second derivative:*

$$x \mapsto \begin{cases} x & \text{if } H_{\min}(x) > 0 \\ x + 2\sqrt{\dfrac{-2H_{\min}(x)}{(H_x F_1)_x F}}(v_1 + v_2 + v_3) + O(x^2) & \text{if } H_{\min}(x) < 0 \end{cases} \tag{33}$$

where $v_1, v_2, v_3 \in \mathbb{R}^n$ are given by

$$v_1 = -\left\{ -\frac{\left((H_x F_2)_x\left(F_1 - \frac{2}{3}F_2\right)\right)_x F}{(H_x F_2)_x F}(F_2 - F_1)_x F \right.$$
$$\left. + \left(F_{1x}F_2 - \frac{1}{3}F_{1x}F_1 - \frac{2}{3}F_{2x}F_2\right)_x F \right\} \frac{H_x x}{(H_x F_1)_x F} \tag{34}$$

$$v_2 = (F_2 - F_1)_x x \tag{35}$$

$$v_3 = -(F_2 - F_1)_x F \frac{(H_x F_2)_x x}{(H_x F_2)_x F} \tag{36}$$

$$H_{\min}(x) = H_x x + O(x^2). \tag{37}$$

28

	Degree	System at grazing point	Map Discontinuity	
	F	**jump in**	Uniform Case	Non-uniform
0	δ-function	x	square-root (Sec. 4)	
1	bounded	F	-	square-root
2	C^0	F_x	(3/2)-type	(3/2)-type
3	C^1	F_{xx}	(5/2)-type	(3/2)-type

Table 1: Relationship between the singularity of the system at the grazing point and the type of singularity in the corresponding local map.

Remarks

1. Note the pattern implied by the non-uniform discontinuity results, Theorem 2.3. If the vector field has a δ-function discontinuity or a finite jump across Σ, we see a local square root singularity in the discontinuity mapping. If, instead, there is a jump in first or second derivative then the DM has a 3/2-law singularity, see Table 1.

2. In contrast, the uniform discontinuity result, Theorem 2.2, gives the more straightforward property that discontinuity of the nth derivative implies a map with a $O(n + 1/2)$ discontinuity to lowest order. In particular, this asserts that the $O(3/2)$ correction term of (33) which does not vanish if $F_{1x} = F_{2x}$ but $F_{1xx} \neq F_{2xx}$ must rely on the disagreement between the two Hessians does not occur with a factor $H(x)^2$ in the Taylor expansion of $F_1 - F_2$ at $x = 0$. We leave it as a (non-trivial!) exercise to the reader to show how the two formulae (33) and (29) agree in the case of uniform discontinuity.

3. In all cases, the ZDM can be seen to reduce to the identity map at each order when the two vector fields F_1 and F_2 are identical.

4. In the general, non-uniform case, equivalent expressions for the PDM applied at some local Poincaré section that contains the grazing point, are given in [22]. Note that the smooth projection that converts from the PDM does not change the order of discontinuity in the map.

Example 2.1 continued (bilinear oscillator)

Let us return to the bilinear oscillator example (4), (5), (6). with a grazing happening at $t = t^*$. First consider when the damping coefficient ζ_i
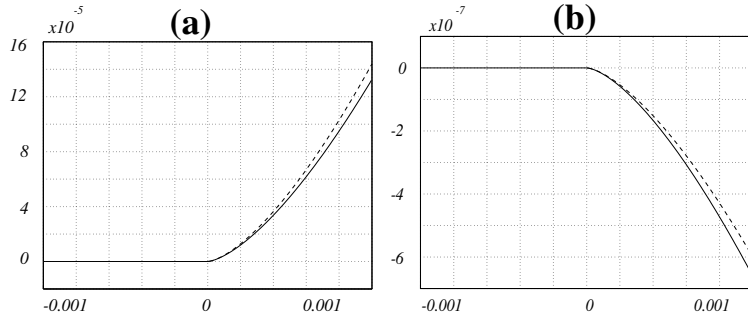
29

Figure 13: Theoretical prediction (dashed line) and numerical computation of the (solid line) of the second component of the local ZDM plotted against $-x_1$ for the bilinear oscillator (3) near grazing. The parameter-values are (a) $k_1 = 1$, $k_2 = 2$, $\zeta_1 = \zeta_2 = 0.1$, $\hat{\beta}_1 = \hat{\beta}_2 = 1$ and (b) $k_1 = k_2 = 1$, $\zeta_1 = 0.1$, $\zeta_2 = 0.2$, $\hat{\beta}_1 = \hat{\beta}_2 = 1$.
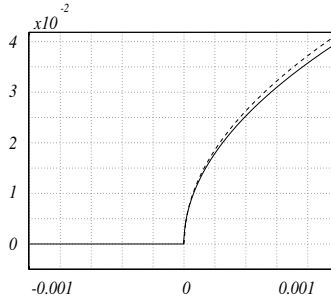

Figure 14: Similar to Fig. 13 but for $k_1 = k_2 = 1, \zeta_1 = \zeta_2 = 0.1, \hat{\beta}_1 = 1, = \hat{\beta}_2 = 2$

or the stiffness coefficient k_i, changes across the switching manifold, while the forcing remain the same. In this case, we set $\hat{\beta}_1 = \hat{\beta}_2 = \hat{\beta}$ in (5) and, using the expressions in Theorem 2.3 one gets for the lowest order approximation to the ZDM for $x_1 < 0$

$$
x \mapsto x + \begin{pmatrix} \frac{2}{3}(\zeta_2 - \zeta_1)\gamma_1^3 \\ \left[\frac{2}{3}\left(\zeta_1^2 - \zeta_1\zeta_2\right) + \frac{1}{3}(k_1^2 - k_2^2) \right]\hat{\beta}\gamma_1^3 + 2(k_1^2 - k_2^2)x_1\gamma_1 \\ 0 \end{pmatrix}, \qquad (38)
$$

where $\gamma_1 = \sqrt{2\frac{|x_1|}{\hat{\beta}}}$, which gives an $|x|^{3/2}$-correction to the leading-order behaviour, which is confirmed numerically (see Fig. 13).

30

Consider next the case where $\beta_1 = \beta_2 := \hat{\beta}$ and, in addition, $\zeta_1 = \zeta_2 = \zeta$. Here we can apply the uniform discontinuity result (29) with $m = 1$. Applying (29), one finds that $H_{\min}(x) = x_{1\min}$ which is equal to x_1 to lowest order. Hence to leading order for $x_1 < 0$ we get

$$x \mapsto x + \frac{2}{3}(k_2^2 - k_1^2)\sqrt{\frac{2}{\hat{\beta}}}\left(0,\ |x_1|^{\frac{3}{2}},\ 0\right)^T .$$

Finally, consider the local dynamics of the bilinear oscillator when the forcing amplitude varies across the switching manifold, i.e. $\hat{\beta}_1 \neq \hat{\beta}_2$ while $k_1 = k_2 = k$, $\zeta_1 = \zeta_2 = \zeta$ in (5). In this case, the bilinear oscillator is characterized by a discontinuous vector field at the grazing point and the formula for the ZDM yields to lowest order for

$$x \mapsto \left(0,\ 2\frac{\hat{\beta}_1}{\hat{\beta}_2}(\hat{\beta}_2 - \hat{\beta}_1),\ \sqrt{2\frac{|x_1|}{\hat{\beta}_1}}.0\right)^T ,\quad \text{for}\quad x_1 < 0. \tag{39}$$

which is a square-root map provided $\hat{\beta}_1 \neq 0$ and $\hat{\beta}_2 \neq 0$, again confirmed numerically in Fig. 14.

Example 2.3 (An explicitly calculable canonical model for grazing)

We now consider an example where we compute the complete Poincaré map. This is an explicitly constructed cannoical model for grazing bifurcations, that takes the form of an autonomous three-dimensional system of ODEs which can be solved in closed form (up to solution of implicit transcendental equations):

$$\begin{aligned} \dot{r} &= \varepsilon_i r(a - r) \\ \dot{\theta} &= \omega_i \\ \dot{z} &= \beta_i z + \gamma_i \end{aligned} \quad ,\quad (i = 1, 2) \quad \text{where}\quad x = r\cos\theta,\ y - 1 = r\sin\theta, \tag{40}$$

where $i = 1$ corresponds to $y > 0$ and $i = 2$ corresponds to $y < 0$. Then the switching manifold is given by

$$\Sigma = \{(x, y, z)|\ y = 0\}, \quad \text{and}\quad H_x = (0, 1, 0),$$

S^+ is the region $y > 0$ and S^- is $y < 0$. A Poincaré section is defined by

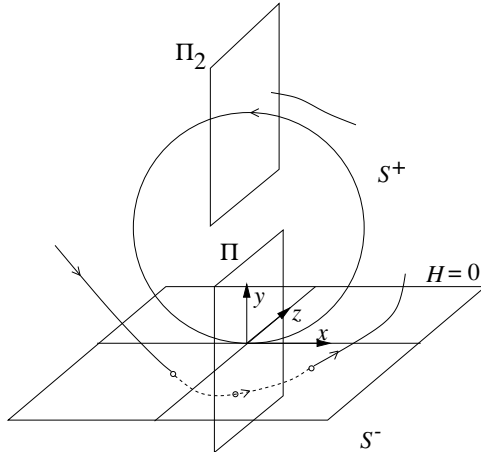$$\Pi = \{(x, y, z)|\ x = 0\},$$

Figure 15: Grazing bifurcation in the explicitly-constructed autonomous system (40)

see Fig. 15.

For simplicity we assume that

$$\omega_1 = 1, \quad \gamma_1 = 0, \quad \varepsilon_1 > 0, \quad \text{and} \quad \beta_1 < 0.$$

Then, for $a = 1$, by construction the system (40) possesses a limit cycle $r = 1$, $\theta = t$ of period 2π which grazes with Σ. Moreover, as $a \to 1^-$ this solution is the limit of a continuous branch of stable 2π-periodic solutions $r = a$ contained within region S^+.

Note that an explicit solution can be found for any point in regions S^+ or S^- with initial conditions (r_0, θ_0, z_0):

$$
\begin{aligned}
r(t) &= \frac{ar_0}{r_0 + (a - r_0)e^{-a\varepsilon_i t}}, \\
\theta(t) &= \theta_0 + \omega_i t, \\
z(t) &= \frac{1}{\beta_i}\left((\gamma_i - \beta_i z_0)e^{\beta_i t} - \gamma_i\right).
\end{aligned}
\tag{41}
$$

Using these solutions, the explicit Poincaré map can be constructed for initial conditions on Π with $y > 0$ (solution entirely in S^+) or $y < 0$ (where solution is required of implicit transcendental equations for transition times between S^+ and S^-). This 'exact' map can be compared with the leading order DM evaluated using the above theory. Consider two separate cases; where the flow is not continuous at the grazing point ($\gamma_2 \neq \gamma_1$ and/or

32

$\omega_1 \neq \omega_2$), and where the flow is continuous ($\gamma_2 = \gamma_1$ and $\omega_1 = \omega_2$). In the first case we obtain the global Poincaré map, defined according to the construction in Fig. 12,

$$P_\Pi \circ P_{PDM} : \quad \begin{bmatrix} y \\ z \end{bmatrix} \mapsto \begin{bmatrix} 0 \\ \frac{2\sqrt{2}\,\gamma_2}{\omega_2} e^{-2\beta_1\pi} \sqrt{|y|} \end{bmatrix} + O(y,z) \quad \text{for} \quad y < 0, \quad (42)$$

where P_Π is the Poincaré map computed around the limit-cycle assuming that region S_- does not exist. Note that it is similarly possible to define the topologically equivalent map $P_{PDM} \circ P_\Pi$. Fig. 16(a) compares both of these two global PDMs with the exact expression in each case plotting the z-component of the map as a function of the y-component of the initial condition. Note how the exact map lies exactly between $P_{PDM} \circ P_\Pi$ and $P_\Pi \circ P_{PDM}$ each of which clearly has a square-root behaviour.

This now raises a subtle point; the constructed maps are only topologically equivalent to the true Poincaré map from $\Pi \to \Pi$, since we have to apply the full DM either at the beginning of the end of the period. To overcome this difficulty, one can work with a new Poincaré section Π_2 that is away from the grazing point. For the present example we could take Π_2 to be the local Poincaré section that is defined by the global extension of Π to a neighbourhood of $(x,y,z) = (0,2,0)$, see Fig. 15. Then the linearisation around the periodic orbit at the grazing point can be composed of two pieces $P_\Pi = P_2 \circ P_1$ where $P_1 : \Pi_2 \to \Pi$, and $P_2 : \Pi \to \Pi_2$. Then we can construct a global PDM from Π_2 to Π_2 via

$$\tilde{P} = P_2 \circ P_{PDM} \circ P_1$$

Thus we obtain

$$\tilde{P} : \quad \begin{bmatrix} y \\ z \end{bmatrix} \mapsto \begin{bmatrix} 0 \\ \frac{2\sqrt{2}\,\gamma_2}{\omega_2} e^{-\beta_1\pi} \sqrt{|e^{-\varepsilon_1\pi}y|} \end{bmatrix} + O(y,z) \quad \text{for} \quad y < 0. \quad (43)$$

Figure 16(b) shows the almost perfect agreement between this map and the equivalent exact expression.

Finally, let us turn to the case where the vector field is continuous at the grazing point ($\gamma_1 = \gamma_2$, $\omega_1 = \omega_2$). Note that if $\beta_1 = \beta_2$, but $\varepsilon_1 \neq \varepsilon_2$ the vector field is not continuous at the whole boundary, but local to the grazing point, the vector field is quadratically equivalent to one that can be written in the form (8) Therefore, to leading order we can use the the simpler formula (29) for calculating the discontinuity mappings.
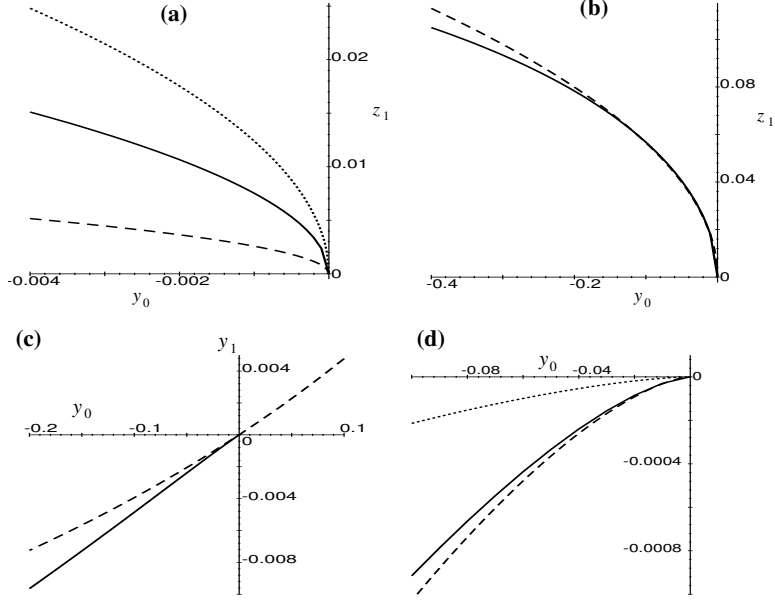
33

Figure 16: Agreement between the 'exact' Poincaré map calculated by solving the implicit equations and the 'calculated' PDM using the theory for the example (40) with $a = 1$, $\beta_1 = \varepsilon_1 = 1/2$, $\gamma_1 = 0$, $\omega_1 = 1$; and (a)–(b) $\beta_2 = \varepsilon_2 = 1/2$, $\gamma_2 = 1$ and $\omega_1 = 3/2$; (c)–(d) $\beta_2 = 1/2$, $\varepsilon_2 = 1/10$, $\gamma_2 = 0$ and $\omega_2 = 1$. In (a), the final value of the z-coordinate is plotted against initial perturbation in $y < 0$ for the exact map (solid line), $P_\Pi \circ P_{\mathrm{PDM}}$ (dashed line) and $P_{\mathrm{PDM}} \circ P_\Pi$ (dotted line). (b) Then compares the exact map with P_{GPDM} defined by (43). (c) Shows, for a case with continuity of the vector field at the grazing, the exact expression for the Poincaré map (solid line) against the unperturbed map as if the boundary were not there (dashed line). Plotted is the final y-value against initial perturbation in y. Finally, (d) shows the difference between these two maps (solid line) together with the curves defined by the nonlinear parts of the $P_{PDM} \circ P_\Pi$ (dotted) and $P_\Pi \circ P_{PDM}$ (dashed)

34

Figure 16(c) shows the exact map for a particular set of parameters showing how the y-component varies as a function of an initial perturbation in y. Figure 16(d) then shows the difference between this map and the map obtained by solving the flow as if the boundary were not there, together with an expression for the nonlinear part of the GPDM calculated as follows. Applying the formula (29) for the ZDM, for simplicity in the case $\gamma_1 = 0$, we find that the correction lies in the Poincaré section Π and so is in fact a PDM:

$$\begin{pmatrix} x \\ y \\ z \end{pmatrix} \mapsto \begin{pmatrix} x \\ y \\ z \end{pmatrix} + \frac{4\sqrt{2}}{3} \frac{(\varepsilon_2 - \varepsilon_1)}{\omega_1} (-y)^{\frac{3}{2}} \begin{pmatrix} 0 \\ 1 \\ 0 \end{pmatrix}.$$

Looking at Fig. 16(d) we see that this gives a good fit to the data from the explicit calculation in this case.

2.2.4 The dynamics of the Poincaré maps

The above analysis derives a complete normal form valid for all grazing bifurcations. This normal form takes the form of a Poincaré map and we have gone to great lengths to explain how they are derived and how the degree of discontinuity of that map relates to assumptions about the discontinuity vector field in the neighbourhood of the gazing points. However, we have so far said almost nothing about the dynamics of the Poincaré maps as a parameter is varied. We shall return to a treatment of maps with a square root singularity in Sec. 4. So let us conclude this section with a few remarks and an applied example that illustrate what can happen in maps with a 3/2-law singularity.

The simplest statement to make is that the 3/2-map is C^1 at the grazing point, so there can be non corresponding local bifurcation of fixed points of the map (assuming as we do that the orbit $p(t)$ is hyperbolic). Thus this NST does not imply bifurcation in the classical sense. However, the slope of the map has square-root singularity, so there can be a rapid (but continuous) change in the Floquet multipliers of the periodic orbit at the grazing point. This can lead to a nearby local bifurcation. The next example illustrates through an application, that such a local bifurcation indirectly caused by the grazing, can occur remarkably close to the grazing point itself.

Example 2.4 (Application: A stick-slip oscillator)

Dankowicz & Nordmark [16] studied the following five-dimensional model of a friction oscillator:

$$\dot{y}_1 = y_2 \tag{44}$$

$$\dot{y}_2 = -1 + \left[1 - \gamma U |1 - y_4| y_2 + \beta U^2 (1 - y_4)^2 \sqrt{K}(y_1)\right] e^{y_1 - d} \tag{45}$$

$$\dot{y}_3 = y_4 \tag{46}$$

$$\dot{y}_4 = -sy_3 + \frac{\sqrt{g\sigma}}{U} e^{-d} \left[\mu(y_5 e^{-y_1} - 1) + \alpha U^2 S(y_1, y_4)\right] \tag{47}$$

$$\dot{y}_5 = \frac{1}{\tau}[(1 - y_4) - |1 - y_4| y_5], \tag{48}$$

where

$$K(y_1) = 1 - \frac{y_1 - d}{\Delta}, \qquad S(y_1, y_4) = (1 - y_4)|1 - y_4| K(y_1) e^{-y_1} - 1 + \frac{d}{\Delta}.$$

This dimensionless model was based on the derivation in [15] aimed at explaining experimentally observed stick-slip motion using more realistic laws than simple coulomb friction. Here the variable y_1 is a vertical, and y_3 a horizontal degree of freedom of a mass being pulled across a horizontal surface by a spring whose other end moves at constant speed U. The extra co-ordinate $y_5 \in [-1, 1]$ is an internal variable measuring the shear deformation between the surface and the mass. The main discontinuity to feature in the dynamics is the set $\Sigma = \{y_4 = 1\}$ and this corresponds to motion with zero relative velocity between the mass and the surface. Motion with $y_4 < 1$ corresponds to the mass being dragged across the surface.

Figure 17 shows a bifurcation diagram where the the bifurcation parameter is s, a rescaling of the spring stiffness (the ordinate k depicted in the plot) for the fixed value of the equilibrium surface separation $d = 0.1$. For the values of the other parameters used, the interested reader is referred to [16]. Note that for $k = 214.2528$, an unstable limit cycle grazes with Σ. This causes the onset, upon decreasing k of so-called *stick-slip* motion that makes repeated tiny penetrations into the region with $y_4 > 1$. This motion can be quite involved and features chaotic dynamics and *period adding bifurcations* (as one would expect in the case of normal-form maps with a square-root dependency [58, 12]).

The onset of this rich dynamics observed upon decreasing k through the grazing value can be explained by the theory treated here. Specificaly, an involved computation in [16] computes the normal form (33) in Theorem 2.3 (actually this was the first ever such computation in the case of discontinuity of degree 2). We omit the details here, but merely reproduce in Fig. 18 the
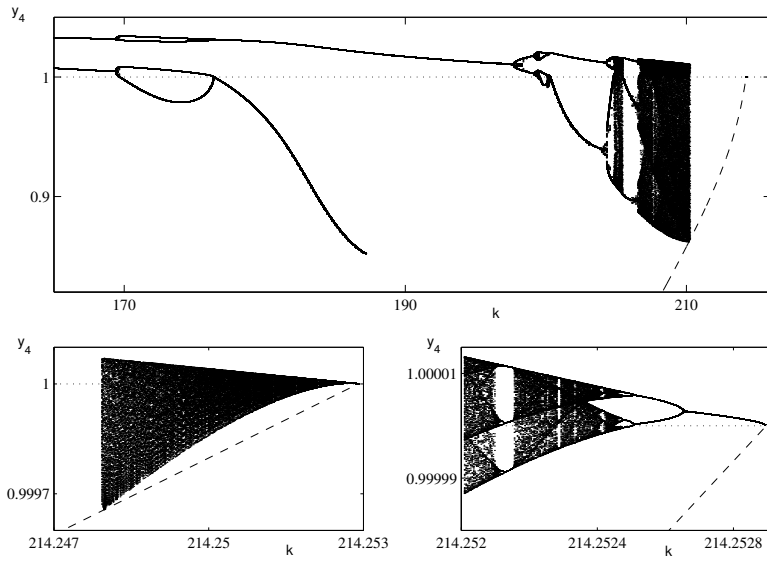
Figure 17: Successive enlargements of a computed bifurcation diagram for $d = 0.1$, depicting local maxima of y_4. The dotted line corresponds to the discontinuity set Σ and the dahsed line to a branch of unstable limit cycles born in a sub-crtical Hopf bifurcation
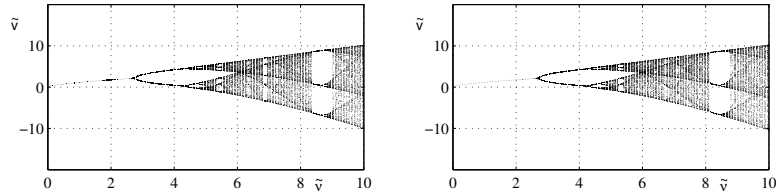
Figure 18: Comparison between the numerical simulations (left panel) and the discontinuity mapping (right panel) local to the grazing bifurcation at $k = 214.2528$. Here $\tilde{v}$ is a rescaling of y_4 and $\tilde{\nu}$ is a rescaling of $-k$ (cf. Fig. 17(c))

results of the iteration of the corresponding map composed with the flow map over a whole period. Note, over this small scale the close agreement between the mapping and the simulations

Further computations in [16] show that a qualitatively similar bifurcation diagram is obtained for $d = 0.01$, but that here the grazing and the fold are $O(1)$ apart.

Now, this example serves to illustrate a key point about grazing bifurcations where the degree of discontinuity is 2 or more. A local analysis of the normal form shows that it is continuous at the grazing point and has a 3/2-type discontinuity. At the grazing point, there should not be a change in the tangent to the branch of fixed points. One might think that this would rule out any complex dynamics emerging from such transitions. Yet, in the dynamics depicted in Fig. 18 while there is no discontinuous jump in the slope, it is found that there is a fold at a $\tilde{\nu}$-value within 10^{-3} of the grazing point. Returning to the physical co-ordinates, this implies a fold for k within 10^{-7} of the grazing point (see Fig. 17)! So even if no instantaneous transition occurs, grazing in piecewise-continuous systems can cause a rapid change in the curvature of a bifurcation branch giving rise to many nearby classical bifurcations. Moreover, when viewed in the large, the dynamics of the normal form may help explain some more global features of the dynamics such as period-adding cascades.

2.3 Nonsmooth Transitions of Limit Cycles 2; Boundary Intersection Crossing

Consider now a situation where two discontinuity boundaries Σ_1 and Σ_2 cross transversally, see Fig. 19(a). It is clear that it would be of codimension one for a periodic orbit to pass through the $(n-2)$-dimensional intersection C
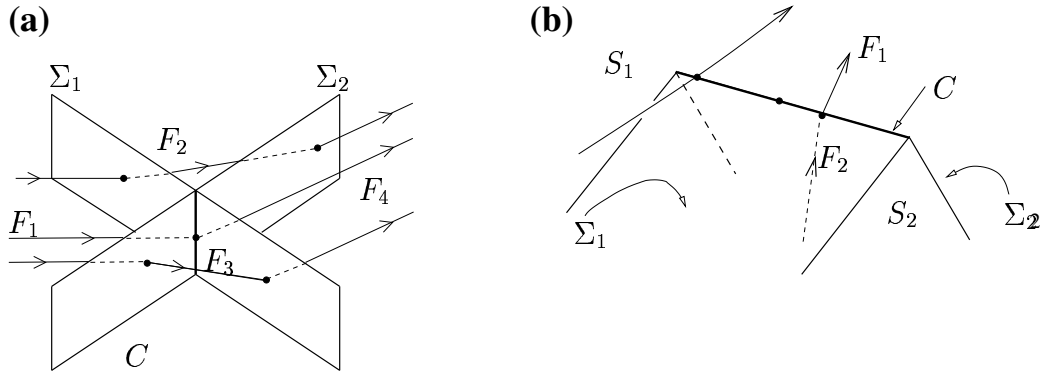
Figure 19: (a) A boundary-intersection crossing trajectory that intersects the crossing manifold C between two discontinuity surfaces Σ_1 and Σ_2, and two nearby trajectories. Here it is assumed that a different smooth vector field F_i applies in each of the four local phase space regions. (b) Shows the special case where only two different vector fields, F_1 and F_2 apply, and the crossing manifold might better be described as the corner in a single discontinuity surface made up of two smooth pieces Σ_1 and Σ_2. Two distinct kinds of corner-intersecting trajectories are depicted, so-called *external* and *internal* corner collisions [21]
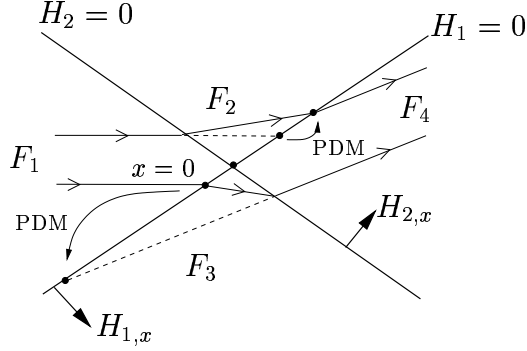
Figure 20: A planar representation of the construction of the local PDM in a neighbourhood of a boundary-crossing intersecting trajectory. Here it is assume that the Poincaré section is $\Sigma_1 : \{H_2 = 0\}$

between these two boundaries. It is this situation that we call a *boundary-intersection crossing*. The special case in Fig. 19(b) has previously been called a *corner-collision bifurcation* [21] We shall consider only the case where the vector field is discontinuous across each of Σ_1 and Σ_2 and shall show that to lowest order this leads to a piecewise linear normal form GPDM. The case where the vector field is continuous can be similarly shown to lead to a discontinuity mapping with a jump at quadratic order.

Consider first the general case depicted in Fig. 19(a) and set up some local co-ordinates such that the point of intersection of the periodic orbit with $C = \Sigma_1 \cap \Sigma_2$ occurs at $x = 0$. Let the boundaries Σ_1 and Σ_2 be given by the zero sets of smooth functions $H_1(x)$ and $H_2(x)$ respectively, which, as in the previous section, we take for simplicity to be linear; $\Sigma_1 = \{H_1 = 0\}$ and $\Sigma_2 = \{H_2 = 0\}$ and the sense of their normal vectors is as depicted in Fig. 20.

Now, it will transpire that the linear approximation to the flow and to the boundaries is sufficient to determine the leading-order expression for the discontinuity mapping in a neighbourhood of $(x, \mu) = (0, 0)$. Thus $F_i(x, \mu)$ is replaced by $F_i(0, \mu)$ and we suppose for simplicity that the local situation near $x = 0$ is unchanged by the variation of μ, so $F_i(x, \mu) \approx F_i(0, 0) := F_i$. Also let a final subscript indicate a component in the normal direction $H_{j,x}$, so that $F_{ij} = H_{j,x}F_i(0)$ and $x_j = H_{j,x}x$, for $j = 1, 2$.

We make the further assumption that there is no sliding or grazing in the neighbourhood of $x = 0$, so that all four vector fields cross both Σ_1 and

Σ_2 transversely and in the same sense. That is,

$$F_{ij} > 0 \quad \text{for} \quad i = 1, \ldots, 4, \quad j = 1, 2. \tag{49}$$

For simplicity, it is easier to work with a Poincaré section that lies in one of the boundaries. Without loss of generality we take the section $\Pi := \{H_1 = 0\}$ as in Fig. 20. Then, constructing the local PDM as in the Figure, we arrive after some algebra at the following

Theorem 2.4 (Local PDM at boundary crossing point intersection)
Under the above assumptions, the local PDM based on the Poincaré section Σ_2 is given by

$$x \mapsto \begin{cases} x + \frac{x_2}{F_{12}} \left(F_2 \frac{F_{11}}{F_{21}} - F_1 \right) + O(|x|^2) & \text{if} \quad x_2 > 0 \\ x + \frac{x_2}{F_{32}} \left(F_4 \frac{F_{31}}{F_{41}} - F_3 \right) + O(|x|^2) & \text{if} \quad x_2 < 0, \end{cases} \tag{50}$$

Here the correction is made to a trajectory for which it is assumed evolves according to vector field F_1 before hitting Σ_1 and vector field F_4 afterwards.

Remarks

1. To lowest order (50) is a piecewise-linear map, such that the each of the maps for $x_2 > 0$ and $x_2 < 0$ is a rank-one update of the identity. This is precisely the form of map studied by Feigin (see [24] and references therein) and in one and two-dimensions by the Maryland group [62, 2], where they were given the name *border collision* bifurcations (of maps). The reader is referred to these works for a detailed description of the dynamics that may ensue under parameter variation. Among other possibilities it is possible for a sharp fold-like transition to occur, a non-smooth period-doubling or a sudden jump to chaotic motion. The chaotic motion has the character of being *robust* [5], that is containing no periodic windows.

2. Obviously in the case of a corner where $F_1 = F_3 = F_4$ (external corner collision) or $F_2 = F_3 = F_4$ (internal corner collision) then the local PDM reduces to the identity for $x_2 < 0$ (see [21] which also derives ZDMs in this case).

Now suppose that the trajectory $p(t)$ that passes through the boundary crossing point at $x = 0$, $\mu = 0$ is part of a periodic orbit. Then, the above discontinuity mapping can be composed with the linear to lowest-order order Poincaré map P_Π around the critical boundary-crossing intersecting periodic orbit. The following examples illustrate the construction of the ensuing piecewise linear maps. Both correspond to the special case in Fig. 19(b).
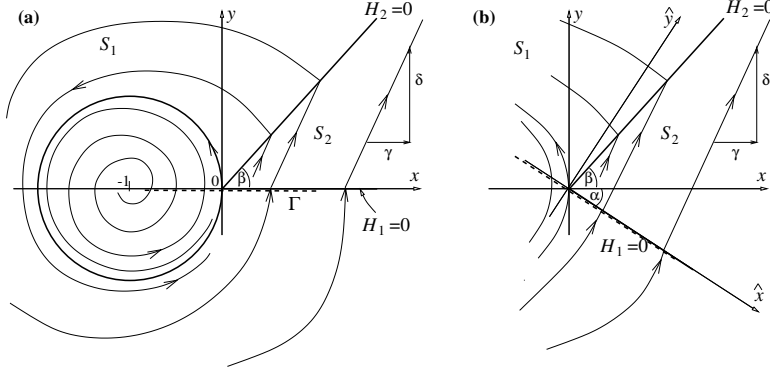
41

Figure 21: (a) Sketch of the phase portrait of (51), (52) with $a = 1$. (b) An adaptation of the system.

Example 2.5 (An explictly calculable canonical model for corner-collision)

We consider first an example where a hyperbolic limit cycle grazes with a corner in an autonomous, piecewise-smooth vector field that is solvable in closed from. Specifically we take a system

$$\begin{aligned} \dot{x} &= \gamma \\ \dot{y} &= \delta \end{aligned} \quad , \quad \text{for } x > 0, \ y > 0, \ y < x \tan \beta \quad (\text{REGION } S_2), \quad (51)$$

$$\begin{aligned} \dot{r} &= \varepsilon r(a - r) \\ \dot{\theta} &= 1 \end{aligned} \quad , \quad \text{otherwise } (\text{REGION } S_1). \quad (52)$$

Here

$$x + 1 = r \cos \theta, \quad y = r \sin \theta,$$

and γ, δ, β, ε and a are real constants satisfying the constraints

$$0 < \beta < \pi/2, \quad \delta > \gamma \tan \beta. \quad (53)$$

See Fig. 21(a). Consider the system (52). For $a > 0$ there is a limit cycle which is stable if $\varepsilon > 0$. At $a = 1$ this limit cycle collides with the boundary of region S_2 in an external corner collision bifurcation. Under this construction we have

$$H_{2,x} = y \cos \beta(-x \sin \beta, \cos \beta)$$

The constraints (53) ensure that no sliding occurs along $\Sigma_{1,2}$
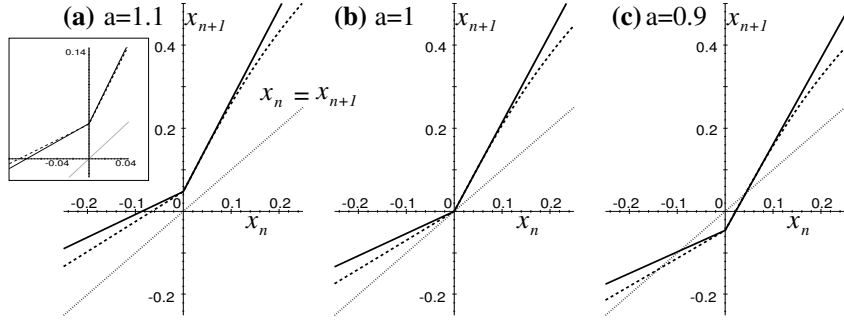
42

Figure 22: Comparison between the PDM given by (56) (solid line) with the map obtained from the exact analytical solution of (51), (52) (dotted line). (Note that there is agreement between the slopes of the two maps on either side of $x_n = 0$. For $x_n < 0$, this agreement is not so obvious but it has been confirmed for *each* of the three a-values by plotting the graphs on a shorter x_n-interval. Just such a zoom for $a = 1.1$ is depicted as an inset to (a).) Intersection of the map with the gray line represents the existence of a fixed point. Numerical values used are $\varepsilon = 1/10$, $\beta = \pi/4$, $\gamma = 3/8$, $\delta = 1/2$ and the three given values of a.

Since the systems in regions S_1 and S_2 are solvable in closed form one can explicitly construct the Poincaré map $x \mapsto \Pi x$ associated with the Poincaré section $\{y = 0, x > -1\}$. After a short calculation, we obtain an explicit expression for this map when $x > 0$,

$$x \mapsto \frac{a\hat{r}\exp[\varepsilon a(2\pi - \hat{\theta})]}{\hat{r}\exp[\varepsilon a(2\pi - \hat{\theta})] + a - \hat{r}} \tag{54}$$

where
$$\hat{t} = \frac{x\tan\beta}{\delta - \gamma\tan\beta}, \quad \hat{r}\cos\hat{\theta} = x + \gamma\hat{t} + 1, \quad \hat{r}\sin\hat{\theta} = \delta\hat{t}. \tag{55}$$

This exact map may be compared to the global PDM calculated using the above theory, for which one easily obtains

$$x \mapsto \begin{cases} \exp(-2\varepsilon\pi)x + (1 - \exp(-2\varepsilon\pi))(a - 1) & \text{if } x < 0 \\ \delta\frac{\exp(-2\varepsilon\pi)}{\delta - \gamma\tan\beta}x + (1 - \exp(-2\varepsilon\pi))(a - 1) & \text{if } x > 0 \end{cases}. \tag{56}$$

Fig. 22 gives the comparison between the PDM and the exact map. Note both the qualitative and quantitative agreement between the two. Note also

43

that for the illustrated numerical values of the various constants, the corner-collision has the effect of destroying the limit cycle. Before the bifurcation, i.e. for $a < 1$, there is the stable limit cycle lying solely in region S_1, but this coexists with an unstable limit cycle which passes through region S_2. At $a = 1$ these two periodic solutions coalesce and for $a > 1$ they have disappeared. Note finally that unlike a saddle-node bifurcation for a smooth system, the Floquet multipliers of the two periodic orbits (the slopes of the two portions of the map) do not approach 1 as $a \to 1^-$.

Example 2.6 (Application: corner-collision in the DC-DC buck converter)

We now study a certain piecewise-linear circuit used widely in power electronics for adjusting a given DC voltage to a lower value. The DC-DC Buck
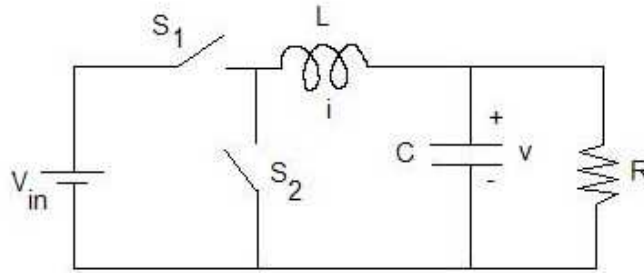

Figure 23: Blocks diagram of the Buck Converter, where $V_{in} = E$.

converter under ramp voltage-mode control is used as an example exhibiting nonsmooth bifurcations. Figure 23 shows the block diagram of the buck converter. A control signal V_r, where

$$V_r(t) = \gamma + \eta(t \bmod T), \qquad \gamma,\ \eta,\ T > 0, \tag{57}$$

is compared with the voltage $V(t)$ in the capacitor. If $V > V_r$ then the switch S_1 opens and the switch S_2 conducts, while if $V < V_r$ then the switch S_1 is closed, S_2 does not conduct, and the battery feeds the load.

Here we shall take the following form of the equations modelling such a circuit used in which are written in terms of a current $I(t)$ and voltage $V(t)$ [18, 20]

$$\dot{V} = -\frac{1}{RC}V + \frac{I}{C}, \tag{58}$$

$$\dot{I} = -\frac{V}{L} + \begin{cases} 0 & V \geq V_r(t) \\ E/L & V < V_r(t). \end{cases} \tag{59}$$

44

C, E, L, and R are positive constants representing a capacitance, battery voltage, inductance and resistance respectively and V_r is a piecewise-linear but discontinuous 'ramp' signal (see 57). For this system we have $\Sigma :=$ $\{V = V_r(t)\}$ which has corners whenever $t = 0$ mod T.

For the details of the electrical circuit represented by the model (58),(59) and for some of the rich features of its dynamics, see [35, 25, 20]. These features include periodic orbits and strange attractors that are characterised by trajectories that are close to both corner-collision (at $t = 0$ mod T) and sliding (with $V(t) = V_r(t)$ for $(m - 1)T < t < mT$ for some m). The parameter values taken were those used in the experiments of [18], which in SI units are

$$R = 22\Omega, \; C = 4.7\mu F, \; L = 20mH, \; T = 400\mu s,$$
$$\gamma = 11.75238V, \; \eta = 1309.524Vs^{-1}, \tag{60}$$

with the bifurcation parameter $E \in (15, 60)$ being the input voltage.

In [21] an analytical explanation was offered for the phenomenon that was merely observed numerically in [20] namely that corner-collision of a periodic orbit causes a fold (actually a sharp corner) in the bifurcation diagram of a branch of periodic orbits. Specifically a sequence of such folds was found for certain 3T and 5T-periodic orbits, as part of a bigger picture of a spiralling bifurcation diagram; see also [35, 25]. See the work of Yuan *et al.* [82] for corner-collision in a related buck-converter configuration.

Figure 24 shows numerically computed 5T-periodic orbits that, in their fourth depicted T-interval, undergo a collision with the upper corner of the function $V_r(t)$ at

$$t = t_0 = 0 \bmod T, \quad V = \gamma + \eta T$$

Moreover, we will consider the possibility of both internal and external corner collision.

As a first step, define local co-ordinates

$$x = V - (\gamma + \eta T), \quad y = I - I_0, \quad z = t - t_0 \tag{61}$$

and rewrite the equation (58),(59) in autonomous form, to give the system

$$\begin{aligned}
\dot{x} &= -a_1 + b_1 x - c_1 y, \\
\dot{y} &= -a_2 \qquad - c_2 y + d\Theta(\sigma(z) - x), \\
\dot{z} &= 1,
\end{aligned}$$

in which

$$a_1 = \frac{\gamma + \eta T - RI_0}{RC}, \; b_1 = \frac{1}{C}, \; c_1 = \frac{1}{RC}, a_2 = \frac{\gamma + \eta T}{L}, \; c_2 = \frac{1}{L}, \; d = \frac{E}{L},$$
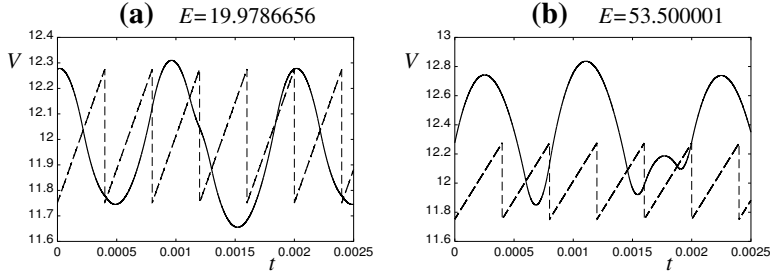
45

(a) E=19.9786656   **(b)** E=53.500001

Figure 24: Periodic orbits of the DC/DC buck converter with period $5T$ undergoing (a) an external and (b) an internal corner collision.

Θ is the Heaviside step function and

$$\sigma(z) = \eta[(z \bmod T) - T].$$

For this system we have

$$\Sigma_1 := \{H_1 = 0\} = \{x = \sigma(t)\}, \quad \Sigma_2 := \{H_2 = 0\} = \{z = 0\},$$

$$\mathcal{C} = \{x = 0, z = 0\}.$$

The corner-collision happens at $x = y = z = 0$, and it can be checked that the conditions of the preceding theory are met there with

$$F_1^0 = (-a_1, -a_2, 1), \quad F_2^0 = (-a_1, -a_2 + d, 1)$$

(observe that F is discontinuous only in the x-direction, and so the jump in derivate of solutions is not seen in graphs of y against t as in Fig. 24).

Using (50), specifically for an *external grazing* the local discontinuity mapping for corner-crossing trajectories using the $\{z = 0\}$ Poincaré section takes the form

$$P_{\text{ZDM}} : \begin{pmatrix} x \\ y \end{pmatrix} \mapsto \begin{pmatrix} x \\ y + k_1(E)x \end{pmatrix} + \text{h.o.t.} \tag{62}$$

where

$$k_1(E) = -d\eta a_1 + \eta = -\frac{E\,RC}{L(\gamma + \eta T - RI_0 + \eta RC)} \tag{63}$$

To compute the full Poincaré map, we must compose the map P_{ZDM} with a global one which is simply found by taking the Jacobian derivative of the flow around the periodic orbit at $E = E_0$ ignoring the effects of the corner.
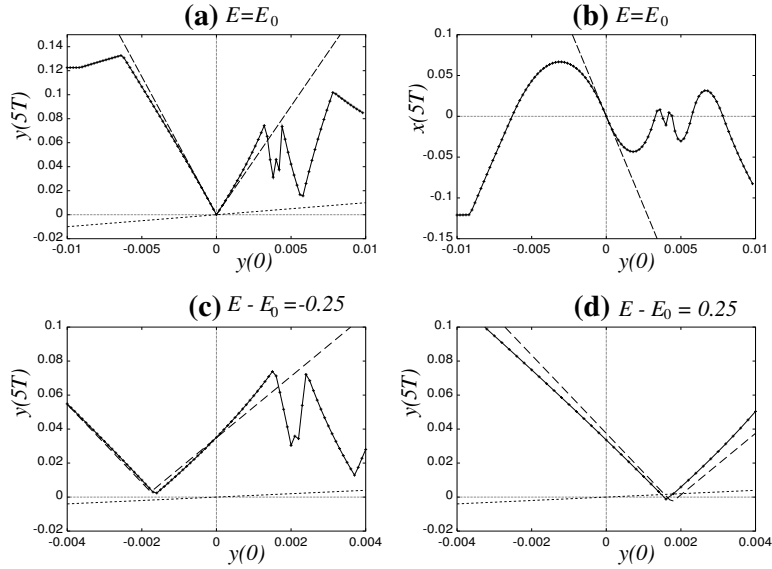
46

Figure 25: The Poincaré map for a $5T$-periodic external corner-colliding orbit at $E_0 = 19.9786656$, computed numerically (solid line with crosses) and via the corner-collision analysis (dashed line). A one-dimensional slice of the map is taken considering the effect of varying only the initial current $y(0)$. (a) and (b) depict the final current and voltage respectively for $E = E_0$; (c) and (d) show the effect on the final current of variation of the bifurcation parameter E. In the final current versus initial current figures, the 45° line is depicted as dotted; viewing the graphs as approximations of 1D maps, intersections with this line are indicative of nearby fixed points of the 2D map.

47

The results for the $5T$-periodic orbit at $E = E_0 = 19.9786656$ are depicted in Fig. 24, for which it was found from examining the numerically computed trajectory that $k_1(E_0) = -0.934$. The map (62) can be compared with a purely numerical evaluation of trajectories in a neighbourhood of the corner-coliding one. We illustrate in Fig. 25 just a one-dimensional approximation to this two-dimensional map, by only displaying the effect of changes in initial current y. This is purely for illustrative convenience (similar results were found with other combinations of $x(0)$ and $y(0)$ varying as initial conditions), but we note from the numerical Jacobian that that initial variations of current y have a much bigger effect (by a factor of about 10) than variations of voltage x.

The results in Fig. 25 (a) and (b) show good quantitative and qualitative agreement between the local theory and the numerics at $E = E_0$. They also illustrate the extent of the region of validity for the local analysis; for $-0.006 < y(0) < -0.0035$ at $E = E_0$, the local map is qualitatively correct, but outside of this region the numerical map shows extra corners. This is due to other corner-collisions taking place at $t = nT$ for some $n \leq 5$. Note from panel (b) in particular that there is no corner in the x-component of the numerically computed map — this component of the map is smooth — which is in complete agreement with the analytical result (62) (there is no change in the x-component in the discontinuity mapping).

Panels (c) and (d) show the effect of variation of E, with the existence of a fixed point on such a graph of $y(5T)$ against $y(0)$ being indicative only of a fixed point of the full 2D map. Here again there is good agreement between theory and numerics on how the map is perturbed as E varies and that two fixed points (corresponding to unstable periodic orbits of the ODEs) are created at $E = E_0$ and coexist for $E > E_0$. See [21] for more details.

3 Filippov PWS system

We consider general system (1) with a single well-defined switching manifold Σ. As mentioned in the introduction, a particular feature of Filippov type systems is the possibility of evolution of the system within its discontinuity set Σ. A subset of Σ where such an evolution is possible is termed as *sliding region* or *sliding subset*. Therefore, the sliding subset represents a region $\hat{\Sigma}$ within the switching manifold Σ where trajectories hitting the manifold are not allowed to switch to another vector field as they are pushed back toward the manifold itself. Thus, there exists a possibility of a motion within Σ which is termed *sliding motion*. An example of a 3-dimensional phase space
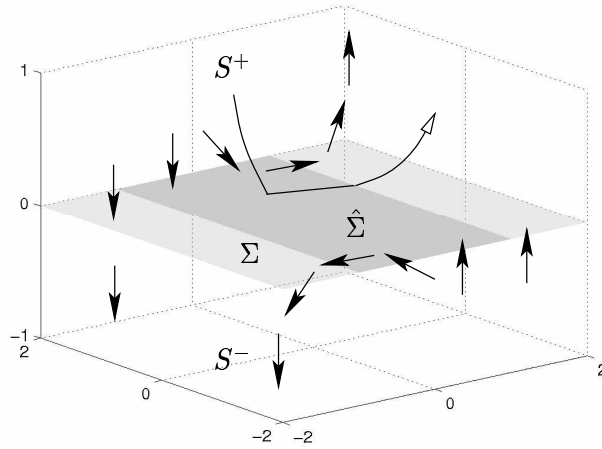
Figure 26: Phase space topology of a system with discontinuous vector fields

with a sliding region, say $\hat{\Sigma}$ is schematically depicted in Fig. 26. Two formalisms exist in the literature for deriving the equations for flows governing the dynamics within the sliding region. These are *Utkin's equivalent control method* [77] and *Filippov's convex method* [34]. In Utkin's method one supposes that the system flows according to the sliding vector field F_s which is the average of the two vector fields F_1 (in region S_+) and F_2 (in region S_-) plus a control $\beta(x) \in [-1, 1]$ in the direction of the difference between the vector fields:

$$F_s = \frac{F_1 + F_2}{2} + \frac{F_2 - F_1}{2}\beta(x). \tag{64}$$

Specifically, the equivalent control is

$$\beta(x) = -\frac{H_x F_1 + H_x F_2}{H_x F_2 - H_x F_1}, \tag{65}$$

where H_x is the gradient vector of $H(x)$. Filippov's method, by contrast, takes a simple convex combination of the two vector fields

$$F_s = (1 - \alpha)F_1 + \alpha F_2$$

with $0 \le \alpha \le 1$, where

$$\alpha = \frac{H_x F_1}{H_x(F_1 - F_2)}.$$

Now it is a simple exercise to show that the above two methods are algebraically equivalent with $\mu = 2\alpha - 1$. In both cases it is straightforward to show that the vector field F_s lies orthogonal to the direction H_x and so lies tangent to Σ. Utkin's method has the interpretation that μ is precisely the

49

control power that is needed to pull the flow back to being in the direction Σ, see Fig. 27(a). Another interpretation, from Filippov's method, is that just the right convex combination of the vector fields needs to be taken for the resulting field F_s to lie in Σ (Fig. 27(b)).

The control $\beta = -1$ (equivalently $\alpha = 0$) means that the flow is governed by F_1 alone, which must by definition be tangent to Σ there. Similarly $\beta = 1$ ($\alpha = 1$) represents a tangency of flow F_2 with Σ. Hence, we can define the sliding region as

$$\hat{\Sigma} := \{x \in \Sigma : -1 \leq \beta(x) \leq 1\},$$

and the boundaries of the sliding region as

$$\partial \hat{\Sigma}^{\pm} := \{x \in \Sigma : \beta(x) = \pm 1\}$$

where one of the vector fields is tangent to Σ.

In Section 3.1, we will discuss the most significant types of nonsmooth transitions of equilibria using a planar Filippov system as a representative example. Nonsmooth transitions of equilibria in this class of systems have been little studied in the literature. An overview of local phenomena in planar Filippov systems was presented in [51]. A non-generic class of Filippov systems was studied in [49]. It was shown that a class of transitions, termed in [49] *generalized Hopf bifurcations*, can be observed in such systems when a family of limit cycles is generated, under parameter variations, as a focus located on the switching surface is perturbed. The transition to sliding cycles (a cycle with a segment of sliding motion) in a class of different Filippov planar systems is studied in [40]. Also, global phenomena can occur with heteroclinoc connections to equilibrium points [51]. An interesting set of examples in applications is given by certain models of DC-DC converters. We will study in some detail a model of a buck converter, an adaption of Example 2.6 above [65]. In [14] a different circuit topology, the Boost converter, is also studied.

In Section 3.2 we focus our attention on *sliding bifurcations* of limit cycles. We depict four possible cases of this type of NSTs which are a distinct feature of *Filippov*-type systems. Then, their heuristic description is followed by the presentation of the normal forms capturing the essence of sliding bifurcations. Finally, an example where one of these bifurcations leads to the sudden onset of chaos is discussed.
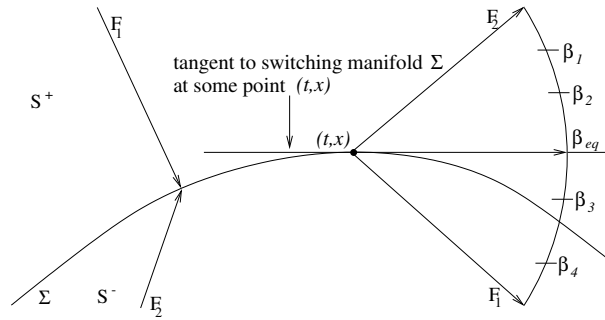
(a) Utkin's method
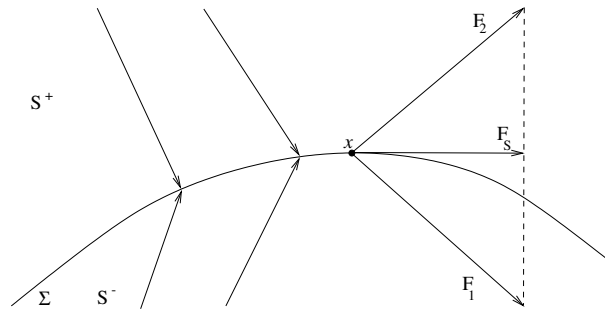
(b) Filippov's method

Figure 27: (a) Utkin's equivalent control method and (b) Filippov's convex method allowing for the definition of the vector field governing the sliding flow – schematic representations

3.1 Equilibrium bifurcations

We consider Filippov systems of the form:

$$\dot{x} = \begin{cases} F_1(x,\mu), & \text{if } H(x,\mu) > 0 \\ F_2(x,\mu), & \text{if } H(x,\mu) < 0 \end{cases}, \tag{66}$$

where $F1 \neq F2$ on $H = 0$. It is possible to identify different types of equilibria in a Filippov system. We give the following definitions.

Definition 3.1 *We say that a point $x \in D$ is a* regular equilibrium *of (66) if*

$$\begin{align} F_1(x,\mu) &= 0 \tag{67} \\ H(x,\mu) := \lambda_1 &> 0 \end{align}$$

or

$$\begin{align} F_2(x,\mu) &= 0 \\ H(x,\mu) := \lambda_2 &< 0 \end{align}$$

Definition 3.2 *We say that a point $\tilde{x}$ is a* pseudo-equilibrium *if it is an equilibrium of the sliding flow, i.e.*

$$\begin{align} F_1(\tilde{x},\mu) + \tilde{\lambda}(F_2 - F_1) &= 0, \\ H(\tilde{x},\mu) &= 0, \tag{68} \\ \tilde{\lambda} &> 0. \end{align}$$

Definition 3.3 *A point $\hat{x}$ is termed a* boundary equilibrium *of (66) if*

$$\begin{align} F_1(\hat{x},\mu) &= 0, \\ H(\hat{x},\mu) &= 0. \end{align}$$

or

$$\begin{align} F_2(\hat{x},\mu) &= 0, \\ H(\hat{x},\mu) &= 0. \end{align}$$

Note that a boundary equilibrium is always located on the boundary of the sliding region defined by where the H_x component of the vector fields is vanishes.

As shown in Sec. 2.1 for nonsmooth continuous systems, in Filippov systems, a boundary equilibrium can appear for some value of the system parameters μ. We shall seek to unfold the bifurcation scenarios that can occur when μ is perturbed away from the origin, i.e. the possible branches of solutions originating from a boundary equilibrium. Specifically we give the following definition.

Definition 3.4 *A regular or pseudo- equilibrium* $x^* = x^*(\mu)$, *which we assume depends smoothly on* μ, *is said to undergo a* boundary equilibrium *transition at* $\mu = \mu^*$ *if*

- $F_i(x^*, \mu^*) = 0, \quad i = 1 \ or \ 2,$

- $H(x^*, \mu^*) = 0,$

- $F_{ix}(x^*, \mu^*)$ *is invertible (or equivalently* $det(F_{ix}) \neq 0$).

3.1.1 Overview of the possible cases

Without loss of generality, we assume that $F_1(0,0) = 0, H(0,0) = 0$, i.e. $x = 0$ is a boundary equilibrium when $\mu = 0$. We shall now seek to find conditions to distinguish between the simplest possible unfoldings of a boundary equilibrium as μ is perturbed away from the origin. We will show that scenarios similar to those presented in Sec. 2.1 for nonsmooth continuous-systems are possible. Namely, we can observe *persistence* where a branch of regular equilibria can turn into a branch of pseudo-equilibria or *nonsmooth saddle-node* where a branch of regular equilibria can disappear after colliding with a branch of pseudo-equilibria. We will not investigate here the case of Filippov systems without sliding. In that case, two branches of regular equilibria can exist and be involved in the nonsmooth transition scenario.

3.1.2 Persistence and Nonsmooth Saddle-Node

Let x be a regular equilibrium of (66) and $\tilde{x}$ a pseudo-equilibrium. Then, linearising (67) and (68) about the boundary equilibrium point at the origin, we have

$$
\begin{aligned}
Ax + B\mu &= 0, \\
Cx + D\mu &= \lambda_1 > 0
\end{aligned}
\tag{69}
$$

and

$$A\tilde{x} + B\mu + E\tilde{\lambda} = 0,$$
$$C\tilde{x} + D\mu = 0, \qquad (70)$$
$$\tilde{\lambda} > 0$$

where $A = F_{1x}, B = F_{1\mu}, C = H_x, D = H_\mu$ and $E = F_2 - F_1$ all evaluated at $x = 0, \mu = 0$.

Now, from (69) we have $x = -A^{-1}B\mu$ and:

$$\lambda_1 = (D - CA^{-1}B)\mu. \qquad (71)$$

Moreover, from (71), $\tilde{x} = -A^{-1}B\mu - A^{-1}E\tilde{\lambda}$. Hence, we find

$$\tilde{\lambda} = \frac{(D - CA^{-1}B)\mu}{CA^{-1}E}, \qquad (72)$$

or, equivalently,

$$\tilde{\lambda} = \frac{\lambda_1}{CA^{-1}E}. \qquad (73)$$

In order for x and $\tilde{x}$ to exist for the same value of μ, both λ_1 and $\tilde{\lambda}$ must share the same sign. While they will exist for opposite values of μ if λ_1 and $\tilde{\lambda}$ have opposite sign. Therefore, using (73), we can state the following theorem.

Theorem 3.1 (Equilibrium points branching from a boundary equilibrium)
For the systems of interest, assuming

$$det(A) \neq 0 \qquad (74)$$
$$D - CA^{-1}B \neq 0 \qquad (75)$$
$$CA^{-1}E \neq 0 \qquad (76)$$

- *persistence is observed at the boundary equilibrium bifurcation point if*

$$CA^{-1}E < 0; \qquad (77)$$

- *a* nonsmooth saddle-node *is instead observed if*

$$CA^{-1}E > 0; \qquad (78)$$

Note, that the conditions found are different, as expected, from those presented in Sec. 2.1 for nonsmooth-continuous systems and are valid for any n-dimensional Filippov system of the given type.

3.1.3 Planar Filippov Systems

A comprehensive analysis of possible bifurcations in Filippov systems is given by Kuznetsov, Rinaldi, & Gragnani in [51]. In reviewing this material, we will consider in this section, only transitions which involve sliding on the discontinuity boundary. Actually, the appearance or disappearance of a sliding segment is already a transition.

Following [51], we term a point T on the switching manifold *tangent point* if the vectors $F_i(T), i = 1, 2$ are nonzero but at least one of them is tangent to Σ. Suppose that a tangent point $T \in \Sigma_s$ is such that

$$H_x(T)F_1(T) = 0.$$

We say that this tangent point is *visible* if the orbit of $\dot{x} = F_1(x, \mu)$ starting at T belongs to S_1 for all sufficiently small $|t| \neq 0$. We say that it is invisible if the orbit belongs to S_2. Similar definitions hold for F_2. In a neighbourhood of a generic tangent point orbits are like in Fig.28, with a possible reversal of all arrows and/or reflection with respect to the vertical axis.

Figure 28: Visible (a) and invisible (b) tangent points.

To meet all generic one-parameter transitions involving the discontinuity boundary Σ we use the following criterion: for a given parameter value μ, we consider the sliding set $\hat{\Sigma}$ and find all the pseudo-equilibria and tangent points in it. These points are finite in number but can collide as μ varies, leading to local codimension-1 transitions. Another local codimension-1 transition can occur when a standard hyperbolic equilibrium in S_1 or S_2 collides with Σ, i.e. a boundary equilibrium bifurcation. There are no other local codimension-1 transitions. Global codimension-1 transitions involving sliding are discussed in [51].

3.1.4 Local Transitions

Collisions of equilibria with the boundary
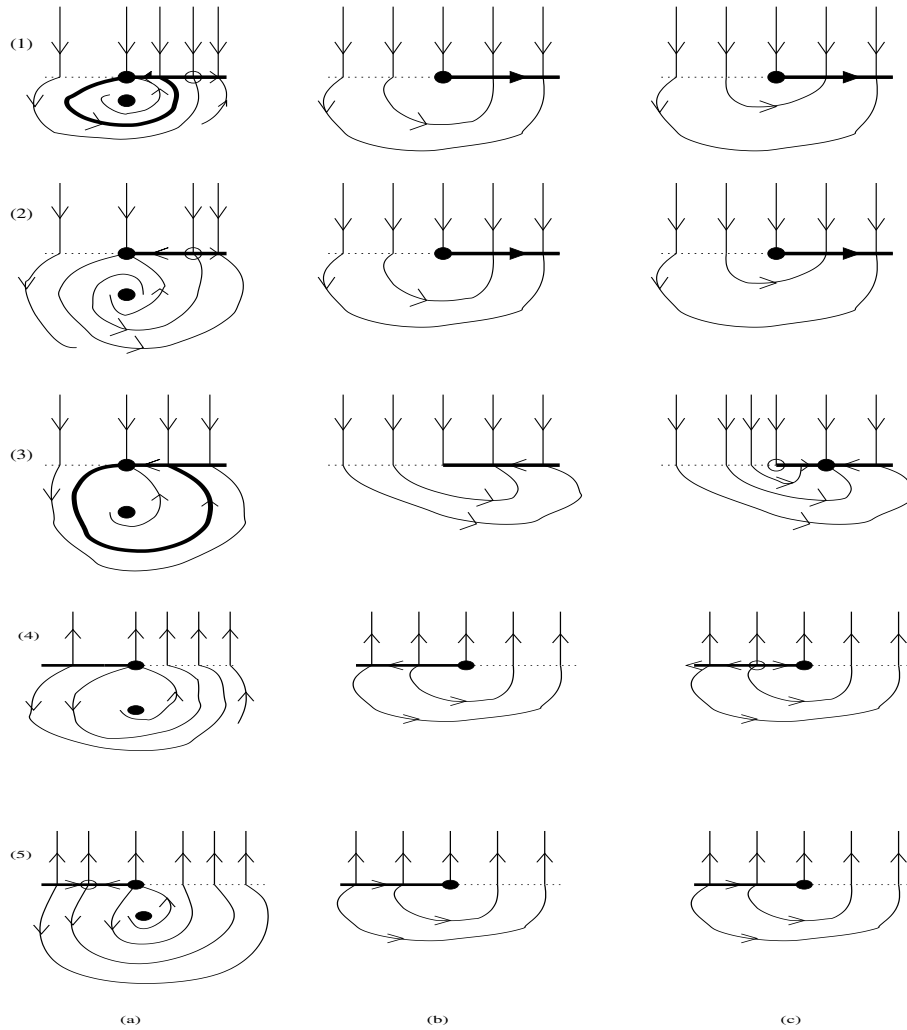
55

Figure 29: Boundary focus transitions. (a) $\mu < 0$, (b) $\mu = 0$, (c) $\mu > 0$. (1),(2) and (5) are nonsmooth saddle-node bifurcations, while (3) and (4) correspond to Persistence.

We can distinguish three main cases:

- Boundary focus: there are five generic critical cases (see Fig. 29(b)). In all of them there is a visible tangent point for $\mu < 0$ and an invisible tangent point for $\mu > 0$. The cases are distinguished by the relative position of the focus zero-isoclines and the behaviour of the orbit departing from the visible tangent point into S_1, as well as by
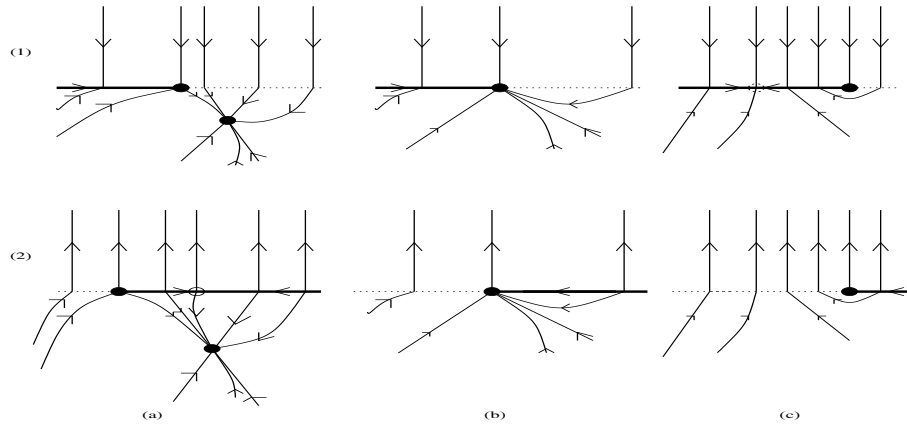
56

Figure 30: Boundary node transitions. (a) $\mu < 0$, (b) $\mu = 0$, (c) $\mu > 0$. (1) is a persistence bifurcation while (2) corresponds to saddle-node.
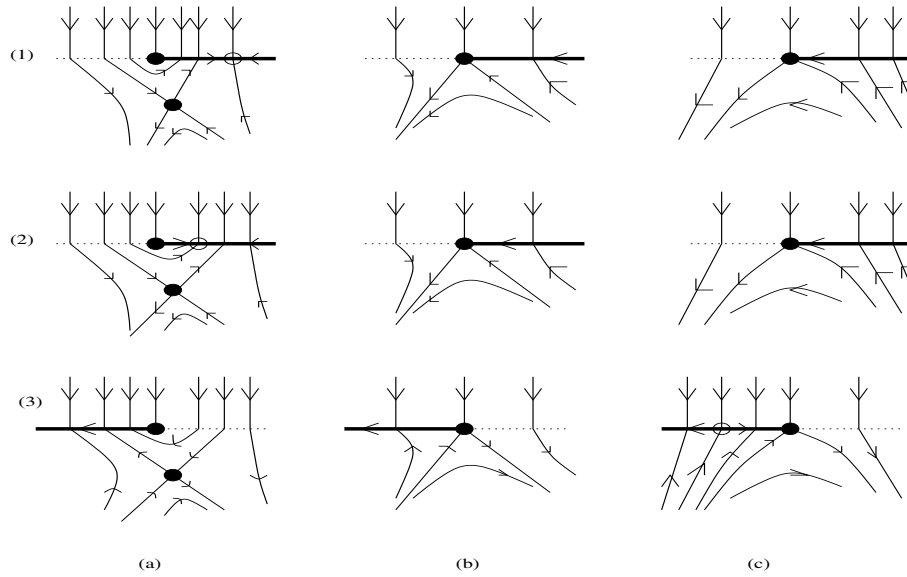
Figure 31: Boundary saddle transitions. (a) $\mu < 0$, (b) $\mu = 0$, (c) $\mu > 0$. (1) and (2) are Saddle-node bifurcations, while (3) corresponds to persistence.

the direction of the motion in S_2. If we assume that the colliding focus is unstable and has counter-clockwise rotation nearby, we can distinguish all five cases in Fig. 29. Cases (1),(2) and (5) are nonsmooth saddle-node bifurcations, while (3) and (4) correspond to persistence.

- Boundary node: Depending on the direction of motion in S_2, there are two generic critical cases, which are shown in Fig. 30. Case (1) is a persistence bifurcation while (2) corresponds to saddle-node.

- Boundary saddle: When the colliding equilibrium is a saddle, there are three generic cases determined by the slope of the saddle zero-isoclines, as can be seen in Fig. 31. In all cases, there is an invisible tangent point for $\mu < 0$ and a visible tangent point for $\mu > 0$. These points delimit the sliding segments on the discontinuity boundary. Cases (1) and (2) are saddle-node bifurcations, while (3) corresponds to persistence.
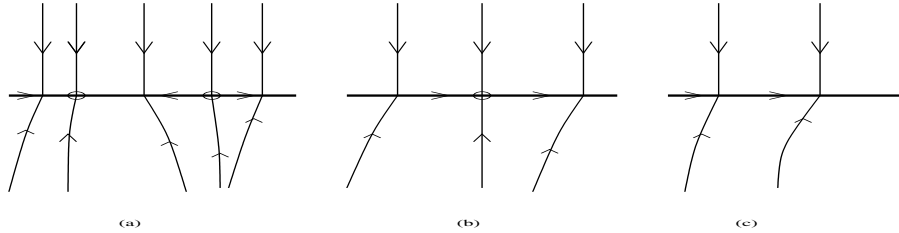

Figure 32: Pseudo-saddle-node transition. (a) $\mu < 0$, (b) $\mu = 0$, (c) $\mu > 0$.

Note that, when μ varies, two pseudoequilibria can collide and dissappear via a standard saddle-node bifurcation on the sliding set $\hat{\Sigma}$, which in this case we will call a pseudo-saddle-node transition. Figure 32 shows this transition in the case of a stable sliding segment.

Global phenomena such as those depicted in Fig. 33 are also possible and were studied in [51]. For example, a pseudo-equilibrium $\tilde{x}(\mu)$ can have a sliding orbit that starts and returns back to it for $\mu = 0$. This is possible if $\tilde{x}(0)$ is either a pseudo-saddle-node or a pseudo-saddle (Fig. 33 (1),(2)). Moreover, a standard saddle x_μ can have a homoclinic orbit containing a sliding segment at $\mu = 0$ (Fig. 33 (3)).

3.1.5   Non-generic situations

Other phenomena concerning equilibria in Filippov systems have been reported in some non-generic cases. For example, it has been observed that a branch of limit cycles can appear after a focus changes its stability on the boundary.

In a non-generic case, where the focus is always in the origin, Küpper and Moritz [49] study parameter dependent Filippov dynamical systems of
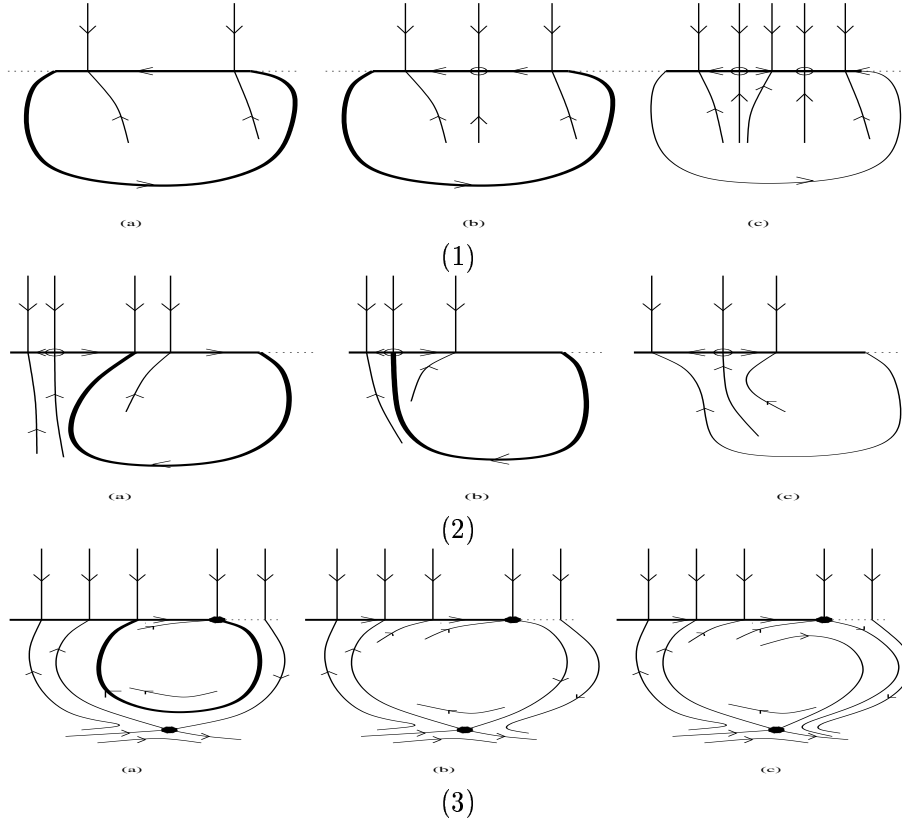
Figure 33: Global phenomena: (1) Sliding homoclinic orbit to a pseudo-saddle-node, (2) Sliding homoclinic orbit to a pseudo-saddle, (3) Sliding homoclinic orbit to a saddle. (a) $\mu < 0$, (b) $\mu = 0$, (c) $\mu > 0$.

the form

$$\left(\begin{array}{c} \dot{x}(t) \\ \dot{y}(t) \end{array} \right) = \left\{ \begin{array}{ll} K^+(x(t), y(t), \lambda) & \text{if} \quad x(t) > 0 \\ K^-(x(t), y(t), \lambda) & \text{if} \quad x(t) < 0 \end{array} \right. ,$$

where the right-hand sides $K^+, K^- : \mathbb{R}^2 \times I \mapsto \mathbb{R}^2$ for some interval I containing 0 are given by:

$$K^+(x, y, \lambda) = A^+_\alpha(\lambda) \left(\begin{array}{c} x \\ y \end{array} \right) + \left(\begin{array}{c} g^+_1(x, y, \lambda) \\ g^+_2(x, y, \lambda) \end{array} \right),$$

and

$$K^-(x, y, \lambda) = A^-_\alpha(\lambda) \left(\begin{array}{c} x \\ y \end{array} \right) + \left(\begin{array}{c} g^-_1(x, y, \lambda) \\ g^-_2(x, y, \lambda) \end{array} \right).$$
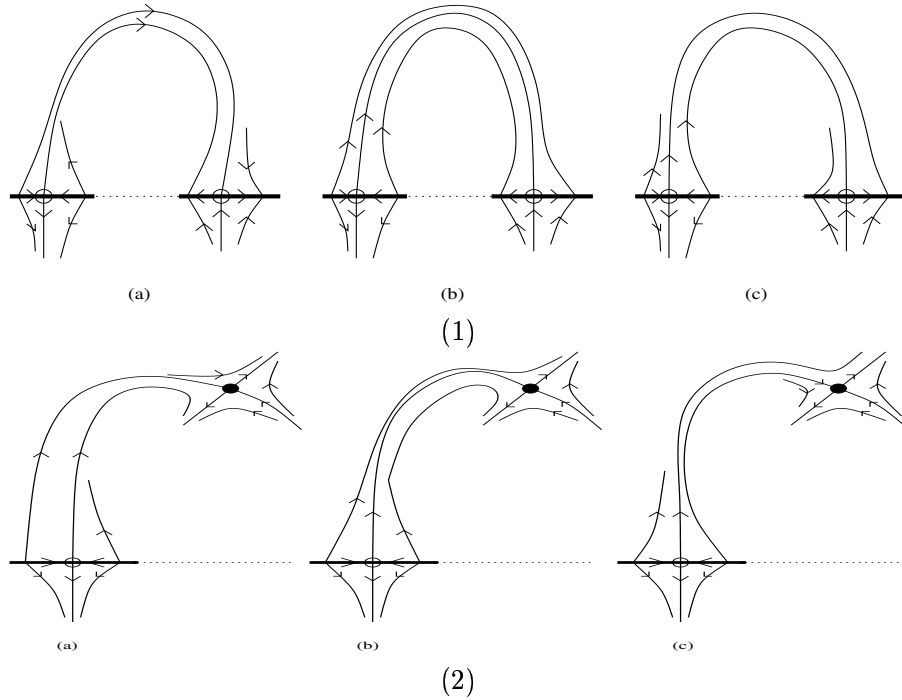
Figure 34: Global phenomena: (1) Heteroclinic connection between two pseudo-saddles, (2) Heteroclinic connection between a pseudo-saddle and a saddle. (a) $\mu < 0$, (b) $\mu = 0$, (c) $\mu > 0$.

The parameter dependent matrices $A_\alpha^+(\lambda)$ and $A_\alpha^-(\lambda)$ are assumed to be of the standard form used in the treatment of Hopf bifurcation in smooth systems, i.e.:

$$A_\alpha^+(\lambda) = \begin{pmatrix} \lambda & w^+(\lambda) \\ -w^+(\lambda) & \lambda \end{pmatrix}$$

and

$$A_\alpha^-(\lambda) = \begin{pmatrix} \alpha\lambda & w^-(\lambda) \\ -w^-(\lambda) & \alpha\lambda \end{pmatrix}$$

where $\alpha = 1$ or $\alpha = -1$. Then, as shown in [49], it is possible to give conditions for a continuous isolated branch of periodic orbits to bifurcate from the boundary equilibrium at the origin.

Another special case is described in Zou & Küpper [85], where the existence of periodic orbits bifurcating from a corner-like manifold in a planar Filippov dynamical system. There, the creation of a branch of cycles is

60

determined by interactions between the geometrical structure of the corner and the eigenstructure of each smooth subsystem.

Still another non-generic Filippov system (with symmetry) modeling a relay system is studied by Giannakopoulos and Pliete in [40]. Specifically, a piecewise-linear system is considered of the form

$$\dot{u} = Au + \text{sgn}(w^T u)v$$

where A is a 2×2 real matrix, u, v, w are two-dimensional real vectors. The theory of point transformation is applied to obtain conditions for the existence and stability of periodic solutions without sliding motion. The case where A has complex eigenvalues with a non-zero real part is studied completely. It is further shown that, if A has real or purely imaginary eigenvalues, then the system has no periodic solutions with sliding motion. Further results are given concerning branches of periodic solutions both with and without sliding motions.

Return to Example 2.6
In fact, Example 2.6 is a Filippov system which at other parameter values than those in Section 2 there can be equilibrium solutions on the ramp. In [14] a DC-DC Boost converter was shown to exhibit several nonsmooth transitions. In [65] a DC-DC Buck converter was initially studied as a Filippov system. We review this example in the following, where a nonsmooth transition is reported.

So we have equations (58),(59) but in this case we assume mixed voltage and a current control, so that the reference signal (57) is

$$V_r = V_{low} - ZI(t),$$

where Z is an impedance constant. The differential equations which drive the system are

$$\begin{pmatrix} \dot{V} \\ \dot{I} \end{pmatrix} = \begin{pmatrix} -1/(RC) & 1/C \\ -1/L & 0 \end{pmatrix} \begin{pmatrix} V \\ I \end{pmatrix} + \begin{pmatrix} 0 \\ E/L \end{pmatrix} u$$

where $u = 0$ if $V_{con} := V(t) + ZI(t) > V_{low}$ and $u = 1$ otherwise.

Thus we have two linear topologies in continuous conduction mode. We will not consider discontinuous conduction mode in this paper, since we will assume that we have bidirectional switches, which allow negative currents. If we fix a set of initial conditions $V_0 = V(t_0)$ and $I_0 = I(t_0)$, since the systems of differential equations are linear, we will be able to compute exactly the solution of each one.

61

Let us write

$$k = \frac{1}{2RC} \qquad w = \sqrt{\frac{1}{LC} - k^2}, \qquad\qquad (79)$$

and suppose that

$$\frac{1}{LC} - k^2 > 0, \qquad\qquad (80)$$

which is the usual case since oscillatory solutions are desired. We also define the real matrix

$$A = \begin{pmatrix} -k/w & 1/(Cw) \\ -1/(Lw) & k/w \end{pmatrix}.$$

Then we have the following solutions for the systems:

system 1: $V_{con} > V$

$$\begin{pmatrix} V(t) \\ I(t) \end{pmatrix} = e^{-k(t-t_0)} \left[I \cos w(t - t_0) + A \sin w(t - t_0) \right] \begin{pmatrix} V_0 \\ I_0 \end{pmatrix}$$

system 2: $V_{con} < V$

$$\begin{pmatrix} V(t) \\ I(t) \end{pmatrix} = \begin{pmatrix} E \\ E/R \end{pmatrix} + e^{-k(t-t_0)} \left[I_Z \cos w(t - t_0) + A \sin w(t - t_0) \right] \begin{pmatrix} V_0 - E \\ I_0 - E/R \end{pmatrix}$$

where I_Z is the identity matrix. It follows that, between two commutation consecutive ramp intersection times, we know exactly the state variables of the system. Essentially, they are a combination of exponential and sinusoidal functions.

In each linear topology we can compute the equilibrium points and their stability. The equilibrium point when $u = 0$ is $P_0 := (0, 0)$, and when $u = 1$ $P_1 := (V_{in}, V_{in}/R)$. It is easy to check that the equilibrium points are spiral sinks with eigenvalues $-k + iw$. But we should not forget that the system switches topologies depending on the switching condition

$$V(t) + ZI(t) = V_{low}$$

and thus, in the nonlinear switched system it can happen that none, one or the two equilibrium points are active.

One of the equilibrium points is always at the origin, and the other moves as parameter E is varied. The corresponding bifurcation diagrams are plotted in Figs. 35-37. The line corresponding to the switching condition is also plotted in the figures, and some representative orbits are also shown. The fixed parameters are $R = 22\Omega$, $C = 47\mu F$, $L = 0.02H$, $V_{low} = 5V$,
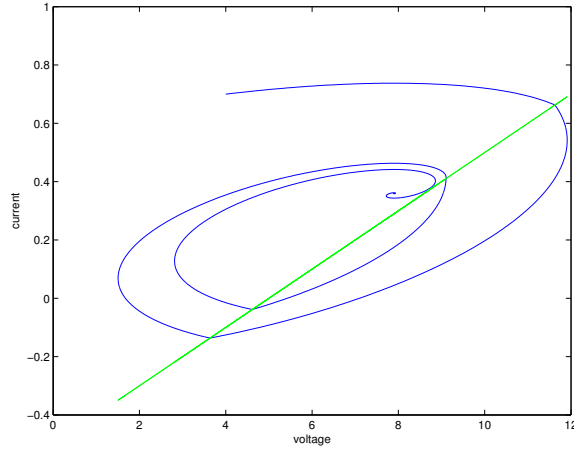
62

Figure 35: E=7.9 V. The only attractor is a stable focus at $(E, E/R)$.
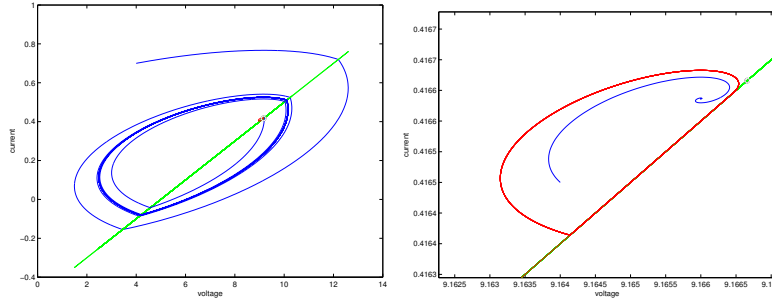
Figure 36: E=9.166 V. The stable limit cycle is coloured blue, while the unstable one is coloured red. The unstable limit cycle contains the stable focus inside. They are close to the boundary equilibrium bifurcation, where the unstable limit cycle dissapears and the unstable focus changes its stability and remains in the switching manifold. The figure on the right is a zoom of the figure on the left.

$Z = -10$ and E is varied between 7.9 and 9.5 as a bifurcation parameter to obtain the different configurations.

For E=7.9, there exists only a stable focus at $(E, E/R)$. For E=8.0012 a standard saddle-node bifurcation of cycles occurs, and a stable limit cycle and an unstable limit cycle are created. The unstable limit cycle is inside the stable one, and the stable focus is inside the unstable cycle, which delimits its basin of attraction. As parameter E is continuously increased the amplitude
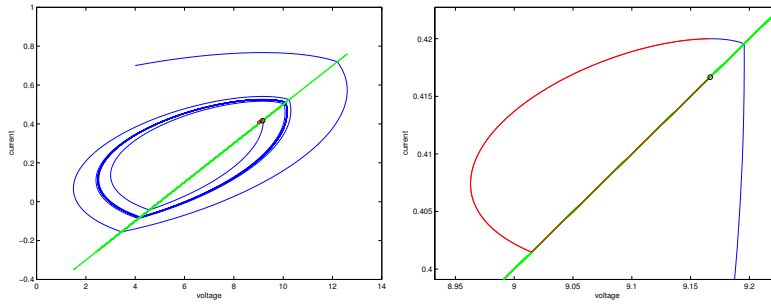
Figure 37: $E=9.167$ V. The stable limit cycle is coloured blue, while the unstable one (previously red) has dissapeared after the boundary equilibrium bifurcation. The figure on the right is a zoom of the figure on the left.

of the unstable limit cycle gets smaller and smaller, and finally it disappears in a nonsmooth transition, when the stable focus collides with the cycle at

$$E = \frac{V_{low}}{1 + Z/R}.$$

The stability of the focus changes and an unstable equilibrium point remains on the switching manifold as E_{in} is further increased.

3.1.6   Open Challenges and Problems

We have seen that equilibria in Filippov systems can undergo several non-smooth transitions involving their sudden disappearance, persistence and, in some cases, the generation of branches of limit cycles. Currently, we can only characterise the simplest possible cases in general n-dimensional systems, while only special (often non-generic) planar models are studied in the literature. A pressing open problem is the study in a more general framework of those transitions involving the occurrence (or disappearance) of one or more families of limit cycles at a boundary equilibrium bifurcation.

Also, Filippov systems can also exhibit sets of equilibria (see [8]) that can be attracting or repelling. Nonsmooth bifurcations of sets of equilibria, which are bound to occur under parameter variations, have not been studied sofar in the literature. Thus, the study of such bifurcations remain an important open challenge for further study.
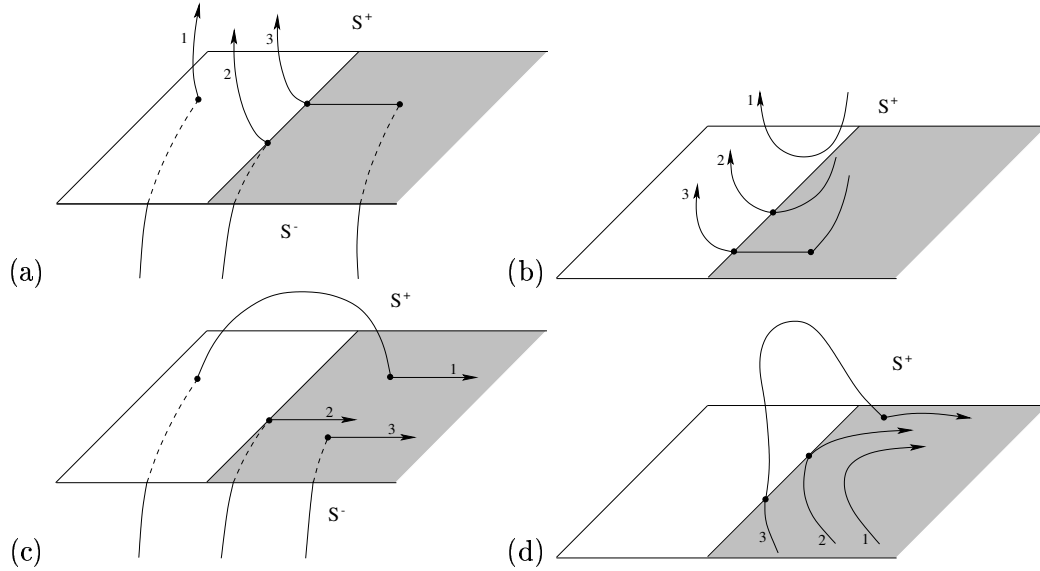
Figure 38: The four possible bifurcation scenarios involving collision of a segment of the trajectory with the boundary of the sliding region $\partial\hat{\Sigma}^-$

3.2 Sliding Bifurcations of Limit Cycles

Sliding bifurcations are defined here as interactions between limit cycles of the system and the sliding region $\hat{\Sigma}$. According to the results presented in [29, 47, 48], and in more detail in [33], we can identify four possible cases of interactions between the system flow and the sliding section. These can be generalised to the case of n-dimensional piecewise-smooth dynamical systems of the form (66). A three-dimensional schematic representation is given in Fig. 38, where we assume the phase space topology introduced in Sec. 2.1 and depict only segments of trajectories (denoted in the figure by '1', '2' and '3') which interact with the sliding region. In order for a NST to occur as a parameter is varied, we suppose that these depicted trajectories represent parts of a limit cycle for three different parameter values.

Figure 38(a) depicts the scenario we term a **crossing-sliding bifurcation**. Here, under parameter variation, a part of the system trajectory transversally crosses the boundary of the sliding strip at the bifurcation point (trajectory labelled '2' in Fig. 38(a)). Further variations of the parameter cause the trajectory to enter the sliding region $\hat{\Sigma}$, leading to the onset of sliding motion. Note that the sliding trajectory then moves locally

65

toward the boundary of $\hat{\Sigma}$. Since at the boundary $F_s = F_1$ or F_2 (without loss of generalty we henceforth assume $F_s = F_1$ there, i.e. we are on $\partial\hat{\Sigma}^-$) the trajectory leaves the switching manifold tangentially.

In the case presented in Fig. 38(b), a section of trajectory lying in region S^+ grazes the boundary of the sliding region from above. Again, this causes the formation of a section of sliding motion which locally tends to leave $\hat{\Sigma}$. We term this transition a **grazing-sliding bifurcation**. We note that this transition is the natural generalisation of grazing bifurcations (see Sec. 2.2) to dynamical systems with sliding.

A different bifurcation event, which we shall call a **switching-sliding bifurcation**, is depicted in Fig. 38(c). This scenario is similar to the crossing-sliding bifurcation shown in Fig. 38(a). We see a section of the trajectory transversally crossing the boundary of the sliding region. Now, though, the trajectory stays locally within the sliding region instead of leaving the switching manifold Σ.

The fourth and last case is the so-called **adding-sliding bifurcation**, shown in Fig. 38(d). It differs from the scenarios presented above since the segment of the trajectory which undergoes the bifurcation lies entirely within the sliding region $\hat{\Sigma}$. Thus, as parameters are varied, a sliding section of the system trajectory tangentially (*grazes*) hits the boundary of the sliding region. Further variation of the parameter causes the formation of an additional segment of trajectory lying above the switching manifold, i.e. in region S^+.

3.2.1 Normal forms for sliding bifurcations

To capture the dynamics of sliding bifurcations one can obtain normal form mappings using the concept of the zero-time discontinuity mapping (see Sec. 2.2). Similarly, we will not give details of the construction of the discontinuity mappings but only present final results; a detailed derivation can be found in [30]. It is assumed that we have uniform discontinuity (see earlier Definition 2.1) across the switching manifold Σ. Since Σ is a well-defined surface, at the bifurcation point x^* we have $H(x^*) = 0$ and $H_x(x^*) \neq 0$. The additional condition

$$H_x(F_2 - F_1) > 0, \tag{81}$$

which we assume to hold across $\hat{\Sigma}$ ensures that the sliding region is simultaneously attracting from both regions S^+ and S^-. Under these assumptions we shall introduce conditions which need to be satisfied at every sliding bifurcation. These are presented in Tab. 2

66

Bifurcations	Defining Conditions
crossing-sliding	$H_x F_1 = 0, \ (H_x F_1)_x F_1 > 0$
grazing-sliding	$H_x F_1 = 0, \ (H_x F_1)_x F_1 > 0$
switching-sliding	$H_x F_1 = 0, \ (H_x F_1)_x F_1 < 0$
adding-sliding	$H_x F_1 = 0, \ (H_x F_1)_x F_1 = 0, \ ((H_x F_1)_x F_1)_x F_1 < 0$

Table 2: Analytical conditions determining a particular sliding bifurcation scenario

Theorem 3.2 *Given the above assumptions and that condition (81) holds, then under the appropriate additional conditions summarised in Tab. 2, we have the following zero-time discontinuity mappings*

- **crossing-sliding**; *given by*

$$x \mapsto \begin{cases} x & \text{if } \mu_x x \leq 0 \\ x + \mathbf{v} + O(x^3) & \text{if } \mu_x x > 0, \end{cases} \tag{82}$$

  where μ_x denotes vector normal to the manifold defined by the equivalent control μ (see Eq. 65)

- **grazing-sliding**

$$x \mapsto \begin{cases} x & \text{if } H_{\min}(x) \geq 0 \\ x + \mathbf{u} + O(x^{3/2}) & \text{if } H_{\min}(x) < 0, \end{cases} \tag{83}$$

- **switching-sliding**

$$x \mapsto \begin{cases} x & \text{if } \mu_x x \leq 0 \\ x + \mathbf{w} + O(x^4) & \text{if } \mu_x x > 0, \end{cases} \tag{84}$$

- **adding-sliding**

$$x \mapsto \begin{cases} x & \text{if } \mu_{min} \geq 0 \\ x + \mathbf{z} + O(x^{5/2}) & \text{if } \mu_{min} < 0, \end{cases} \tag{85}$$

where:

$$H_{min} = H_x x + O(x^2), \quad \mu_{min} = \mu_x x + O(x^2), \tag{86}$$

$$\mathbf{v} = \frac{1}{2} \frac{((H_x F_1)_x x)^2}{(H_x F_d)((H_x F_1)_x F_1)} F_d, \tag{87}$$

67

$$\mathbf{u} = -\frac{H_x x}{H_x F_d} F_d, \tag{88}$$

$$\mathbf{w} = \frac{2}{3} \frac{((H_x F_1)_x x)^3}{(H_x F_d)^2 ((H_x F_1)_x F_1)^2}$$
$$[(H_x F_d)(F_{1x} F_d - F_{dx} F_1) - (H_x (F_{1x} F_d - F_{dx} F_1)) F_d], \tag{89}$$

$$\mathbf{z} = -\frac{9}{2} \frac{((H_x F_1)_x x)^2}{(H_x F_d)^2 (((H_x F_1)_x F_1)_x F_1)}$$
$$[(H_x F_d)(F_{1x} F_d - F_{dx} F_1) - (H_x (F_{1x} F_d - F_{dx} F_1)) F_d], \tag{90}$$

where $F_d = F_2 - F_1$.

As shown on examples in Sec. 2.2.3 the appropriate composition of the discontinuity mapping with some affine transformation gives rise to a map which describes the behaviour of a limit cycle which undergoes a C-bifurcation. We can state that generically, the type of discontinuity found in the discontinuity map will be characterising the full Poincaré map. Thus, the leading order term characterising a particular discontinuity map has direct influence on the system dynamics following any sliding bifurcation scenario.

Let us briefly discuss consequences following from the character of each ZDM.

3.2.2 Dynamical consequences of the character of the ZDMs. Discussion

The ZDM characterising crossing-sliding bifurcation scenario causes discontinuity in the second-derivative terms ($\mathbf{v} = \mathcal{O}(x^2)$). Thus, the Poincaré mapping describing the bifurcating orbit will be continuous with continuous first derivative, but there will be a second derivative discontinuity across the boundary of the sliding region. The mapping will have co-rank 1 on the sliding side of the discontinuity (note that sliding introduces loss of system dimension by 1). The eigenvalues of the Jacobian matrix of the Poincaré map describing the bifurcating cycle vary continuously across the discontinuity. Thus, a hyperbolic cycle undergoing the crossing-sliding bifurcations will preserve its stability properties and period. Moreover, non-standard bifurcations can be expected in the case when the bifurcating cycle is non-hyperbolic.

The second case of sliding bifurcations considered here is the grazing-sliding scenario. The correction which needs to be made to account for the sliding flow in this case influences terms at the linear order, $\mathbf{u} = \mathcal{O}(x)$. Thus, for such a mapping we can not conclude that the periodic orbit will persist under parameter variations that wolude cause it to acquire a sliding portion. If the orbit survives the bifurcations, we can expect a jump in eigenvalues as the periodic orbit goes through a tangency with the boundary of the sliding set. The presence of the higher order term in the ZDM (the $\mathcal{O}(3/2)$-term) will cause the eigenvalues to have a square root singularity with respect to parameter variations as the border is approached from the sliding side. The jump in eigenvalues is nicely illustrated by the fact that a sliding periodic orbit must have at least one eigenvalue 0, whereas there is no such restriction for an orbit which does not contain any sliding segments. It is worth mentioning here that in the case of grazing bifurcations in systems with degree of discontinuity one that do not slide, the normal form map is characterised by a square-root singularity (see Sec. 2.2). Grazing in the presence of sliding changes the nature of C-bifurcations giving rise to a normal form that is piecewise linear to leading order.

To classify the possible bifurcation scenario we can use the classification strategies for border-collision bifurcations in maps [2, 3, 24, 62, 63]. Note, however that sliding motion introduces loss of the rank of the map on one side of the discontinuity. Therefore, not all classification strategies developed for PWS maps can be applied to describe bifurcations in PWL maps which are non-invertible in one of their region of definition. This point has been further elucidated in [46] where a classification strategy for bifurcations arising due to grazing-sliding in 3-dimensional Filippov type flows is introduced.

The third case, namely switching-sliding leads to a normal form which has continuous derivatives up to order 2 ($\mathbf{w} = \mathcal{O}(x^3)$). Hence, as for crossing-sliding, a hyperbolic trajectory will persist under parameter variation since the mapping has continuous first parameter derivatives, but the second parameter derivative is discontinuous. Finally, we shall consider the ZDM for the adding-sliding bifurcations. Since the first derivative is continuous, a hyperbolic orbit persists under parameter variations, but the first parameter derivative of the eigenvalues has a jump over the boundary, and the second parameter derivative approaches infinity on one side, due to the presence of a 5/2 term in the higher order term of the Poincaré mapping.

Example 3.1 (Application to a simple dry-friction oscillator)

In what follows, we present an example of a dry friction oscillator model

69

which serves as an illustration of how the ZDMs can be used to explain and also predict a particular bifurcation scenario arising in Filippov systems. More details can be found in [46].

Friction oscillators are of Filippov type when the friction characteristic is modelled by some discontinuous function and gives rise to a system with discontinuous right hand side [69, 68, 38]. A characteristic feature of the dynamics of friction systems is so-called stick-slip motion. As shown in [72] the stick phase of an oscillatory motion corresponds to sliding . Therefore, different transitions from slip motion to more complex stick-slip oscillations, often present in friction oscillators, correspond to sliding bifurcations. Examination of slip to stick-slip transitions found in [69, 68, 39, 38] will reveal that at least three of the four aforementioned cases of sliding bifurcations have been observed there, namely crossing-sliding, switching-sliding and grazing-sliding. In fact all the four sliding-bifurcations scenarios have been reported to be have been exhibited in a simple model of friction oscillator (see [33] for details).

Here we focus on a more intricate stick-slip transition which lead to the sudden onset of chaotic stick-slip behaviour. Following [81], the dry friction oscillator under investigation in dimensionless form can be expressed as

$$\ddot{y} + y = f(1 - \dot{y}) + F\cos(\nu t), \tag{91}$$

where

$$f(1 - \dot{y}) = \alpha_0 \mathrm{sgn}(1 - \dot{y}) - \alpha_1(1 - \dot{y}) + \alpha_2(1 - \dot{y})^3 \tag{92}$$

is a kinematic friction characteristic and $1 - \dot{y}$ corresponds to the relative velocity between the driving belt and moving block. In the case when $\dot{y} = 1$ the relative velocity is 0 and the kinematic friction is set valued i.e.: $-\alpha_0 < f(1 - \dot{y}) < \alpha_0$. The coefficients of the kinematic friction characteristic are positive constants, which in our example shall take the values

$$\alpha_0 = \alpha_1 = 1.5, \quad \alpha_2 = 0.45, \quad \text{while} \quad F = 0.1$$

is the amplitude of forcing. As a bifurcation parameter, we take ν, the normalized angular velocity, and let $T = 2\pi/\nu$ represent the forcing period. We focus, in particular, on the bifurcation scenario for $\nu \approx 1.7078$ that gives rise to the sudden emergence of chaotic stick-slip motion. As shown in Fig. 39(a), at the bifurcation point, a $4T$-periodic orbit grazes the switching manifold $\Sigma = \{\dot{y} = 1\}$ at the boundary of the sliding region (denoted in the figure by a short vertical line). The observed scenario corresponds to a grazing-sliding bifurcation, as the bifurcating orbit grazes from below the
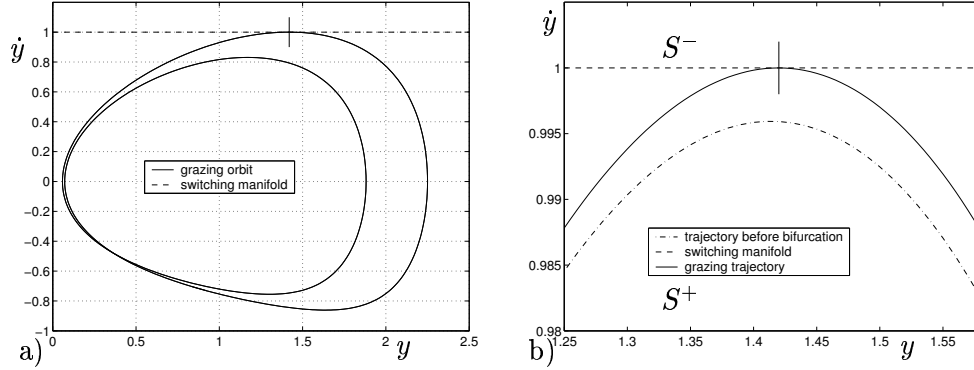
70

Figure 39: (a) Orbit of (91) of period $4T$ ($8\pi/\nu$) undergoing grazing-sliding bifurcation for $\nu = 1.7077997$. (b) Enlargement of the region where grazing-sliding occurs; the dash-dotted segment correspond to the periodic orbit for $\nu = 1.7082$ that clearly does not reach the switching manifold.

boundary of the region where stick motion can take place. This can be more clearly seen in Fig. 39(b).

To study the dynamics ensuing due to this bifurcation we can proceed similarly as in Sec. 2.2 for grazing bifurcations. That is, we need to obtain a global Poincaré mapping which describes the behaviour of the bifurcating cycle. Such a mapping is obtained by a composition of the ZDM for the grazing-sliding bifurcation with an affine transformation such as (93) which captures the dynamics of the non-sliding hyperbolic cycle. Here we have a forced dynamical system with the bifurcating orbit being of period $4T$, i.e. four times the period of the external forcing term, the natural Poincaré map is a $4T$-stroboscopic mapping, say P_{4T}, which we assume to be affine and well represented by its linear terms i.e.

$$P_{4T} : x_{n+1} = Ax_n + B\nu = \left(\begin{array}{cc} a_{11} & a_{12} \\ a_{21} & a_{22} \end{array} \right) x_n + \left(\begin{array}{c} b_1 \\ b_2 \end{array} \right) \nu, \qquad (93)$$

where x_n is the two-dimensional state vector, in our case corresponding to position and velocity of the dry-friction oscillator, obtained by sampling the system states at time instants that are multiples of $4T$. Note that we assume the map to be affine and sufficiently smooth away from the bifurcation point, i.e. when the orbit does not contain any segments of sliding (stick) motion. Smoothness is lost under parameter variation as the orbit grazes and then enters the sliding region.

To capture the influence of the grazing-sliding event we then need to

71

compose (93) with the normal-form map for grazing-sliding given by (83) with correction term (88). Thus, the final map obtained from a composition of (93) with the ZDM takes the form:

$$
x_{n+1} = \begin{cases} \begin{pmatrix} a_{11} & a_{12} \\ a_{21} & a_{22} \end{pmatrix} x_n + \begin{pmatrix} b_1 \\ b_2 \end{pmatrix} \nu & \text{if} \quad x_{2n} < 0, \\ \begin{pmatrix} a_{11} & 0 \\ a_{21} & 0 \end{pmatrix} x_n + \begin{pmatrix} b_1 \\ b_2 \end{pmatrix} \nu & \text{if} \quad x_{2n} > 0. \end{cases}
\tag{94}
$$

A detailed derivation leading to the mapping (94) was presented in [31]. Following [31] we introduce numerical values of the matrix coefficients: $a_{11} = -1.85$, $a_{12} = 4.396$, $a_{21} = -1.14$, $a_{22} = 2.704$, $b_1 = 4.498$ and $b_2 = -1.755$. Bifurcations that can be observed in (94) under the variation of the bifurcation parameter ν correspond to bifurcations in the friction oscillator. Note, that map (94) is non-invertible in one of its regions of definition. Non-invertibility can be heuristically understood form the fact that *sliding motion* introduces loss of a system dimension by 1 which appears in the map as a loss of rank. Under appropriate coordinate transformation (94) can be written as:

$$
x_{n+1} = \begin{cases} \begin{pmatrix} \delta_1 & 1 \\ \tau_1 & 0 \end{pmatrix} x_n + \begin{pmatrix} 1 \\ 0 \end{pmatrix} \mu & \text{if} \quad x_{1n} < 0, \\ \begin{pmatrix} \tau_2 & 1 \\ 0 & 0 \end{pmatrix} x_n + \begin{pmatrix} b_1 \\ b_2 \end{pmatrix} \nu & \text{if} \quad x_{1n} > 0. \end{cases}
\tag{95}
$$

where δ_1, τ_1, τ_2 are the determinant and traces of the matrices on either side of the discontinuity. The map (95) is a canonical normal form for grazing-sliding bifurcations in 3-dimensional Filippov type flows. Here we have that $\tau_1 = 0.854$, $\delta_1 = 0.009$ and $\tau_2 = -1.85$ which according to the criterion developed in [46] implies sudden onset of chaos under variation of μ. The bifurcation diagram computed from numerical integration of the system is depicted in Fig. 40(a). Note that the chaos is *robust* in the sense introduced in [5], that is it has no enbedded periodic windows. A part of the chaotic trajectory born in the bifurcation is shown in Fig. 40(b).

4 Impacting Systems

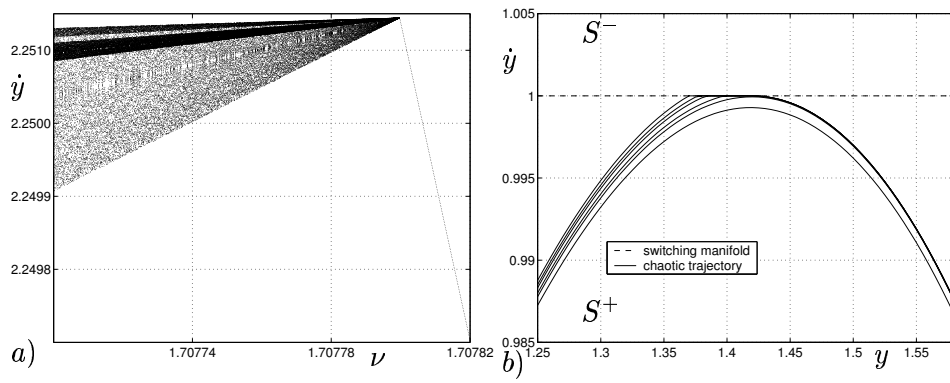**Example 4.1 (A motivating example, a driven linear impact oscillator)**

Figure 40: Bifurcation diagram obtained from the numerical integration of the system under consideration (a) and a chaotic trajectory in the neighbourhood of the switching manifold.

Suppose a 1 one-degree-of-freedom linear, damped, harmonically driven oscillator is constrained to displacements to the right of its equilibrium position. When the oscillator reaches the constraint with non-zero velocity, a rebound will take place, where we assume the outgoing velocity to be proportional to the incoming velocity.

The non-impact dynamics can be written

$$\ddot{q} + \delta\dot{q} + \omega_0^2 q = \cos(t),$$

where $q > 0$ and the impact law

$$\dot{q}^+ = -r\dot{q}_-$$

at $q = 0$. Using instead the state variables

$$
\begin{aligned}
x_1 &= q, \\
x_2 &= \dot{q}, \\
x_3 &= t \bmod 2\pi,
\end{aligned}
$$

the impact system can be more abstractly described by

$$\dot{x} = F(x) = \begin{pmatrix} x_2 \\ -\delta x_2 - \omega_0^2 x_1 + \cos(x_3) \\ 1 \end{pmatrix}, \tag{96}$$

when $H(x) = x_1 > 0$

$$x^+ = R(x^-) = \begin{pmatrix} x_1^- \\ -r x_2^- \\ x_3^- \end{pmatrix}. \tag{97}$$

This last equation (97) can also be written

$$x^+ = x^- + G(x^-)H_x F(x^-) = x^- + \begin{pmatrix} 0 \\ -(r+r) \\ 0 \end{pmatrix} x_2^-. \tag{98}$$

73

We will in the next section study impact systems described by the three functions F, G, and H. The chosen form of the impact law covers systems with multiple impacting rigid bodies, when no friction is assumed in the impact. When friction is present, the assumption of low incoming velocity $H_x F$ leading to a small change of state in (98) does not necessarily hold (see for example the Painlevé paradox studied in [55]).

Apart from motion with $H > 0$ interrupted by isolated impacts, there are some special types of motion in these systems. In the linear oscillator, if we start at

$$x = \begin{pmatrix} 0 \\ 0 \\ 3\pi/2 \end{pmatrix}$$

which is at the boundary with zero velocity, we find that we cannot leave the boundary through the vector field, as the acceleration $(H_x F)_x F = \cos(3\pi/2)$ is negative. The impact law will just return us to the same state, so we have to assume that *sticking* motion takes place along the boundary until the acceleration becomes positive again at $x_3 = 0 \bmod 2\pi$, which can be thought of as higher order sliding, i.e. motion along a codimension-two surface. Further, if the coefficient of restitution satisfies $0 < r < 1$, then starting at

$$x = \begin{pmatrix} 0 \\ \text{small} \\ 3\pi/2 \end{pmatrix}$$

will lead to a rapid series of impacts accumulating in finite time (like a ping-pong ball coming to rest) which we call *chattering*, see [10]. After the chattering has completed, sliding motion will follow until the acceleration becomes positive again.

4.1 Nonsmooth transitions of Boundary Equilibria

In structural mechanical systems with friction, the question of the existence and uniqueness of equlibrium points has been investigated recently, for example in [45]. Here we will present results in a more abstract and general setting, albeit one that precludes impact with friction.

As stated above, we will consider system of the form

$$\dot{x} = F(x) \quad \text{if } H(x) > 0 \tag{99}$$

with impact at the surface Σ defined by $H(x) = 0$, and where the impact law takes the form

$$x^+ = R(x^-) = x^- + G(x^-)H_x F(x^-). \tag{100}$$

74

For convenience, we will also define the velocity $v(x)$ and acceleration $a(x)$ (of the vector field F relative to H) as

$$
\begin{align}
v(x) &= H_x F(x), \tag{101} \\
a(x) &= (H_x F)_x F(x). \tag{102}
\end{align}
$$

These systems also have the possibility of *sliding* motion, through points satisfying

$$
\begin{align}
H(x) &= 0, \tag{103} \\
v(x) &= 0, \tag{104}
\end{align}
$$

where the impact mapping is the identify. The mechanism for maintaining sliding motion is the same as for low velocity impacts, so the sliding vector field should be

$$
\dot{x} = F_s(x) = F(x) - \lambda(x) G(x), \tag{105}
$$

where $\lambda > 0$ is chosen to keep $H = 0$, $v = 0$. This is possible for the typical mechanical impacting system since, at these points, we must have $H_x G = 0$ as the impact mapping should map points in the impact surface back to the impact surface, and thus G must be parallel to the impact surface for small impact velocities. Further, defining

$$
b(x) = (H_x F)_x G(x),
$$

we have for the typical system that $b \leq -1$ at these points, since a negative incoming velocity should produce a positive outgoing velocity. The requirement that the acceleration also vanishes for the sliding flow, i.e. that $a(x)$ defined by (102) with F replaced by F_s is zero for the sliding flow (105) leads to the condition that

$$
\lambda(x) = a(x)/b(x).
$$

Now since $\lambda(x) > 0$ we find this equivalent to $a(x) < 0$ that the acceleration is directed towards the boundary. We can interpret λ physically as the contact force provided by the boundary. Thus the sliding set $\hat{\Sigma}$ is determined by

$$
\begin{align}
H(x) &= 0, \\
v(x) &= 0, \\
a(x) &< 0.
\end{align}
$$

75

4.1.1 Existence of equilibrium points

In addition to regular equilibrium points x^*, with $F = 0$, $H > 0$, there is a possibility of having pseudo-equilibrium points x^* with $F_s = 0$, $H = 0$. The equations to solve are

$$
\begin{aligned}
F(x^*) &= 0, \\
H(x^*) &> 0,
\end{aligned}
$$

and

$$
\begin{aligned}
F(x^*) - \lambda^* G(x^*) &= 0, \\
H(x^*) &= 0, \\
\lambda^* &> 0,
\end{aligned}
$$

respectively. In the later case, λ^* is most conveniently regarded as an independent variable.

Now assume that the system depends on a single parameter μ, and that $x = \bar{x}$, $\mu = \bar{\mu}$ satisfies

$$
\begin{aligned}
F(\bar{x}, \bar{\mu}) &= 0, \\
H(\bar{x}, \bar{\mu}) &= 0.
\end{aligned}
$$

This point may be called a boundary equilibrium point. If the parameter μ is changed, regular and/or pseudo-equilibrium points may branch off the boundary equilibrium. Assuming for simplicity $\bar{x} = \bar{\mu} = 0$ and linearizing, we find

$$
\begin{aligned}
Ax^* + M\mu^* &= 0, \\
Cx^* + N\mu^* &> 0,
\end{aligned}
$$

for a regular equilibrium, and

$$
\begin{aligned}
Ax^* + M\mu^* + B\lambda^* &= 0, \\
Cx^* + N\mu^* &= 0, \\
\lambda^* &> 0,
\end{aligned}
$$

for a boundary equilibrium, where

$$
\begin{aligned}
A &= F_x(\bar{x}, \bar{\mu}), \\
M &= F_\mu(\bar{x}, \bar{\mu}), \\
C &= H_x(\bar{x}, \bar{\mu}), \\
N &= H_\mu(\bar{x}, \bar{\mu}), \\
B &= -G(\bar{x}, \bar{\mu}), \\
CB &= 0.
\end{aligned}
$$

If the linear systems are not degenerate, they will be representative for what happens locally in the full system. We find

Theorem 4.1 (Equilibrium points branching from a boundary equilibrium)
For systems in this class, and assuming

$$
\begin{aligned}
\det(A) &\neq 0 \\
e = N - CA^{-1}M &\neq 0 \\
s = CA^{-1}B &\neq 0,
\end{aligned}
$$

there exists a unique regular equilibrium point branching off from $\bar{x}$ when $e(\mu^* - \bar{\mu})$ is small and positive, and a unique pseudo-equilibrium point branching off from $\bar{x}$ when $(e/s)(\mu^* - \bar{\mu})$ is small and positive. The derivative of the points with respect to the parameter exists and has a limit as $\mu^* \to \bar{\mu}$ from the side where the point exists.

Note the similarity of this result to Theorem 3.1; the proof follows along similar lines. We note that if $s > 0$, the regular and pseudo points are both present for one sign of $\mu^* - \bar{\mu}$ and none are present for the other sign. Thus one can say that the points annihilate each other as μ^* changes, in a *saddle-node like* bifurcation. If $s < 0$, one equilibrium point is present for any small value of $\mu^* - \bar{\mu}$, and the regular equilibrium *persists* into a pseudo point as μ^* changes.

Stability The stability of a regular equilibrium point is determined by the eigenvalues of the matrix A. The question of stability of a pseudo-equilibrium point can be split into stability of the sliding set, and stability of the sliding vector field when restricted to the sliding set, respectively.

A simple calculation shows that stability of the sliding set is guaranteed if

$$
-2 < b(\bar{x}) \leq -1,
$$

atleast in the case when G is linear (essentially because expression $-(1+b)$ acts like a "coefficient of restitution"). If this is fulfilled a small disturbance in initial condition will decay towards the sliding set through an infinite number of impacts in finite time ("chattering").

The linearization of the sliding vector can be attained by linearising with x replacing x^* and $\dot{x}$ on the right hand side of the first equation about $x = \bar{x}$, $\lambda = \bar{\lambda}$ at fixed μ. The result is

$$A_s = \left(I - \frac{BCA}{CAB} \right) A,$$

and we see that there is a 2x2 Jordan block corresponding to eigenvalue 0 with left eigenvector CA and left generalized eigenvector C. This of course corresponds to the invariance of the codimension two sliding set. The rest of the eigenvalues of A_s correspond to dynamics within the sliding set, and if all have negative real part, the pseudo-equilibrium is stable within the sliding set.

Example 4.2 (A simple 2D system)

Consider the system

$$
\begin{aligned}
F(x, \mu) &= \begin{pmatrix} x_2 \\ \mu - kx_1 + x_2 \end{pmatrix} \\
H(x) &= x_1 \\
G &= -(1 + r) \begin{pmatrix} 0 \\ 1 \end{pmatrix}
\end{aligned}
\tag{106}
$$

describing a 1DOF mechanical system with position x_1, velocity x_2, a spring force with spring constant k, damping coefficient -1, and an impact coefficient of restitution r. Note this is like an unforced, but negatively damped (energy inputting) version of Example 4.1. At $\bar{x} = 0$, $\bar{\mu} = 0$ we have a

78

boundary equilibrium. We find

$$
\begin{aligned}
v(x) &= x_2, \\
a(x) &= \mu - kx_1 + x_2, \\
b(x) &= -(1 + r), \\
F_s(x, \mu) &= \begin{pmatrix} x_2 \\ 0 \end{pmatrix}, \\
A &= \begin{pmatrix} 0 & 1 \\ -k & 1 \end{pmatrix}, \\
M &= \begin{pmatrix} 0 \\ 1 \end{pmatrix}, \\
C &= \begin{pmatrix} 1 & 0 \end{pmatrix}, \\
N &= 0, \\
B &= (1 + r) \begin{pmatrix} 0 \\ 1 \end{pmatrix}, \\
e &= 1/k, \\
s &= -(1 + r)/k, \\
A_s &= \begin{pmatrix} 0 & 1 \\ 0 & 0 \end{pmatrix}, .
\end{aligned}
$$

This is consistent with the explicit solution for the regular equilibrium

$$
\begin{aligned}
x^* &= \begin{pmatrix} \mu^*/k \\ 0 \end{pmatrix}, \\
\mu^*/k &> 0,
\end{aligned}
$$

and the pseudo-equilibrium

$$
\begin{aligned}
x^* &= \begin{pmatrix} 0 \\ 0 \end{pmatrix}, \\
\lambda^* &= -\mu^*/(1 + r), \\
\mu^*/(1 + r) &< 0.
\end{aligned}
$$

If $k = 1$ the regular equilibrium exists for $\mu > 0$ and the pseudo one for $\mu < 0$. If $k = -1$ none exist for $\mu > 0$ and both exist for $\mu < 0$. The regular equilibrium point is unstable (a saddle point if $k < 0$). The pseudo-equilibrium point is stable if $0 \leq r < 1$ (owing to stability of the sliding set; A_s has no non-trivial eigenvalues).

4.1.2 Existence of other invariant sets

Little is known about the existence of invariant sets besides equilibrium points when perturbing a boundary equilibrium. The type of analysis required clearly has a strong resemblance to the what would be needed in the corresponding cases for Filippov and nonsmooth continuous systems in Sections 2.1 and 3.1, where planar systems are fully understood, but only relatively weak results apply in three and higher dimensions. We will here merely give some examples where a single-impact limit cycles exist for the Example 4.1, equation (106). In each case, the limit cycle will branch off the boundary equilibrium as μ passes through 0. In particular we can show after some calculations that

- If $k = 1$, $0 \leq r < \exp(-\pi/\sqrt{3})$, and $\mu > 0$, a stable impacting limit cycle surrounds the regular unstable focus equilibrium point.

- If $k = 1$, $\exp(-\pi/\sqrt{3}) < r < 1$, and $\mu < 0$, an unstable impacting limit cycle surrounds the stable pseudo-equilibrium point.

- If $k = -1$, $(3 - \sqrt{5})/2 < r < 1$, and $\mu < 0$, an unstable impacting limit cycle surrounds the stable pseudo-equilibrium point, but not the regular saddle point.

Figure 41 shows one example of each these situations.

4.2 Nonsmooth transitions of Limit Cycles 1; Grazing

We will again consider systems that (at least locally) take the form, given at the beginning of this section,

$$\dot{x} = F(x) \quad \text{if } H(x) > 0$$

with impact at the surface defined by $H(x) = 0$, and where the impact law takes the form

$$x^+ = R(x^-) = x^- + G(x^-)H_x F(x^-).$$

In such a system, there is the possibility of having a periodic orbit that contains an isolated point of zero impact velocity $H_x F$. This is called a *grazing* impact. Due to the assumed form of the impact law R, it will have no effect on the orbit, so we may or may not regard this as an impact. Nearby trajectories may have a low velocity impact close to the grazing
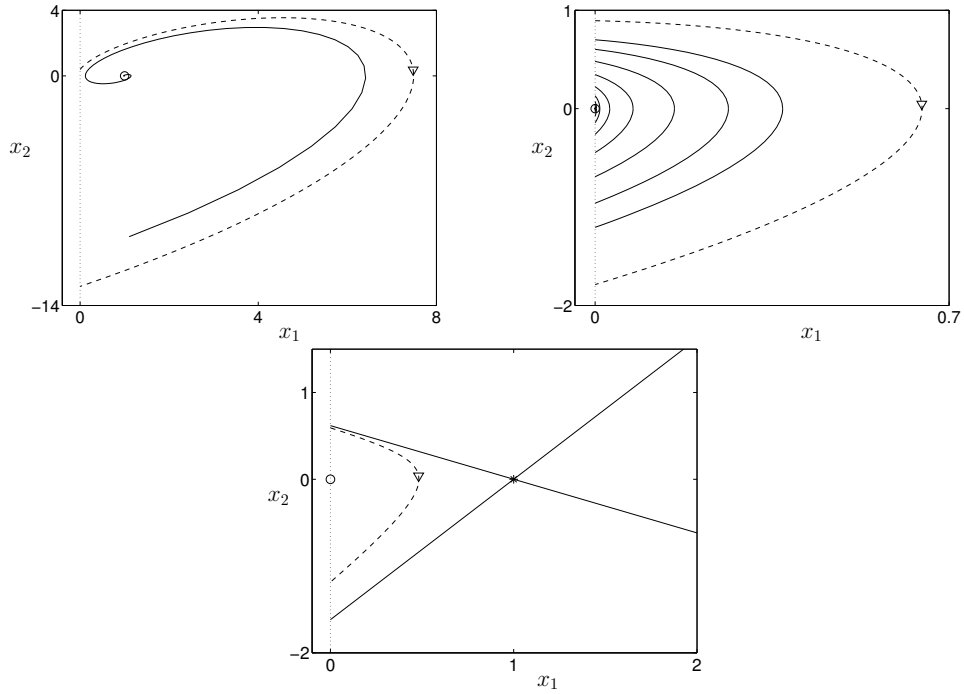
Figure 41: Limit cycles in boundary equilibrium bifurcations. Top left: $k=1$, $r = 0.03$, $\mu = 1$. Impacting stable limit cycle (dashed) together with orbit (solid) starting near unstable focus (circle). Top right: $k=1$, $r = 0.5$, $\mu = -1$. Impacting unstable limit cycle (dashed) together with chattering orbit (solid) converging to the stable pseudo-equilibrium (circle). Bottom: $k=-1$, $r = 0.5$, $\mu = -1$. Impacting unstable limit cycle (dashed) together with stable pseudo-equilibrium (circle), saddle point (star), and the non-impacting parts of its stable and unstable manifolds.
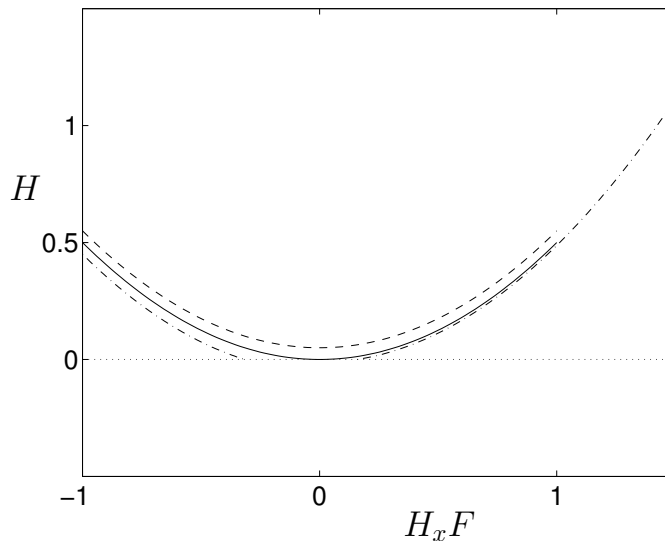
Figure 42: A grazing trajectory (solid), an impacting trajectory (dot-dashed), and a missing trajectory (dashed), all simulated for the same amount of time. Note the large shift in endpoint for the trajectory with a low velocity impact.

impact point, or they may miss the impact surface, see Figure 42. Since nearby trajectories can undergo different events, it is suitable to encapsulate this into a discontinuity mapping acting on a neighborhood of the grazing point.

4.2.1 Discontinuity mappings for grazing impact

The derivation and form of the discontinuity mapping for grazing impact has been presented for one degree driven impact oscillators in [58], and for more general systems in [36]. The results presented here have been adapted to the more general form of system specified by arbitary F, G, and H.

Consider the *grazing set* $\Sigma_0 \subset \Sigma$ where the

$$
\begin{aligned}
H(x) &= 0, \\
H_x F(x) &= 0, \\
(H_x F)_x F(x) &> a_0 > 0.
\end{aligned}
$$

We assume all functions to be as smooth as necessary in a neighborhood of Σ_0. Through each point of Σ_0 passes a grazing trajectory of the system that

82

has a quadratic tangency to the impact surface. The form of the impact law ensures that grazing trajectories are well defined whether they are considered as impacting or not, and that incoming trajectories that are close stay close after passing trough a neighborhood of Σ_0. In a neighborhood of Σ_0 we define a ZDM as the identity if the trajectory does not impact, and as the result of going through an impact and returning to time zero along the flow, if the trajectory impacts. See Figure 43. We find
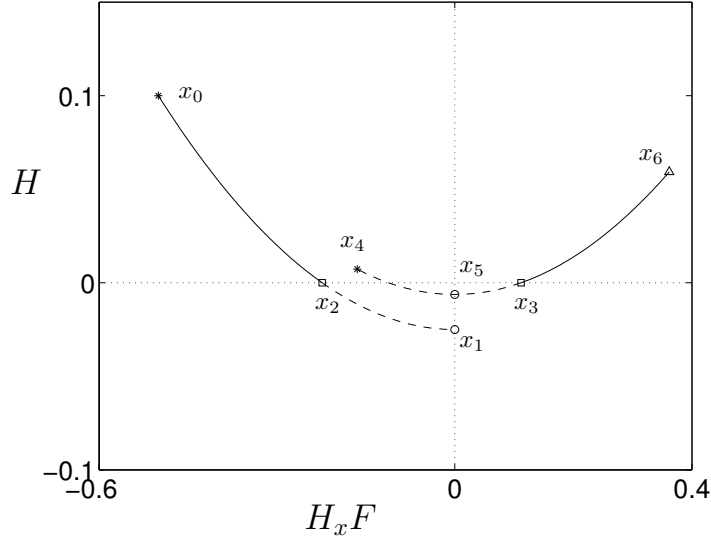
Figure 43: Discontinuity mappings for grazing impact. A trajectory starts at x_0, impacts at x_2, is mapped to x_3 by the impact law, and continues to x_6. The ZDM maps x_0 to x_4. The PDM maps x_1 to x_5.

Theorem 4.2 (The ZDM for grazing impact) *For systems in this class, there is a neighborhood of Σ_0 where the ZDM can be written*

$$ZDM(x) = x + \begin{cases} 0 & \textit{if } H_{\min}(x,v) \geq 0, \\ \beta(x,y,v)y & \textit{if } H_{\min}(x,v) < 0 \end{cases}, \qquad (107)$$

83

where

$$\begin{aligned}
\beta(x,y,v) &= -G(x)\sqrt{2a} + r_2(x,y,v), \\
r_2(x,y,v) &\to 0 \quad \text{if } y, v \to 0, \\
y(x,v) &= \sqrt{-H_{\min}(x,v)}, \\
H_{\min}(x,v) &= H(x) - v^2\left(\frac{1}{2a} + r_1(x,v)\right), \\
r_1(x,v) &\to 0 \quad \text{if } v \to 0, \\
v(x) &= H_x F(x), \\
a(x) &= v_x F(x),
\end{aligned} \tag{108}$$

and β and $H_{\min}$ are smooth in their arguments.

Note that the set Σ_0 is determined by H and $H_x F$ being zero and that the auxiliary variables v and y are independent variables measuring the closeness of x to Σ_0. Note also that y is not smooth when $H_{\min} = 0$. Thus the full ZDM is not smooth at points where $H_{\min} = 0$. The lowest order approximation is

$$\begin{aligned}
\beta(x,y,v) &\approx -G(x)\sqrt{2a}, \\
H_{\min}(x,v) &\approx H(x).
\end{aligned}$$

By choosing an incoming and a (possibly different) outgoing surface that are both transversal to the flow and that both contain Σ_0, we can derive PDMs for grazing impact. A convenient surface to use is $H_x F = 0$, which satisfies all requirements. For this choice, also illustrated in Figure 43, we find

Theorem 4.3 (A PDM for grazing impact) *For systems in this class, there is a neighborhood of Σ_0 where the PDM from an incoming to an outgoing $H_x F = 0$ surface can be written*

$$PDM(x) = x + \begin{cases} 0 & \text{if } H(x) \geq 0 \\ \beta(x,y)y & \text{if } H(x) < 0 \end{cases}, \tag{109}$$

where

$$\begin{aligned}
\beta(x,y) &= -\sqrt{2a}\left(G(x) - \frac{b}{a}F(x)\right) + r_2(x,y), \\
r_2(x,y) &\to 0 \quad \text{if } y \to 0, \\
y(x) &= \sqrt{-H(x)}, \\
a(x) &= (H_x F)_x F(x), \\
b(x) &= (H_x F)_x G(x),
\end{aligned} \tag{110}$$

and β is smooth in its arguments.

Note that H attains its minimum in the Poincaré surface, so no calculation of the minimum value is needed. Note also that if F and G are parallel, the lowest order term of β drops out.

Example 4.3 (An explicitly calculable model)

Consider an undamped, undriven single-degree-of-freedom linear impact oscillator model with angular frequency 1, where x_1 is displacement and x_2 is velocity, the equilibrium position is at $x_1 = 1$, and there is impact at $x_1 = 0$. We write the state variables collectively as

$$x = \begin{pmatrix} x_1 \\ x_2 \end{pmatrix}.$$

The ODE system is

$$\dot{x} = \begin{pmatrix} x_2 \\ 1 - x_1 \end{pmatrix}$$

when $x_1 > 0$. At $x_1 = 0$ an impact with coefficient of restitution r takes place: $x_2^+ = -r v_2^-$. In the notation of the general theory, we have

$$
\begin{aligned}
F(x) &= \begin{pmatrix} x_2 \\ 1 - x_1 \end{pmatrix}, \\
H(x) &= x_1, \\
G(x) &= -(1 + r) \begin{pmatrix} 0 \\ 1 \end{pmatrix}.
\end{aligned}
$$

At $x_1 = 0$ there is a grazing impact with acceleration

$$a(x) = (H_x F)_x F = 1 - x_1 > 0.$$

For this system the ZDM can be explicitly computed and we find

$$
H_{\min}(x, v) = 1 - \sqrt{(1 - x_1)^2 + v^2}, \tag{111}
$$

$$
\beta(x, y, v) = (1 + r)\frac{\left[\sqrt{2(1 - \chi_1) - y^2} + \chi_2 y/(1 - \chi_1) \right]}{(1 - \chi_1)\sqrt{(1 - x_1)^2 + v^2}},
$$

$$
\begin{pmatrix} y(1 - x_1)\sqrt{2(1 - \chi_1) - y^2} + v(1 - \chi_1 - y^2) \\ (1 - x_1)(1 - \chi_1 - y^2) - vy\sqrt{2(1 - \chi_1) - y^2} \end{pmatrix}, \tag{112}
$$

85

where

$$y = \sqrt{-H_{\min}(x)},$$

$$\chi_1 = 1 - \frac{(1-x_1)^2 + x_2 v}{\sqrt{(1-x_1)^2 + v^2}},$$

$$\chi_2 = \frac{(x_2 - v)(1 - x_1)}{\sqrt{(1-x_1)^2 + v^2}},$$

$$v = x_2.$$

The result is seen to be in agreement with equations (107)–(108). Using the relations between y, v and x, we can simplify (111)–(112) into

$$H_{\min}(x) = 1 - \sqrt{(1-x_1)^2 + x_2^2},$$

$$\beta(x,y) = (1+r)\frac{\sqrt{2+y^2}}{(1+y^2)^2}\left(\frac{x_2 + (1-x_1)y\sqrt{2+y^2}}{(1-x_1) - x_2 y\sqrt{2+y^2}}\right).$$

The PDM can also be explicitly computed and we find

$$\beta(x,y) = \frac{(1-x_1)(\sigma - 2\tau - y\tau^2)}{\sqrt{1+y\sigma}(\sqrt{1+y\sigma} + 1 + y\tau)}\binom{1}{0}, \qquad (113)$$

where

$$y = \sqrt{-x_1},$$

$$\sigma = -y\frac{1+r}{(1-x_1)^4}\{(2(1-x_1) - y^2)(1-x_1)^2(1-r),$$

$$-x_2 y[x_2 y(1+r) + 2\sqrt{2(1-x_1) - y^2}(1-x_1)r]\},$$

$$\tau = -\frac{1+r}{(1-x_1)^4}\{y(2(1-x_1) - y^2)(1-x_1)^2(1-r),$$

$$-x_2[x_2 y(1 - x_1 + ry^2),$$

$$+\sqrt{2(1-x_1) - y^2}(1 - x_1 - y^2 + 2y^2(1-x_1)r + x_1 y^2)]\}.$$

This lengthy expression is seen to be in agreement with equations (109)–(110). Setting $x_1 = -y^2$ and $x_2 = 0$ simplifies (113) into

$$\beta(x,y) = \frac{y(1-r^2)\sqrt{2+y^2}}{1+y^2 + \sqrt{1+r^2 y^2(2+y^2)}}\binom{1}{0}.$$

86

4.2.2 Poincaré mappings for the full system

The PDM

$$D(x) = x + \begin{cases} 0 & \text{if } H(x) \geq 0 \\ \beta(x,y)y & \text{if } H(x) < 0 \end{cases},$$

where

$$y(x) = \sqrt{-H(x)}$$

can now be composed with a mapping $P(x)$ from the outgoing surface to the incoming, where any low velocity impacts in the beginning or towards the end is disregarded, and it is assumed that no low velocity impacts are taking place elsewhere. In that case, the mapping P is smooth, and the full mapping from the outgoing surface back to itself is $D \circ P$ and contains all dynamics.

Note again that this mapping is not the usual Poincaré mapping derived from the same section, as the low velocity impact is always taken into account at the end of the mapping, whereas in the usual Poincaré mapping, low velocity impacts could come either in the beginning or at the end. Usual Poincaré mappings are best taken at a section away from Σ_0. On the other hand, the mapping $D \circ P$ is *topologically equivalent* to any Poincaré mapping using a section away from Σ_0, and so it can be used to analyze the dynamics. These observations echo those made for Example 2.3 earlier for non-impacting systems.

Example 4.4 (Another explicitly calculable model)

We now consider a somewhat artificial example where we can compute all mappings explicitly. Let x_1 and x_2 be position and velocity, and the x_3 be a variable defined modulo 4 that keeps track of the driving phase. We write the state variables collectively as

$$x = \begin{pmatrix} x_1 \\ x_2 \\ x_3 \end{pmatrix}.$$

The three-dimensional ODE system for $x_1 > 0$ will be taken to have different forms depending on the values of x_3. For $x_1 > 0$, $0 < x_3 < 2$ (region S_1) we use

$$\dot{x} = \begin{pmatrix} x_2 \\ \dot{x}_{2p} - (2d/w)(x_2 - x_{2p}) - (1/w^2)(x_1 - x_{1p}) \\ 1 \end{pmatrix},$$

where the particular solution x_p is

$$\begin{pmatrix} x_{1p} \\ x_{2p} \end{pmatrix}(x_3) = \begin{pmatrix} 1/2 + \mu + x_3 - x_3^2/2 \\ 1 - x_3 \end{pmatrix}.$$

For $x_1 > 0$, $2 < x_3 < 4$ (region S_2) we use

$$\dot{x} = \begin{pmatrix} x_2 \\ 1 \\ 1 \end{pmatrix}.$$

As $\dot{x}_3 = 1$ there is no possibility of sliding of the boundary between regions S_1 and S_2. At $x_1 = 0$ an impact with coefficient of restitution r takes place: $x_2^+ = -rx_2^-$.

In S_1 the system is controlled towards the particular solution x_p using the positive control parameters d and w, and the position of the particular solution is determined by the parameter μ. In this region, the particular solution represents those initial conditions that lead to constant negative acceleration equal to -1. In region S_2, the acceleration is constant and equal to 1.

When $\mu > 0$, the system admits a non-impacting periodic solution

$$\begin{pmatrix} x_1 \\ x_2 \end{pmatrix} = x_p = \begin{pmatrix} 1/2 + \mu + x_3 - x_3^2/2 \\ 1 - x_3 \end{pmatrix}$$

in S_1, and

$$\begin{pmatrix} x \\ v \end{pmatrix} = \begin{pmatrix} 1/2 + \mu - (x_3 - 2) + (x_3 - 2)^2/2 \\ -1 + (x_3 - 2) \end{pmatrix}$$

in S_2. The minimal x_1 value of this orbit is μ at $x_3 = 3$. When $\mu = 0$ we have a periodic orbit with a grazing impact at

$$x^* = \begin{pmatrix} 0 \\ 0 \\ 3 \end{pmatrix}.$$

The grazing orbit is shown in Figure 44.

For this system we can explicitly write down mappings for trajectories close to the grazing one. The flow mapping for region S_1 is, assuming no impacts and $0 \leq x_3, x_3 + t \leq 2$,

$$\Phi_1(x,t) = \begin{pmatrix} A_1(t)\left[\begin{pmatrix} x_1 \\ x_2 \end{pmatrix} - \begin{pmatrix} x_1 \\ x_2 \end{pmatrix}_p(x_3)\right] + \begin{pmatrix} x_1 \\ x_2 \end{pmatrix}_p(x_3 + t) \\ x_3 + t \end{pmatrix}$$
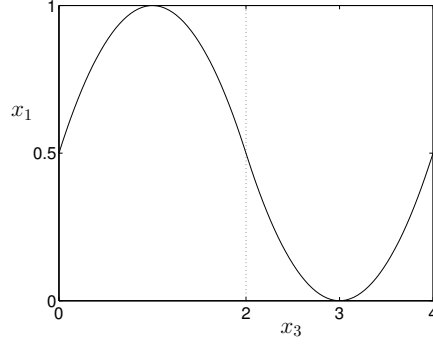
88

Figure 44: Grazing periodic orbit of Example 4.4.

where

$$A_1(t) = e^{B_1 t},$$

$$B_1 = \begin{pmatrix} 0 & 1 \\ -(2d/w) & -(1/w^2) \end{pmatrix}.$$

In region S_2, there is at most one impact. Assuming no impacts and $2 \leq x_3, x_3 + t \leq 4$ the flow mapping is

$$\Phi_2(x, t) = \begin{pmatrix} x_1 + x_2 t + t^2/2 \\ x_2 + t \\ x_3 + t \end{pmatrix}.$$

For initial conditions with $x_3 < 3$ near the grazing periodic orbit, there is a low velocity impact near $x_3 = 3$ precisely if

$$H_{\min}(x) = x_1 - x_2^2/2$$

is negative. If we take an impact into account whenever $H_{\min}(x) < 0$ (regardless of whether the impact takes place inside or outside of the time interval studied), we arrive at the mapping

$$\Phi_2'(x, t) = \Phi_2(x, t) + \begin{cases} 0 & \text{if } H_{\min}(x) \geq 0, \\ \sqrt{2}(1 + r) \begin{pmatrix} \sqrt{2}y + x_2 + t \\ 1 \\ 0 \end{pmatrix} y & \text{if } H_{\min}(x) < 0, \end{cases}$$

$$(114)$$

where $y = \sqrt{-H_{\min}(x)}$. Setting $t = 0$ in (114) gives us the ZDM

$$D(x) = x + \begin{cases} 0 & \text{if } H_{\min}(x) \geq 0 \\ \beta(x, y)y & \text{if } H_{\min}(x) < 0 \end{cases},$$

89

where

$$\beta(x, y) = \sqrt{2}(1 + r) \begin{pmatrix} \sqrt{2}y + x_2 \\ 1 \\ 0 \end{pmatrix}.$$

These results for $H_{\min}$ and β are in agreement with the equations (107)–(108) of the grazing ZDM for a system with impact, if the expression for $v = x_2$ is introduced.

Knowing these mappings we can easily build other mappings. For example, a Poincaré mapping from the surface $x_3 = 0$ back to itself, is $\Phi_2(\cdot, 1) \circ D \circ \Phi_2(\cdot, 1) \circ \Phi_1(\cdot, 2)$ near the grazing periodic orbit. An equivalent mapping is $D \circ \Phi_2(\cdot, 1) \circ \Phi_1(\cdot, 2) \circ \Phi_2(\cdot, 1)$, which is essentially the Poincaré mapping at $x_3 = 3$, except the impact is always taken into account last. Using only

$$z = \begin{pmatrix} x_1 \\ x_2 \end{pmatrix}$$

as the variables, the mapping can be written $D \circ P$, where

$$P(z) = Az + M\mu,$$

and

$$
\begin{aligned}
A &= \begin{pmatrix} 1 & 1 \\ 0 & 1 \end{pmatrix} A_1(2) \begin{pmatrix} 1 & 1 \\ 0 & 1 \end{pmatrix}, \\
M &= \begin{pmatrix} 1 \\ 0 \end{pmatrix} - \begin{pmatrix} 1 & 1 \\ 0 & 1 \end{pmatrix} A_1(2) \begin{pmatrix} 1 \\ 0 \end{pmatrix},
\end{aligned}
$$

and

$$D(z) = z + \begin{cases} 0 & \text{if } h(z) \geq 0 \\ b(z, y)y & \text{if } h(z) < 0 \end{cases},$$

where

$$
\begin{aligned}
b(z, y) &= \sqrt{2}(1 + r) \begin{pmatrix} \sqrt{2}y + x_2 \\ 1 \end{pmatrix}, \\
H(z) &= x_1 - x_2^2/2.
\end{aligned}
$$

4.2.3 Unfolding a grazing periodic orbit

The dynamical behaviour nearby (in state and parameter space) to a grazing orbit can be quite rich, with the grazing orbit being at the limit point of an infinite series of other smooth and non-smooth transitions. Various aspects

90

of it have been studied in [58, 12, 11, 59, 36, 60]. It has been shown that up to an infinite number of different periodic orbits can branch off the grazing orbit as a parameter is varied, and also that a chaotic attractor may exist. Here we will present some results that are valid in any finite number of space dimensions.

4.2.4 Existence of low period periodic orbits

Assume that the system depends on single parameter μ, and that $x = \bar{x}$, $\mu = \bar{\mu}$ satisfies

$$
\begin{aligned}
P(\bar{x}, \bar{\mu}) &= \bar{x}, \\
H(\bar{x}, \bar{\mu}) &= 0.
\end{aligned}
$$

This means that $\bar{x}$ lies on a grazing periodic orbit. If the parameter μ is changed, non-impacting and/or impacting periodic orbits (fixed or periodic point for the mapping) may branch off the grazing orbit. Finding all of these is a difficult task, given that the Poincaré mapping has different expressions depending on the sign of H at each iterate, but if one decides to look for a specific period and a specific pattern of signs of H for each iterate, one can formulate a smooth system of equations to solve, whose solutions are subject to the condition that they must agree with the assumed pattern. In the following, when an iterate is referred to as being "impacting" or not, we mean the presence or not of a low velocity impact near the grazing point. There may well be other impacts along the trajectory.

Thus, the conditions for a non-impacting period-one point are

$$
\begin{aligned}
P(x^*, \mu^*) &= x^*, \\
H(x^*, \mu^*) &> 0,
\end{aligned}
$$

and the conditions for a single-impact period-one point are

$$
\begin{aligned}
P(x^*, \mu^*) + \beta(P(x^*, \mu^*), y^*, \mu^*)y^* &= x^*, \\
H(P(x^*, \mu^*), \mu^*) + y^2 &= 0, \\
y^* &> 0.
\end{aligned}
$$

Assuming for simplicity $\bar{x} = \bar{\mu} = 0$ and linearizing, we find

$$
\begin{aligned}
Ax^* + M\mu^* &= x^* \\
Cx^* + N\mu^* &> 0
\end{aligned}
$$

91

for the non-impacting period-one point

$$
\begin{aligned}
Ax^* + M\mu^* + By^* &= x^*, \\
CAx^* + (CM + N)\mu^* &= 0, \\
y^* &> 0,
\end{aligned}
$$

for the single-impact period-one point, where

$$
\begin{aligned}
A &= P_x(\bar{x}, \bar{\mu}), \\
M &= P_\mu(\bar{x}, \bar{\mu}), \\
C &= H_x(\bar{x}, \bar{\mu}), \\
N &= H_\mu(\bar{x}, \bar{\mu}), \\
B &= \beta(\bar{x}, 0, \bar{\mu}), \\
CB &= 0.
\end{aligned}
$$

If the linear systems are not degenerate, they will be representative of what happens locally in the full system. Introducing the notation

$$
s(\lambda, n) = CA^n(\lambda I - A^n)^{-1} B
$$

we find

Theorem 4.4 (Period 1 orbits branching from a grazing orbit) *For systems in this class, and assuming*

$$
\begin{aligned}
\det(I - A) &\neq 0 \\
e = N + C(I - A)^{-1}M &\neq 0 \\
s(1, 1) = CA(I - A)^{-1}B &\neq 0,
\end{aligned}
$$

there exists a unique non-impacting period-one point branching off from $\bar{x}$ when $e(\mu^* - \bar{\mu})$ is small and positive, and a unique single-impact period-one point branching off from $\bar{x}$ when $(e/s(1, 1))(\mu^* - \bar{\mu})$ is small and negative. The derivative of the points with respect to the parameter exist and has a limit as $\mu^* \to \bar{\mu}$ from the side where the point exists.

We note that if $s(1, 1) < 0$, the non-impact and single-impact points are both present for one sign of $\mu^* - \bar{\mu}$ and none are present for the other sign. Thus one can say that the points annihilate each other as μ^* changes, much like in a saddle-node bifurcation for smooth systems. If $s(1, 1) > 0$, one equilibrium point is present for any small value of $\mu^* - \bar{\mu}$, and the non-impact is transformed into a single-impact point as μ^* changes. Note the similarity of this result to Theorem 4.1 for equilibria.

Concerning orbits of period-two, a non-impacting orbit branching off the grazing orbit will in general (if A does not have an eigenvalue -1) just be the the non-impacting period-one orbit traversed twice, and likewise for a double-impact orbit, so the interesting case is when a period-two point has a single impact. Then we find the equations

$$
\begin{aligned}
P(x_1^*, \mu^*) &= x_2^* \\
P(x_2^*, \mu^*) + \beta(P(x_2^*, \mu^*), y^*, \mu^*)y^* &= x_1^* \\
H(P(x_2^*, \mu^*), \mu^*) + y^2 &= 0 \\
H(x_2^*, \mu^*) &> 0 \\
y^* &> 0
\end{aligned}
$$

(note that suffixes means iterate numbers here, not component numbers). Linearizing as before, we find

Theorem 4.5 (Period 2 orbits branching from a grazing orbit) *For systems in this class, and assuming*

$$
\begin{aligned}
\det(I - A) &\neq 0 \\
\det(I + A) &\neq 0 \\
e = N + C(I - A)^{-1}M &\neq 0 \\
s(-1, 1) = -CA(I + A)^{-1}B &< 0 \\
s(1, 2) = CA^2(I - A^2)^{-1}B = (s(1,1) + s(-1,1))/2 &\neq 0,
\end{aligned}
$$

there exists a unique single-impact period-two point branching off from $\bar{x}$ when $(e/s(1,2))(\mu^* - \bar{\mu})$ is small and negative. The derivative of the points with respect to the parameter exist and has a limit as $\mu^* \to \bar{\mu}$ from the side where the point exists.

Note that $s(-1, 1)$ determines if the orbit is possible, and $s(1, 2)$ on which side of the transition the orbit exists. Note also that the relation between $s(1, 1)$, $s(-1, 1)$ and $s(1, 2)$ shows the impossibility of having a non-impacting and a single-impact period-one orbit on one side of the transition, and a single-impact period-two orbit on the other side.

One can note that these results have a strong resemblance to the results for existence in continuous piecewise smooth mappings [24]. This is a strong hint that there are underlying topological properties that may be used to shed light on these results.

For higher periods the analytical solution of the linearized equation and conditions becomes more complicated, but there is of course no problem with

solving the linearized equations numerically for a given system, and then checking the linearized inequalities. In this way the existence of periodic orbit up to say period-ten can be quickly established for a given grazing bifurcation.

For two-dimensional mappings, the situation is known more completely, see [60].

Stability The stability of the non-impacting orbit is determined by the eigenvalues of A. If all eigenvalues are within the unit circle, the orbit is stable. For the single-impact period-one orbit, if $CAB \neq 0$ the orbit must be unstable with an eigenvalue approaching $-CAB/(2y)$ as the transition point is approached. For the single-impact period-two orbit, if $CA^2B \neq 0$ the orbit must likewise be unstable with an eigenvalue approaching $-CA^2B/(2y)$. In general, all impacting orbits that branch off the grazing orbit are violently unstable close to the transition point unless there is some additional degeneracy. Away from the transition point, the branches may well turn stable, of course (see e.g. [60] for an example where this happens).

4.2.5 Attractors

Although all impacting periodic orbits are in general found to be unstable close to the transition point, there is nonetheless a possibility of finding an attractor branching off the grazing orbit. An attractor is guaranteed, if we can show that the grazing orbit is asymptotically stable. The stability of the grazing orbit, depends on whether repeated low velocity impacts can be avoided, as each such impact, through the square root terms, tend to shift motion away from the grazing orbit by a (relatively) large amount. Repeated impacts are avoided if $CA^nB > 0$ for all $n > 0$, Thus we have

Theorem 4.6 (Stability of a grazing orbit) *For systems in this class, a grazing orbit is stable if A is stable (all eigenvalues within the unit circle) and $CA^nB > 0$ for all $n > 0$. If $CA^{n_1}B < 0$ for some $n_1 > 0$, the grazing orbit is unstable.*

For a 2D mapping, the conditions for stability (and the existence of an attractor) are fulfilled if the eigenvalues of A satisfy $0 < \lambda_2 < \lambda_1 < 1$ and $CAB > 0$. For N-dimensional mappings, if A has a single positive stable eigenvalue λ_1 of largest modulus with right eigenvector ϕ and left eigenvector ϕ^*, and $(C\phi)(\phi^*B)/(\phi^*\phi) > 0$, then $CA^nB > 0$ for large enough n, so only a finite number of CA^nB need be checked.

94

Assuming we have this situation of a single positive stable eigenvalue λ_1 of largest modulus, and a non-zero value of e, we will have 1 stable non-impacting period 1 orbit when $e(\mu - \bar{\mu}) > 0$. When $e(\mu - \bar{\mu}) < 0$ there is an attractor of size proportional to $\sqrt{-e(\mu - \bar{\mu})}$. The dynamics of this attractor depends mainly on the value of λ_1, see [59].

- If $2/3 < \lambda_1 < 1$ there will be a chaotic attractor for all small negative $e(\mu - \bar{\mu})$.

- If $1/4 < \lambda_1 < 2/3$ there will be an alternating sequence of chaotic and stable periodic motion for small negative $e(\mu - \bar{\mu})$. Each chaotic or periodic band is mapped to the next if $\mu - \bar{\mu}$ is multiplied by a factor that has the asymptotic value λ_1^2 as $\mu - \bar{\mu} \to 0$. The period of the periodic motion is increased by 1 from one band to the next ("period-adding"). For λ_1 close to $2/3$ the periodic bands will be narrow, and for λ_1 close to $1/4$ the chaotic bands will be narrow.

- If $0 < \lambda_1 < 1/4$ the periodic bands start to overlap and there is no attracting chaotic motion for small negative $e(\mu - \bar{\mu})$. The same parameter scaling as before applies. For each parameter value, there is either a unique stable periodic orbit, or two different stable orbits with periods differing by 1.

The chaotic attractor, when it exists, has a general structure consisting of segments in the positive $A^n B$ directions for $0 \leq n \leq N$. The segments gets thinner and their number increases as $\mu \to \bar{\mu}$.

Let us end this discussion on grazing in impacting systems with two examples that illustrate this period-adding and chaos.

Return to Example 4.4
In the example system, set $d = 0.7$, $w = 2$, and $r = 0.8$. This gives

$$
\begin{aligned}
A &= \begin{pmatrix} 0.4663 & 1.4337 \\ -0.2277 & -0.1713 \end{pmatrix}, \\
M &= \begin{pmatrix} 0.5337 \\ 0.2277 \end{pmatrix}, \\
B &= \begin{pmatrix} 0 \\ 2.5456 \end{pmatrix}, \\
C &= \begin{pmatrix} 1 & 0 \end{pmatrix}, \\
N &= 0.
\end{aligned}
$$

Checking orbits up to period-three, we find for small positive μ there is a non-impacting period-one orbit and single impact period-three orbit, and for small negative μ there are single-impact unstable orbits of periods one and two, as well as a double impact orbit of period three. Since $CA^3B < 0$, there is no continuous transition from the non-impacting orbits into an attractor as μ decreases through 0. All impacting orbits are highly unstable close to the transition point. In the left panel of Figure 45 we can see how the stable non-impacting period-one orbit existing when $\mu = 0.4$ vanishes at $\mu = 0$. The single impact orbit of period three becomes stable in a saddle-node bifurcation near $\mu = 0.1$, but vanishes in another grazing transition just below $\mu = 0$. The single impact orbit of period-two becomes stable in a period-doubling bifurcation near $\mu = -0.3$, and is still stable at $\mu = -0.6$. There are several other bifurcations/transitions in this plot.
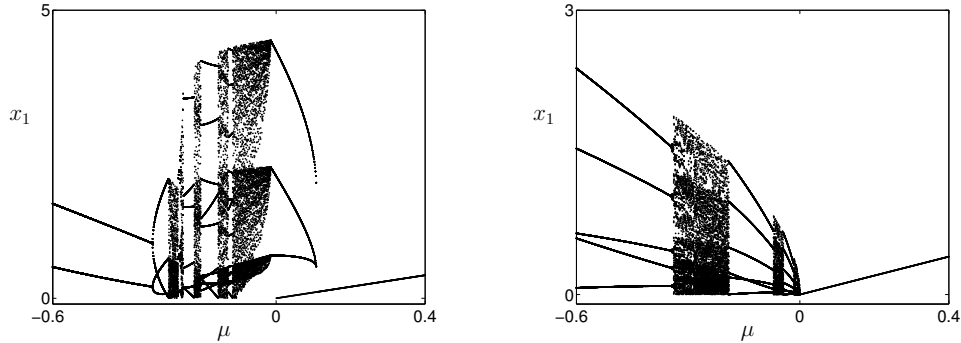

Figure 45: Grazing transitions in the example system. Left: $d = 0.7$, $w = 2$, $r = 0.8$. Discontinuous transition. Right: $d = 1.5$, $w = 5$, $r = 0.8$. Continuous transition.

Now change the parameters to $d = 1.5$, $w = 5$, and $r = 0.8$. This gives

$$
A = \begin{pmatrix} 0.7883 & 1.6660 \\ -0.0895 & -0.0175 \end{pmatrix},
$$
$$
M = \begin{pmatrix} 0.2117 \\ 0.0895 \end{pmatrix}.
$$

The eigenvalues of A are 0.50 and 0.27 and thus we should have a continuous transition from a non-impacting periodic orbit to an attractor. Since the largest eigenvalue is between $1/4$ and $2/3$, we expect periodic windows with increasing periods, with the size of the windows scaling by 0.50^2 near the transition point. This is shown in the right panel of Figure 45. Periodic

96

windows of periods 5, 6, and 7 can be distinguished, with the higher periodic windows being too narrow to be seen. When there is a chaotic attractor, it has a charatcteristic *fingered structure*, as shown in Figure 46.
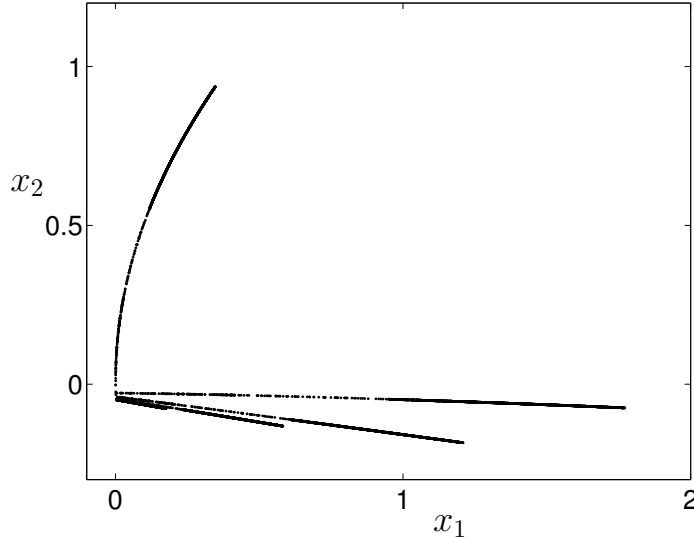

Figure 46: Star-shaped chaotic attractor when $d = 1.5$, $w = 5$, $r = 0.8$, $\mu = -0.3$.

Example 4.5 (Application to an impacting pendulum)

In [67] a simple rigid-arm pendulum that strikes an impact surface is considered experimentally (see right panel of Fig. 1). By horizontally shaking the supporting pivot of the pendulum a variety of dynamic behavior can be observed including chaos. However, with the impact barrier located at static equilibrium the velocity of impact tends to be relatively high and thus grazing bifurcations of the fundamental period-one orbit do not typically occur. But, by inclining the angle $\hat{\theta}$ at which the pendulum mass strikes the barrier (see left panel of Fig. 1), it is possible to observe a transition between non-impacting and impacting dynamic behavior.Due to speed limitations of the forcing mechanism the assembly isinclined at an angle of Θ (out of plane, see middle panel of Fig. 1) in order to change the effect of gravity, i.e., $g_e = \cos(\Theta)g$, and thus reduce the natural frequency of the system. For a more careful discussion of this system see [6, 73, 67].

The nondimensionalized equations of motion for the mechanism described above can be written

$$
\dot{x} = \begin{pmatrix} \dot{x}_1 \\ \dot{x}_2 \\ \dot{x}_3 \end{pmatrix} = \begin{pmatrix} x_2 \\ \alpha \cos(x_1 + \hat{\theta}) \sin(x_3) - \frac{2\beta}{\eta} x_2 - \frac{1}{4\eta^2} \sin(x_1 + \hat{\theta}) \\ 1 \end{pmatrix},
$$
(115)

where $(x_1, x_2, x_3)^T = \left(\theta - \hat{\theta}, \theta', \tau \mod 2\pi \right)^T$ and

$$
\eta = \frac{\omega}{\omega_0}, \quad \omega_0 = 2\sqrt{\frac{g_e}{L}}, \quad \tau = \omega t, \quad \alpha = \frac{A}{L}, \quad \beta = \frac{\kappa}{2\omega_0}.
$$
(116)

Here ω_0 is the frequency of small amplitude motion of the impacting oscillator (when $\hat{\theta} = 0$), which is twice the natural frequency of the non-impacting system. At impact, as $x_1 = 0$, we assume a simple restitution law of the form (100) is applied, thus

$$
x^+ = x^- + \begin{pmatrix} 0 \\ 1 + r \\ 0 \end{pmatrix} x_2^-,
$$
(117)

where r is the coefficient of restitution. We assume further that x_{im} an τ_{im} is the point and time of grazing, respectively, i.e. $h(x(\tau_{\mathrm{im}})) = h(x_{\mathrm{im}}) = 0$. Following (107) and (108) the ZDM for the present system can be written

$$
D(x) = \begin{cases} x + \begin{pmatrix} 0 \\ 1 + r \\ 0 \end{pmatrix} \sqrt{-2x_1 a(x_{\mathrm{im}})}, & h(x) \leq 0, \\ x, & h(x) > 0, \end{cases}
$$
(118)

where we have used $y = \sqrt{-x_1}$, $a = x_2'$ and $x_{\mathrm{im}} = (0, 0, \tau_{\mathrm{im}})^T$. The complete Poincaré map Π around the grazing periodic orbit can be written as

$$
\Pi(x, T) = \Phi_2(x, T - \tau_{\mathrm{im}}) \circ D(x) \circ \Phi_1(x, \tau_{\mathrm{im}}),
$$
(119)

where $T > 0$ is the period of the grazing periodic orbit, Φ_1 and Φ_2 are the flow function before and after the grazing (cf. sect. 4.2.2). Estimation of the motion near grazing using the map (119) can be compared with experimental results and direct numerical simulations. In Figs. 47(a) and (b) bifurcation diagrams close to grazing using direct numerical simulations and the full Poincaré map (119) are shown, respectively. As expected, a striking
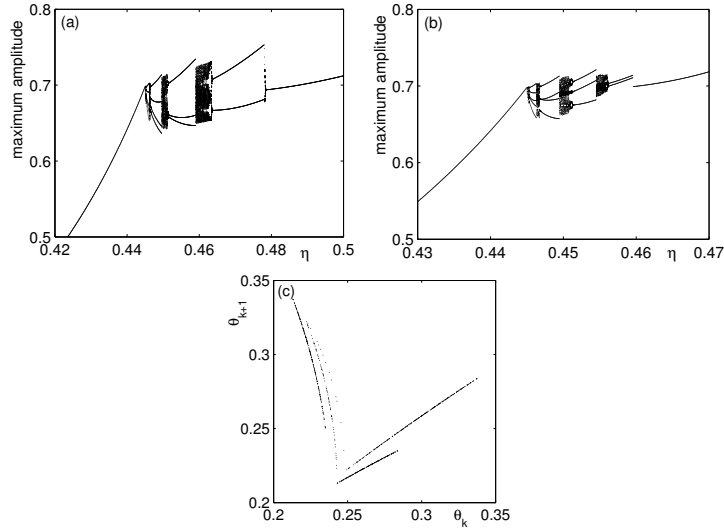
Figure 47: Grazing transitions in the forced impacting pendulum under variation of η and using (a) direct numerical simulation, (b) the full Poincaré map including the ZDM. (c) Delay plots for the impacting pendulum near grazing using direct numerical simulation (cf. Fig.1). In all figures the angle of the impact barrier $\hat{\theta} = 40°$.

similarity between the two methods are found. In this particular example the in magnitude largest eigenvalue is $|\lambda_{\max}| \approx 0.51$ for the grazing orbit and therefore, as expected (see sect. 4.2.5), a period-adding sequence is clearly visible. Figure 47(c) shows a finger shaped delay plot of the system close to grazing using direct numerical simulation. The square root term in the grazing normal form (118) clearly shows its presence as the almost vertical finger, and if the full Poincaré map is used very similar results are found (not depicted). If Fig. 47(a) is compared with Fig. 2(a) the η-value at which grazing occurs is almost the same. While there are also some differences in the details between the simulations and the experiment, there is clear experimental evidence for a period adding sequence (upon decreasing η) interspersed with regions of chaos, just as predicted by the theory.

4.3 Nonsmooth Transitions of Limit Cycles 2; Multiple Impacts

In general, the sort of impacting problems that are likely to be met in many applications are *systems* of impact oscillators which have many components, each of which can collide of others. In the simplest case this could be a system like the Newton cradle, in which a line of balls can each collide with its nearest neighbour. At the extreme limit of complexity we can look at a granular material with many particles each of which can collide with any other. Other problems, such as the cantilever beam, can be considered (by looking at the different modes of oscillation) as being systems of impact oscillators where the modes evolve independently between impacts, but are coupled together by the impacts. Certain types of the behaviour of systems can be considered to be extensions of the theory for single impact oscillators. However, there are new phenomena to be considered which simply do not arise in the simple impact oscillator. Roughly speaking, this is the dynamics which arises when we have a simultaneous collision of several particles. Whilst the probability of such an incident occurring for an isolated system is zero, as a parameter in the system varies then such incidents will be observed. We show presently that this is a codimension-one phenomenon. Significant changes of behaviour then occur to the dynamics of the overall system as a parameter varies through the multiple impact scenario. In particular, we see that several new types of periodic motion are generated. This makes it hard to say precisely what the dynamics will be following a multiple impact, as several scenarios are possible.

There is far less existing literature (if any) on analysis of multiple impacts using bifurcation theory, than there is for grazing. So rather than attempt to be completely general we shall stick here to the mechanical framework of rigid particles described by positions and velocities.

Thus, we can think of a set of particles x_i, with velocities v_i, moving smoothly in a set S_i. In the simplest case we might consider a set of such particles in an ordered line so that $x_i \leq x_{i+1}$ with the motion of the particle x_1 excited by impact with a moving wall x_0. Under the motion induced by the moving wall, each particle will move independently so that a $2N$-dimensional phase space

$$S = (x_1, v_1) \times (x_2, v_2) \times \ldots \times (x_N, v_N), \qquad (120)$$

with the restriction that $x_i < x_{i+1}$. This phase space is bounded by a piecewise smooth $(N - 1)$-dimensional surface Σ comprising the union of

the N separate surfaces

$$\Sigma_i = \{(x,v) = (x_1, x_2, \ldots) \times (v_1, v_2, \ldots) : x_i = x_{i+1}\}, \quad i = 0, \ldots, N-1. \tag{121}$$

The combined surface Σ thus has *corners* and resembles the discontinuity surfaces examined in Section 2.3 above for piecewise smooth systems without impacts. Interesting dynamics occurs when a trajectory intersects one of these corners. In S itself we have smooth dynamics.

An example is given by a simplified version of Newton's cradle in which balls at positions x_i are suspended by vertical strings and we have simply

$$\frac{dx_i}{dt} = v_i, \quad \frac{dv_i}{dt} = -\omega_i^2(x_i - \bar{x}_i) - \zeta_i v_i. \tag{122}$$

where $\bar{x}_i$, ω_i, and ζ_i are the rest position, the natural frequency, and the damping coefficient of each particle, respectively. The dynamics changes when two particles collide and the trajectory in S intersects *one* of the surfaces Σ_i. The simplest description of the resulting dynamics is that (as in Example 4.1) we have an instantaneous impact in which the combined momentum of the particles is conserved but the relative impact velocity is reversed. This leads to the following system of equations

$$x_i^+ = x_i^-, \quad x_{i+1}^+ = x_{i+1}^- \tag{123}$$

$$m_i v_i^- + m_{i+1} v_{i+1}^- = m_i v_i^+ + m_{i+1} v_{i+1}^+, \quad \left(v_{i+1}^+ - v_i^+\right) = -r\left(v_{i+1}^- - v_i^-\right). \tag{124}$$

so that

$$\begin{pmatrix} x_i^+ \\ x_{i+1}^+ \\ v_i^+ \\ v_{i+1}^+ \end{pmatrix} = \begin{pmatrix} 1 & 0 & 0 & 0 \\ 0 & 1 & 0 & 0 \\ 0 & 0 & \frac{m_i - r m_{i+1}}{M_i} & \frac{(1+r)m_{i+1}}{M_i} \\ 0 & 0 & \frac{(1+r)m_i}{M_i} & \frac{m_{i+1} - r m_i}{M_i} \end{pmatrix} \begin{pmatrix} x_i^- \\ x_{i+1}^- \\ v_i^- \\ v_{i+1}^- \end{pmatrix} \tag{125}$$

where

$$M_i = m_i + m_{i+1}.$$

The linear equation (125) then describes the action of the impact map

$$(x_i^+, x_{i+1}^+, v_i^+, x_{i+1}^+) = f_i(x_i^-, x_{i+1}^-, v_i^-, x_{i+1}^-, r)^T \tag{126}$$

on the surface Σ_i which is a natural generalisation of the impact map $v^+ = -rv$ used in the analysis of single-degree-of-freedom impact oscillators (Example 4.1). If it is assumed that $m_i \gg m_{i+1}$ then the map (125)

101

reduces to

$$
\begin{pmatrix} x_i^+ \\ x_{i+1}^+ \\ v_i^+ \\ v_{i+1}^+ \end{pmatrix} = \begin{pmatrix} 1 & 0 & 0 & 0 \\ 0 & 1 & 0 & 0 \\ 0 & 0 & 1 & 0 \\ 0 & 0 & 1+r & -r \end{pmatrix} \begin{pmatrix} x_i^- \\ x_{i+1}^- \\ v_i^- \\ v_{i+1}^- \end{pmatrix}, \tag{127}
$$

which is the standard restitution law for a rigid impact of a particle with a moving wall.
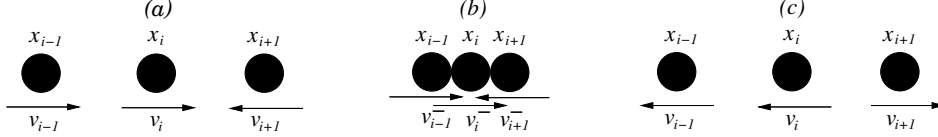

Figure 48: Three particles and their (possible) velocities (a) before, (b) during, and (c) after collision. The velocity directions in (c) depend of the associated impact map (cf. (125)).

The overall behaviour of the system of impact oscillators is thus described by the hybrid motion of the smooth map in S and the various maps f_i on the surfaces Σ_i. As before, we will see the usual mix of periodic fixed points and chaotic behaviour. Similarly, we will see grazing behaviour in a neighbourhood of any trajectory which intersects any of the surfaces Σ_i tangentially.

4.3.1 Corner-bifurcations

The similarities between systems of impact oscillators and the single-degree of freedom impact oscillator break down in a neighbourhood of a trajectory which intersects one of the corners of the surface Σ. Generically these are manifolds of codimension-two and we denote these by Γ_i so that for the Newton's cradle type problem we have

$$
\Gamma_i = \{x : x_{i-1} = x_i = x_{i+1}\}, \tag{128}
$$

representing a simultaneous collision between x_i, x_{i-1} and x_{i+1} (see Fig. 48). It is simply not known at present how to define what sort of dynamics arises in such a collision using bifurcation theory, as several, equally likely scenarios are possible. A complete analysis of this situation is difficult, so we restrict our discussion to the following scenario, which encapsulates much of the interesting dynamics observed in multiple impacting problems.

102

4.3.2 Saw-tooth forcing

Consider an infinitely massive moving wall x_1, moving sinusoidally and impacting with a massive particle at position $x_2(t) \geq x_1(t)$ which rebounds from it periodically. This scenario is a familiar example of a single degree of freedom impact oscillator. Whilst the motion of the wall is smooth, that of x_2 is not, and its periodic motion, in the simplest case takes the form of a rectified sine wave of which the simplest example is the function

$$\kappa + \beta |\sin(\omega t)|, \tag{129}$$

where in this case $\kappa, \beta, \omega \in \mathbb{R}$ and the points of impact with the wall are given by

$$t_k = k\frac{\pi}{\omega}.$$

(The motion resembles the teeth of a saw). More generally, close to the point of impact with the wall, so that $t \approx t_0$ we may approximate the motion of the particle x_2 by the function

$$x_2(t) = \begin{cases} \kappa + \theta_1(t_k - t), & t < t_0, \\ \kappa + \theta_2(t - t_k), & t > t_0, \end{cases} \tag{130}$$

for $\theta_i > 0$ with the overall motion of x_2 having a period T so that $t_k = t_0 + kT$.
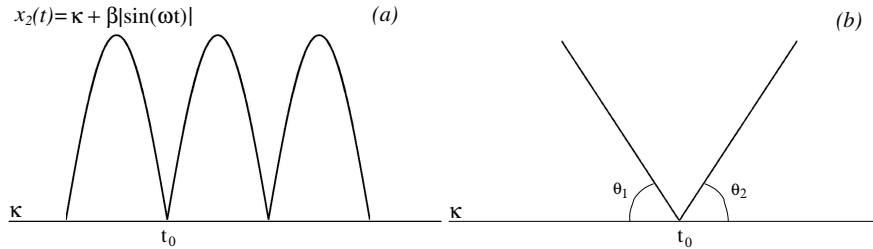

Figure 49: (a) The function $x_2(t) = \kappa + \beta |\sin(\omega t)|$. (b) A blow-up of the area in the vicinity of t_0 (cf. eq. (130)).

Now consider a third particle at position $x_3(t) \geq x_2(t)$ which impacts with the particle at x_2. In the simplest case we take x_2 to be very massive when compared to x_3 so that its is unaffected by the impact. As a useful simplification of a multiple impacting system we can this study the motion of a particle x_3 driven by impacting with a *non-smooth* moving surface $x_2(t)$

103

described, in particular, by the function (129) or more generally by the function (130) locally. For simplicity, we will also consider the particle to move in free space between impacts according to the the harmonic equation

$$\frac{d^2 x_3}{dt^2} + x_3 = 0. \tag{131}$$

As parameters in this system vary, we expect to see a change in the various points impact τ_j between x_2 and x_3. Under smooth changes in these parameters, there will be values at which x_3 impacts x_2 at a point t_k at which x_2 loses smoothness (see Fig. 50). As τ_j varies through such a point, we would also expect to see a qualitative behaviour in the solution.
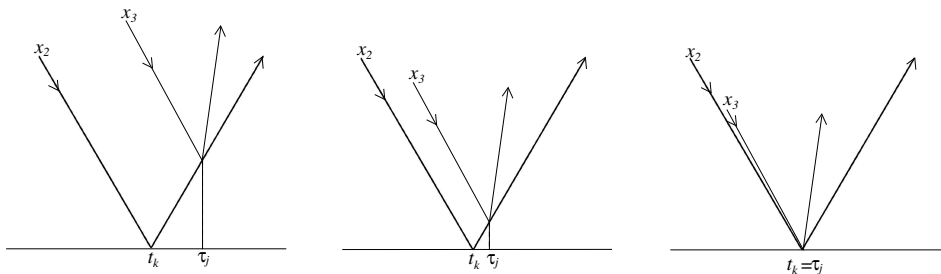

Figure 50: A schematic on how a saw-tooth event can locally be approached.

To illustrate this, we present in Fig. 51 some simulations of the behaviour of this system by considering the bifurcation diagram of the ω-limit sets of the motion in the case of the saw-tooth forcing function (129) with κ fixed, $\beta = 1$ and ω treated as the bifurcation parameter. In these simulations an event driven numerical code is used with a semi-analytical solution of the motion obtained by using the MATLAB `expm` command.

From the Figs. 51(a),(b) it can be seen that over significant parts of the bifurcation diagram, the behaviour of x_3 is simply periodic (with one impact per period). However, as ω is reduced through a point $\omega = \omega_S$, a dramatic change is observed as the point of impact passes through the discontinuity point t_S. In the case of Fig. 51, for which $\kappa = 0$ this occurs when $\omega_S = 2$, $t_S = \pi/2$. For ω slightly less than ω_S we then see the creation of three distinct types of periodic motion I, II and III illustrated below in Fig. 52. It is notable that in this case each solution type, with period nT, has $2n$ equivalent solutions but separated with a time shift of $k\frac{\pi}{\omega}$, $k = 0, \cdots, n-1$.

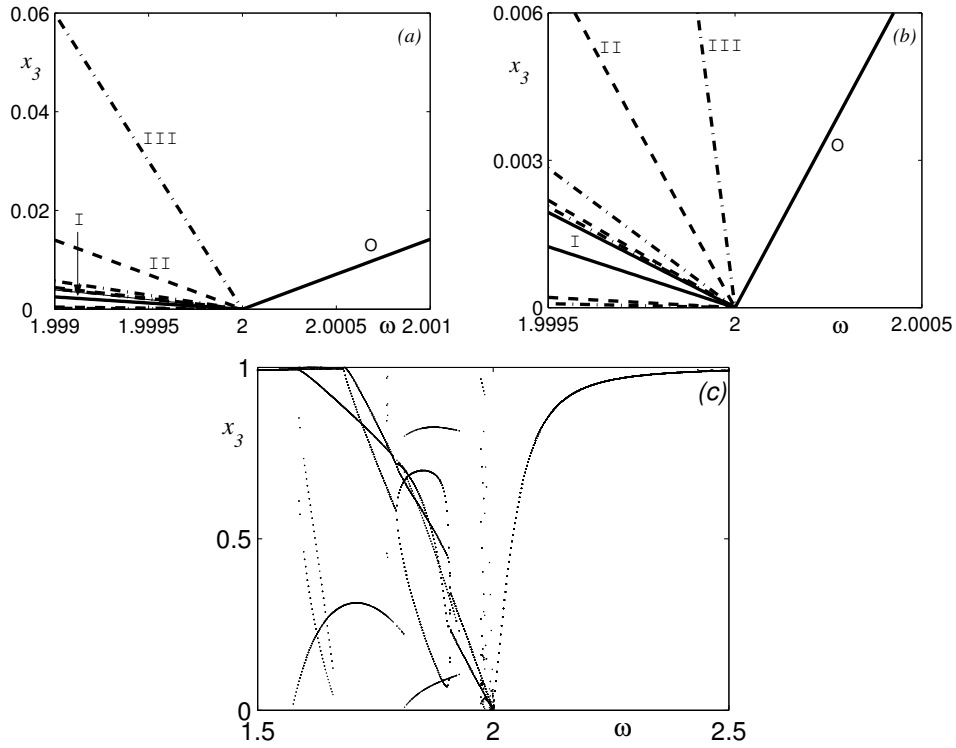We now proceed to give a brief explanation of this behaviour.

Figure 51: Bifurcation diagrams showing the position of the particle x_3 at impact for varying frequency ω. In (a) and (b) the local behaviour in the vicinity of the nonsmooth transition (at $\omega = 2$) is depicted and in (c) a bifurcation diagram for $1.5 < \omega < 2.5$. The different curves in (a) and (b) represent period-one (O - 'solid' and I - 'solid'), period-two (II - '--'), and period-three (III - '- · -') motion. See also Fig. 52, where the actual trajectories are depicted.

4.3.3 Bifurcation condition

Let us make the presumption that a simple periodic orbit of x_3 exists, and that as a parameter varies, this orbit has a point of impact which coincides with a point of discontinuity t_k of the forcing function described in (130). To study this, we introduce a Poincare surface Π at the time $t = nT$ so that $(x_3(0), v_3(0)) = (a, b)$ and $(x_3(T), v_3(T)) = (A, B)$ so that close to $t = 0$ we have $x_3(t) = a\cos(t) + b\sin(t)$ and close to $t = T$ we have $x_3(t) =$
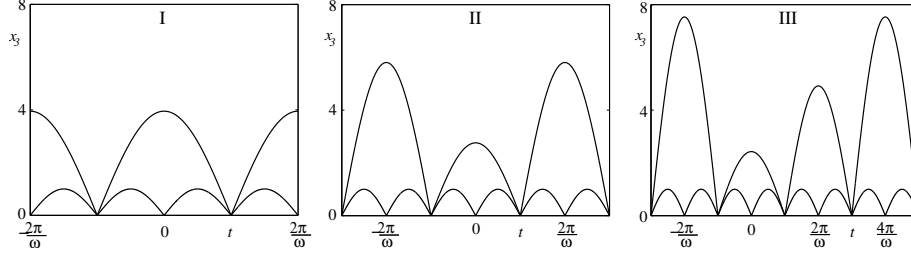
Figure 52: Time series at $\omega = 1.999$ of the three distict types of periodic orbits created at $\omega_s = 2$, where I, II, and III show period-one, period-two, and period-three motion, respectively.

$A \cos(t - T) + B \sin(t - T)$.

We assume at present that there is a single impact orbit of period T for which the impact of x_3 with x_2 occurs at a point τ slightly after the point t_0. The reasons for this choice will become clear presently. In this case it follows that a, b and A, B are related as follows. The condition for an impact gives

$$a \cos(\tau) + b \sin(\tau) = A \cos(\tau - T) + B \sin(\tau - T) = \kappa + \theta_2(\tau - t_0)$$

and the change in the velocity at impact gives

$$-A \sin(\tau - T) + B \cos(\tau - T) = (1 + r)\theta_2 + ra \sin(\tau) - rb \cos(\tau),$$

where the impact law (127) is used. If a, b are known, this gives a nonlinear map to τ, A and B. If $\tau - t_0 = \epsilon$ is small we have to leading order

$$\epsilon = \frac{\delta}{\theta_2 + a \sin(t_0) - b \cos(t_0)}, \quad \delta = a \cos(t_0) + b \sin(t_0) - \kappa. \qquad (132)$$

The condition

$$\delta = 0 \qquad (133)$$

implies that x_3 lies above x_2 at the point t_0 so that the impact occurs after t_0.

The condition for a single period periodic orbit is that $(a, b) = (A, B)$. This orbit will occur at the 'saw-tooth' point t_0 provided that $\tau = t_0$. For given t_0 this leads to the following linear system for a, b and κ

$$\begin{pmatrix} \cos(t_0) & \sin(t_0) & -1 \\ \cos(t_0) - \cos(t_0 - T) & \sin(t_0) - \sin(t_0 - T) & 0 \\ -r \sin(t_0) - \sin(t_0 - T) & r \cos(t_0) + \cos(t_0 - T) & 0 \end{pmatrix} \begin{pmatrix} a \\ b \\ \kappa \end{pmatrix} = \begin{pmatrix} 0 \\ 0 \\ (1 + r)\theta_2 \end{pmatrix},$$

106

with solution

$$(a, b, \kappa) = \theta_2 \frac{(1 + r)}{(1 - r)} \left(\frac{\sin(t_0) - \sin(t_0 - T)}{(1 - \cos(T))}, \frac{\cos(t_0 - T) - \cos(t_0)}{(1 - \cos(T))}, \cot(T/2) \right).$$

$$(134)$$

As an example we consider the case of the forcing $\kappa + \beta |\sin(\omega t)|$ given in (129). In this case we let $\beta = 1$, $t_0 = \pi/\omega$, $T = 2\pi/\omega$ and $\theta_1 = \theta_2 = \omega$. A 'saw-tooth' bifurcation then occurs when $\omega = \omega_S$ satisfies the condition

$$\omega_S \frac{(1 + r)}{(1 - r)} \cot(\pi/\omega_S) = \kappa.$$

For fixed κ this is satisfied by a locally unique value of ω so that we have a codimension-one condition for a bifurcation in this case. If $\kappa = 0$ this occurs when $\omega = 2$ as we can observe from the bifurcation diagram in Fig. 51. Note that for general κ at the bifurcation point we also have

$$a = \omega \frac{(1 + r)}{(1 - r)} \frac{1}{\sin(\pi/\omega)}, \quad b = 0. \tag{135}$$

Note further that the height σ of the point of impact of any such periodic orbit is given by

$$\sigma = f(\omega) \equiv \omega \frac{1 + r}{1 - r} \cot(\pi/\omega).$$

This is an increasing function of ω. Thus σ is greater than κ and the impact occurs on the part of the function $x_2(t)$ with positive slope only if $\omega > \omega_S$. If $\omega < \omega_S$ then the impact is on the part of the curve x_2 with *negative* slope. In this case $a < 0$ and the periodic solution x_3 lies underneath the curve x_2 which is non-physical.

In conclusion, we expect to see regular behaviour if $\omega > \omega_S$ and more complex behaviour is $\omega < \omega_S$ which is consistent with the observed behaviour on the bifurcation diagram (51).

4.3.4 The maps close to the saw-tooth bifurcation point

We now consider the behaviour of the impact close to the point t_0. Generically one of three things can happen for the linear map approximation given in (130):

α-**map** The particle x_3 impacts at a point $\tau_1 < t_0$ and at a second point $\tau_2 > t_0$ τ_1 and τ_2 close to t_0.

β-**map** The particle x_3 impacts at a point $\tau_1 > t_0$ close to t_0.

γ-**map** The particle x_3 impacts at a point $\tau_1 < t_0$ close to t_0 and does not
impact again close to t_0.

The three situations are as illustrated in Fig. 53 and the condition for either
of the maps α and γ to occur is that

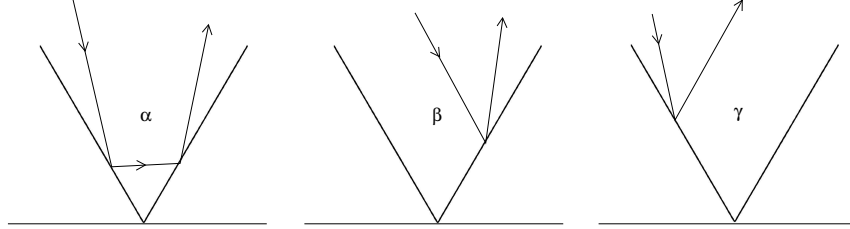$$\delta = a\cos(t_0) + b\sin(t_0) - \kappa < 0.$$

Figure 53: Schematics of the three local maps α, β and γ.

4.3.5   Analysis at the bifurcation point

We now present an analysis of the infinitesimal map associated with an
impact at the sawtooth point. For convenience we consider the *resonant*
case for which $\kappa = 0$, $\omega = 2$ and $t_s = \pi/2$. In this case the resulting algebra
is greatly simplified. The solution can easily then be perturbed to either of
the two cases of $\omega = 2 - \epsilon$ and $\omega = 2 + \epsilon$ where $\epsilon > 0$. In this case we see
a multiplicity of different types of periodic motion when $\omega = 2 - \epsilon$ and a
single periodic motion when $\omega = 2 + \epsilon$.

To analyse this situation, we consider the map P_S from $(a, b) \to (A, B)$
advancing $(u, du/dt)$ over the time $T = \pi$, and show that P_S can take three
different linear forms.

The condition for impact with $\kappa = 0$ at $t = \pi/2$ gives

$$a\cos(\pi/2) + b\sin(\pi/2) = 0, \quad \text{and} \quad A\cos(\pi/2 - \pi) + B\sin(\pi/2 - \pi) = 0.$$

These two conditions are satisfied if and only if

$$b = B = 0.$$

Now, suppose that the impact velocity is v so that

$$v = -a\sin(\pi/2) + b\cos(\pi/2) = -a.$$

After impacting with the sawtooth waveform we have

$$v \to f(v)$$

so that
$$f(v) = -A\sin(\pi/2 - \pi) + B\cos(\pi/2 - \pi) = A.$$

Thus we have an infinitesimal Poincaré map given by

$$P_S(a, 0) = (f(-a), 0).$$

Now, the map $f(v)$ takes one of three affine linear forms, depending upon whether the infinitesimal impact occurs on both sides (the $\alpha-$map), immediately after $\pi/2$ (the $\beta-$map) or immediately before $\pi/2$ (the $\gamma-$map). If the slope of the forcing function before $\pi/2$ is θ_1 and after $\pi/2$ is θ_2 then we have

$$\alpha : f_1(v) = (1 + r)\theta_2 - r[(1 + r)\theta_1 - rv] = (1 + r)\theta_2 - r(1 + r)\theta_1 + r^2 v,$$
$$\beta : f_2(v) = (1 + r)\theta_2 - rv,$$
$$\gamma : f_3(v) = (1 + r)\theta_1 - rv.$$

Observe that in each case, when $\omega = 2$ the impact point is at $x = 0$. For $\omega = 2 \pm \epsilon$ we expect that the point of impact will be proportional to ϵ, as can be seen in Fig. 51.

In the case of forcing with a sinusoidal function $|\sin(\omega t)|$, then when $\omega = 2$ at $t = \pi/2$ we have $-\theta_1 = \theta_2 = 2$ giving

$$\alpha : f_1(v) = 2(1 + r)^2 + r^2 v,$$
$$\beta : f_2(v) = 2(1 + r) - rv,$$
$$\gamma : f_3(v) = -2(1 + r) - rv.$$

(Again with perturbations proportional to ϵ when ω varies from 2). Thus when applying one of these maps we simply have

$$A = g_i(a) \equiv f_i(-a), i = 1, \ldots, 3.$$

It is clear from inspection that none of these maps commutes with any other.

To look for periodic orbits we now seek fixed points of the iterated map

$$F(a) = g_{i_N} \circ g_{i_{N-1}} \circ g_{i_{N-2}} \circ \ldots \circ g_{i_1}.$$

In principle any such combination of the elemental maps, with a free choice of each index i_K will lead to a fixed point. However two conditions restrict our choices

1. If a^* (with $b^* = 0$) is any such fixed point then $a^* > 0$ and the value of
   $$g_{i_K} \circ g_{i_{K-1}} \circ g_{i_{K-2}} \circ \ldots \circ g_{i_1}(a^*) > 0$$
   for all values of $1 \leq K \leq N$.

2. If we perturb ω to $\omega - \epsilon$ and the fixed point perturbs to a^*_ϵ (with the value of b^* similarly perturbing to b^*_ϵ) then the values of (a, b) given by the two dimensional prolongation of the above maps
   $$(a, b) = g_{i_K} \circ g_{i_{K-1}} \circ g_{i_{K-2}} \circ \ldots \circ g_{i_1}(a^*_\epsilon, b^*_\epsilon)$$
   are such that the conditions for the next map to be of the form $g_{i_{K+1}}$ are satisfied.

Condition 1. can be easily verified for any particular fixed point by using the ideas described in these notes. Verification of Condition 2 is rather harder, and we will not give it here.

Prompted by our numerical calculations, we are led to the conjecture that four possible fixed points are given by the respective maps: g_2, g_1, $g_2 \circ g_1$, and $g_3 \circ g_2 \circ g_1$. We examine each in turn.

g_2: The fixed point of the map g_2 is given when

$$a = 2(1 + r) + ra, \quad \text{so that} \quad a = \frac{2(1 + r)}{(1 - r)} > 0.$$

g_1: The fixed point of the map g_1 is given when

$$a = 2(1 + r)^2 - r^2 a, \quad \text{so that} \quad a = \frac{2(1 + r)^2}{(1 + r^2)} > 0.$$

Both maps satisfy Condition 1. A little thought shows that g_2 can only occur when the impact is to the right of the saw-tooth point, so that $\omega \geq 2$. Similarly, the fixed point of g_1 can only arise when the impact is to the left of the saw-tooth point, so that $\omega \leq 2$.

110

$g_2 \circ g_1$: The iterated map $g_2 \circ g_1$ is given by

$$g_2 \circ g_1 = 2(1+r) + r[2(1+r)^2 - r^2 a] = 2(1+r)(1+r+r^2) - r^3 a$$

with fixed point(s)

$$a_1 = \frac{2(1+r)(1+r+r^2)}{(1+r^3)} > 0 \quad \text{and} \quad a_2 = g_1(a_1).$$

Note that

$$
\begin{aligned}
a_2 &= 2(1+r)^2 - \frac{2r^2(1+r)(1+r+r^2)}{(1+r^3)} \\
&= 2(1+r)\left[(1+r) - \frac{r^2(1+r+r^2)}{(1+r^3)}\right] \\
&= \frac{2(1+r)}{(1+r^3)}(1+r-r^2) > 0.
\end{aligned}
$$

$g_3 \circ g_2 \circ g_1$: The iterated map $g_3 \circ g_2 \circ g_1$ is given by

$$
\begin{aligned}
g_3 \circ g_2 \circ g_1 &= -2(1+r) + r[2(1+r)(1+r+r^2) - r^3 a] \\
&= -r^4 a + 2((1+r)(r(1_r + r^2) - 1)).
\end{aligned}
$$

This has fixed points

$$a_1 = \frac{(1+r)(-1+r+r^2+r^3)}{(1+r^4)}, \quad a_2 = g_1(a_1) \quad \text{and} \quad a_3 = g_2(a_2).$$

A similar check to the above shows that these are all positive. The periodic orbits corresponding to the fixed points of the respective maps g_1, $g_2 \circ g_1$, and $g_3 \circ g_2 \circ g_1$ give the three orbits I, II and III visible in Figure 1.5 when $\omega = 1.999$ (with a small perturbation in this case as ω is slightly less than 2). The fact that these orbits can be computed strongly implies that the various compatibility conditions apply in this case, though this remains to be verified in detail. At this stage no other combinations of the maps g_i have been found (numerically) which lead to periodic orbits.

5 Discussion

While we have tried to be comprehensive in this review, there are many things that we have not addressed. For example (in no particular order)

111

we have not dealt with more complex impact laws than (100), for example those required to explain the so called 'Painlevé paradox' [55]. We have also not treated multiple impacts in a generic way (Section 4.3). In the case of equilibrium bifurcation, general unfoldings in N-dimensions remain unknown (Sections 2.1, 3.1). For sliding bifurcations of limit cycles we have not dealt with repelling sliding regions. Perhaps the biggest area that remains open is the unfolding of all the possible dynamics of the normal form we have derived. Set valued Coulomb friction laws [78], chattering (the infinite accumulation of impacts), higher order sliding (sliding along the intersection of two or more discontinuity surfaces), and the possible existence of sets of equilibria in the sliding or sticking set have not been touched on here as often more precise mathematical tools such as differential inclusions are required.

Also, the reviw has (deliberately) limited its scoop to codimension-one equilibrium and periodic orbit bifurcations. For some hints on how certain codimension-two C-bifurcations can act as organising centres, see [23]. There is also literature on global bifurcations in non-smooth systems (an idea that was touched in Section 3.1) see also [51, 70, 74] for other examples. There is also literature on non-smooth invariant tori bifurcations that we have not touched on here [17, 84].

Finally we mention infinite-dimensional systems genersted by PDEs or delay equations, see e.g. [52, 80]. In real continuous structures with impact, for example, many modes may be excited at impact and there may be a delay associated with the dissipation of the shock wave (see e.g. [41, 76, 83] for more realistic models of impact mechanisms).

Clearly we are just scratching on the surface of a bifurcation theory for piecewise smooth systems, yet it is the nnn of the authors that such a theory is pressing since rattles, bangs, and switches are perhaps the most common (and grossest) form of nonlinearity found in applications.

6 Acknowledgment

112

References

[1] D. K. Arrowsmith and C. M. Place. *An Introduction to Dynamical Systems*. CUP, Cambridge, UK, 1990.

[2] S. Banerjee and C. Grebogi. Border collision bifurcations in two-dimensional piecewise smooth maps. *Physical Review E*, 59:4052–4061, 1999.

[3] S. Banerjee and C. Grebogi. Border collision bifurcations at the change of state-space dimension. *CHAOS*, 12:1054–1069, 2002.

[4] S. Banerjee and G. Verghese. *Nonlinear Phenomena in Power Electronics*. IEEE press, New York, 2001.

[5] S. Banerjee, J. A Yorke, and C. Grebogi. Robust chaos. *Physical Review Lett*, 80:3049–3052, 1998.

[6] P.V. Bayly and L.N. Virgin. An experimental study of an impacting pendulum. *Journal of Sound and Vibration*, 164(2):364–374, 1993.

[7] B. Brogliato. *Nonsmooth Mechanics – Models, Dynamics and Control*. Springer–Verlag, New York, 1999.

[8] B. Brogliato. *Impacts in Mechanical Systems – Analysis and Modelling*. Springer–Verlag, New York, 2000. Lecture Notes in Physics, Volume 551.

[9] B. Brogliato. Some perspectives on the analysis and control of complementarity systems. *IEEE Transactions on Automatic Control*, 48:918–935, 2003.

[10] C. J. Budd and F. Dux. Chattering and related behaviour in impact oscillators. *Phil. Trans. Roy. Soc. Lond. A*, 347:365–389, 1994.

[11] C. J. Budd and F. Dux. Intermittency in impact oscillators close to resonance. *Nonlinearity*, 7:1191–1224, 1994.

[12] W. Chin, E. Ott, H. E. Nusse, and C. Grebogi. Grazing bifurcations in impact oscillators. *Physical Review E*, 50:4427–4444, 1994.

[13] S.N. Chow and J. Hale. *Methods of Bifurcation Theory*. Springer–Verlag, New York, 1982.

113

[14] F.B. Cunha, D.J. Pagano, and U.F. Moreno. Sliding bifurcations in planar variable structure systems. *IEEE Transactions on Circuit and Systems*, 50(8):1129–1134, 2003.

[15] H. Dankowicz. On the modelling of dynamic friction phenomena. *ZAMM*, 79:399–409, 1999.

[16] H. Dankowicz and A. B. Nordmark. On the origin and bifurcations of stick-slip oscillations. *Physica D*, 136:280–302, 1999.

[17] H. Dankowicz, P.T. Piiroinen, and A.B. Nordmark. Low-velocity impacts of quasiperiodic oscillations. *Chaos Solitons & Fractals*, 14:241–255, 2002.

[18] J. H. B. Deane and D. C. Hamill. Analysis, simulation and experimental study of chaos in the buck concerter. In *Proceedings of the Power Electronics Specialists Conf. (PESC 1990)*, pages 491–8, New York, 1990. IEEE Press.

[19] M. di Bernardo. Normal fprms of border collisions in high dimensional nonsmooth maps. In *IEEE ISACS*, volume 3, pages 76–79, 2003.

[20] M. di Bernardo, C. J. Budd, and A. R. Champneys. Grazing, skipping and sliding: analysis of the nonsmooth dynamics of the DC/DC buck converter. *Nonlinearity*, 11:858–890, 1998.

[21] M. di Bernardo, C. J. Budd, and A. R. Champneys. Corner–collision implies border–collision bifurcation. *Physica D*, 154:171–194, 2001.

[22] M. di Bernardo, C. J. Budd, and A. R. Champneys. Grazing bifurcations in n-dimensional piecewise-smooth dynamical systems. *Physica D*, 160:222–254, 2001.

[23] M. di Bernardo, A.R. Champneys, S.J. Hogan, M. Homer, P. Kowalczyk, Yu.A. Kuznetsov, and A.B. Nordmark. Two-parameter nonsmooth grazing bifurcations of limit cycles: challanges and open problems. In preparation, 2004.

[24] M. di Bernardo, M. I. Feigin, S. J. Hogan, and M. E. Homer. Local analysis of C-bifurcations in n-dimensional piecewise smooth dynamical systems. *Chaos, Solitons and Fractals*, 10:1881–1908, 1999.

[25] M. di Bernardo, E. Fossas, G. Olivar, and F. Vasca. Secondary bifurcations and high periodic orbits in voltage controlled buck converter. *International Journal of Bifurcations and Chaos*, 7:2755–2771, 1997.

[26] M. di Bernardo, F. Garofalo, L. Glielmo, and F. Vasca. Switchings, bifurcations and chaos in DC/DC converters. *IEEE Transactions on Circuits and Systems, Part I*, 45:133–141, 1998.

[27] M. di Bernardo, F. Garofalo, L. Ianelli, and F. Vasca. Bifurcations in piecewise smooth feedback systems. *International Journal of Control*, 75(16):1–22, 2002.

[28] M. di Bernardo, F. Garofalo, L. Ianelli, and F. Vasca. Bifurcations of piecewise smooth feedback systems. *International Journal of Control*, pages 1–20, 2003.

[29] M. di Bernardo, K. H. Johansson, and F. Vasca. Self-oscillations and sliding in relay feedback systems: Symmetry and bifurcations. *International Journal of Bifurcations and Chaos*, 11(4):1121–1140, 2001.

[30] M. di Bernardo, P. Kowalczyk, and A. Nordmark. Bifurcations of dynamical systems with sliding: derivation of normal-form mappings. *Physica D*, 170:175–205, 2002.

[31] M. di Bernardo, P. Kowalczyk, and A. Nordmark. Sliding bifurcations: A novel mechanism for the sudden onset of chaos in dry-friction oscillators. *International Journal of Bifurcation and Chaos*, 13(10):2935–2948, 2003.

[32] M. I. Feigin. On the structure of C-bifurcation boundaries of piecewise continuous systems. *PMM*, 42:820–829, 1978.

[33] M. I. Feigin. *Forced Oscillations in Systems With Discontinuous Nonlinearities*. Nauka, Moscow, 1994. In Russian.

[34] A. F. Filippov. *Differential Equations with Discontinuous Righthand Sides*. Kluwer Academic Publishers, Dortrecht, 1988.

[35] E. Fossas and G. Olivar. Study of chaos in the buck converter. *IEEE Transactions on Circuits and Systems - I: Fundamental Theory and Applications*, 43:13–25, 1996.

[36] M. H. Frederiksson and A. B. Nordmark. Bifuractions caused by grazing incidence in many degrees of freedom impact oscillators. *Proc. Royal Soc. Lond. A*, 453:1261–1276, 1997.

[37] E. Freire, E. Ponce, F. Rodrigo, and F. Torres. Bifurcation sets of continuous piecewise linear systems with two zones. *International Journal of Bifurcation and Chaos*, 8(11):2073–2097, 1998.

[38] U. Galvanetto. Some discontinuous bifurcations in a two block stick-slip system. *Journal of Sound and Vibration*, 284(4):653 – 669, 2001.

[39] U. Galvanetto and S. R. Bishop. Dynamics of a simple damped oscillator undergoing stick-slip vibrations. *Meccanica*, 34:337–347, 2000.

[40] F. Giannakopoulos and K. Pliete. Planar systems of piecewise linear differential equations with a line discontinuity. *Nonlinearity*, 14:1–22, 2001.

[41] C. Glocker. *Set-valued force laws*. Springer–Verlag, Berlin Heidelberg, 2001. Lecture Notes in Applied Mechanics, Volume 1.

[42] J. Guckenheimer and P. Holmes. *Nonlinear Oscillations, Dynamical Systems, and Bifurcations of Vector Fields*. Springer–Verlag, New York, 1983. Applied Mathematical Sciences, Volume 42.

[43] W.P.M.H. Heemels and B.B. Brogliato. The complementarity class of hybrid dynamical systems. *European Journal of Control*, 9:311–319, 2003.

[44] G. Iooss and D. Joseph. *Elementary stability and bifurcation theory*. Springer–Verlag, New York, 1980.

[45] A Klarbring. Examples of non-uniquess and non-existence of solutions to quasistatic contact problems with friction. *Ingenieur-Archiv*, 60:529–541, 1990.

[46] P. Kowalczyk. Border-collision bifurcations and robust chaos in non-invertible piecewise linear (PWL) maps. Submitted for a journal publication, February 2004.

[47] P. Kowalczyk and M. di Bernardo. Existence of stable asymmetric limit cycles and chaos in unforced symmetric relay feedback systems. In *Proceedings of European Control Conference, Porto*, pages 1999–2004, 2001.

[48] P. Kowalczyk and M. di Bernardo. On a novel class of bifurcations in hybrid dynamical systems - the case of relay feedback systems. In *Proceedings of Hybrid Systems Computation and Control*, pages 361–374. Springer–Verlag, 2001.

[49] T. Küpper and S. Moritz. General hopf bifurcations for non-smooth planar systems. *Phil. Trans. Roy. Soc. Lond. A*, pages 2483–2498, 2001.

[50] Yu. A. Kuznetsov. *Elements of Applied Bifurcation Theory.* Springer–Verlag, New York, second edition, 1998. Applied Mathematical Sciences, Volume 112.

[51] Yu.A. Kuznetsov, S. Rinaldi, and A. Gragnani. One-parameter bifurcations in planar fillipov systems. *Int. J. Bifurcation Chaos*, 2003.

[52] A.C. Lazer and P.J. McKenna. Large-amplitude periodic oscillations in suspension bridges: Some new connections with nonlinear analysis. *SIAM Review*, 32:537ff, December 1990.

[53] R.I. Leine. *Bifurcations in Discontinuous Mechanical Systems of Filippov-Type.* PhD thesis, Teknische Universiteit Eindhoven, The Netherlands, 2000.

[54] R.I. Leine. Some examples of discontinuous bifurcations., 2003. DCT report, Teknische Universiteit Eindhoven, The Netherlands.

[55] R.I. Leine, B. Brogliato, and H. Nijmeijer. Periodic motions induced by the painlev/'e paradox. *IEEE Transactions on Circuits and Systems I*, 1998.

[56] A. Nordmark. *Grazing conditions and chaos in impacting systems.* PhD thesis, Royal Institute of Technology, Stockholm, Sweden, 1992.

[57] A. Nordmark, M. di Bernardo, and G. Olivar. Bifurcations of equilibria in nonsmooth dynamical systems. In preparation.

[58] A.B. Nordmark. Non-periodic motion caused by grazing incidence in impact oscillators. *Journal of Sound and Vibration*, 2:279–297, 1991.

[59] A.B. Nordmark. Universal limit mapping in grazing bifurcations. *Physical Review E*, 55:266–270, 1997.

[60] A.B. Nordmark. Existence of priodic orbits in grazing bifurcations of impacting mechanical oscillators. *Nonlinearity*, 14:1517–1542, 2001.

[61] A.B. Nordmark. Discontinuity mappings for vector fields with higher-order continuity. *Dynamical Systems*, 17:359–376, 2002.

[62] H. Nusse, E. Ott, and J. Yorke. Border collision bifurcations: an explanation for observed bifurcation phenomena. *Phys. Rev. E*, 49:1073–1076, 1994.

[63] L. E. Nusse and J. A. Yorke. Border-collision bifurcations including 'period two to period three' for piecewise smooth systems. *Physica D*, 57:39–57, 1992.

[64] L. E. Nusse and J. A. Yorke. Border–collision bifurcations for piece-wise smooth one-dimensional maps. *International Journal of Bifurcation and Chaos*, 5:189–207, 1995.

[65] G. Olivar, M. di Bernardo, and F. Angulo. Discontinuous bifurcations in DC-DC converters. In *Proceedings of International Conference on Industrial Technology ICIT*, 2003.

[66] F. Peterka. Part 1: Theoretical analysis of n-multiple $(1/n)$-impact solutions. *CSAV Acta Technica*, 19:462–473, 1974.

[67] P.T. Piiroinen, L.N. Virgin, and A.R. Champneys. Chaos and period-adding; experimental and numerical verification of the grazing bifurcation. *Journal of Nonlinear Science*, 14(4):383–404, 2004.

[68] K. Popp, N. Hinrichs, and M. Oestreich. Dynamical behaviour of friction oscillators with simultaneous self and external excitation. *Sadhana (Indian Academy of Sciences)*, 20:627–654, 1995.

[69] K. Popp and P. Shelter. Stick–slip vibrations and chaos. *Philosophical Transactions of the Royal Society A*, 332(1624):89–105, 1990.

[70] M.N. Rabinder, editor. *Chua's circuit: a paradigm for chaos.* World Scientific Series on Nonlinear Science, Series B. World Scientific, 1993.

[71] S. W. Shaw and P. J. Holmes. A periodically forced piecewise linear oscillator. *J. Sound and Vibration*, 90:129–144, 1983.

[72] S.W. Shaw. On the dynamic response of a system with dry friction. *Journal of Sound and Vibration*, 108(2):305–325, 1986.

[73] K.N. Slade, L.N. Virgin, and P.V. Bayly. Extracting information from interimpact intervals in a mechanical oscillator. *Physical Review E*, 56(3):3705–3708, 1997.

[74] C. Sparrow. Chaos in a three-dimensional single loop system with a piecewise linear feedback function. *Journal of Mathematical Analysis and Applications*, 83:275–291, 1981.

[75] D.E. Stewart. Rigid-body dynamics with friction and impact. *SIAM Review*, 42(1):3–39, 2000.

[76] W.J. Stronge. *Impact Mechanics*. CUP, Cambridge, 2000.

[77] V. I. Utkin. *Sliding Modes in Control Optimization*. Springer–Verlag, New York, 1992.

[78] N. van de Wouv and R.I. Leine. Attractivity of equilibrium sets of systems with dry friction. *Nonlinear Dynamics*, 35:19–39, 2004.

[79] A. J. van der Schaft and J. M. Schumacher. *An Introduction to Hybrid Dynamical Systems*. Springer–Verlag, New York, 2000.

[80] D.J. Wagg, Karpodinis G., and Bishop S.R. An experimental study of the impulse response of a vibro-impacting cantilever beam. *J. Sound Vib,*, 228:242–264, 1999.

[81] Y. Yoshitake and A. Sueoka. Forced self-excited vibration with dry friction. In Marian Wiercigroch and Bram de Kraker, editors, *Applied nonlinear dynamics and chaos of mechanical systems with discontinuities*, pages 237–259. World Scientific, 2000.

[82] G. Yuan, S. Banerjee, E. Ott, and J. A. Yorke. Border-collision bifurcations in the buck converter. *IEEE Transactions on Circuits and Systems–I*, 45:707–716, 1998.

[83] G. Zhou and S.R. Reid, editors. *Impact on Composites*. Woodhead Publishers, 2000.

[84] Zh.T. Zhusubaliyev, E.A. Soukhoterin, and E. Mosekilde. Border-collision bifurcations on a two-dimensional torus. *Chaos, Solitons, and Fractals*, 13:1889–1915, 2003.

[85] Y. Zou and T. Küpper. Generalized hopf bifurcation emanated from a corner for piecewise smooth systems, 2003. In submission.